Graphene: Applications in Surface Science Studies

Boix, Virginia

2022

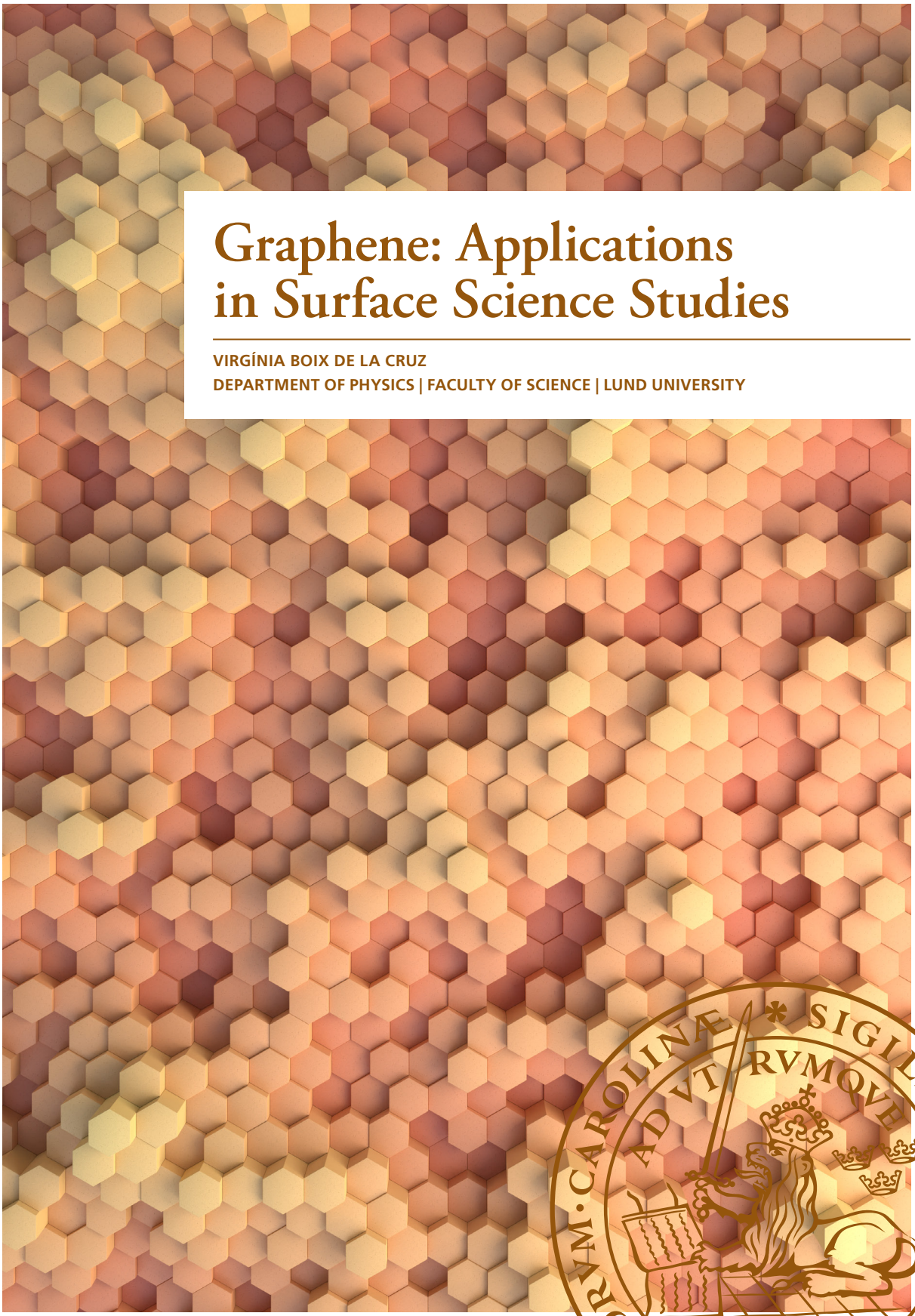

Graphene: Applications in Surface Science Studies

VIRGÍNIA BOIX DE LA CRUZ
DEPARTMENT OF PHYSICS | FACULTY OF SCIENCE | LUND UNIVERSITY

Graphene: Applications in Surface Science Studies

Virgínia Boix de la Cruz

LUND
UNIVERSITY

DOCTORAL DISSERTATION

Doctoral dissertation for the degree of Doctor of Philosophy (PhD) at the Faculty of Science at Lund University to be publicly defended on the 2nd of December 2022 at 13.15 in Rydberg lecture Hall, Department of Physics

Faculty opponent
José Ángel Martín Gago, Research professor and Institute director at Instituto de Ciencia de Materiales de Madrid, ICMM, CSIC

Organization LUND UNIVERSITY	**Document name** Doctoral Dissertation
	Date of issue 2022-12-02
Author Virgínia Boix de la Cruz	Sponsoring organization

Title and subtitle Graphene: Applications in Surface Science Studies

Abstract

This thesis addresses how graphene can be a valuable asset for surface science studies. Using a combination of X-ray photoelectron spectroscopy, scanning tunneling microscopy, and low-energy electron diffraction, we take advantage of graphene's sensitivity to changes in its chemical environment to obtain an atomic scale understanding of different reactions occurring above and below the film.

As a substrate, graphene provides an inert base for studying growth mechanisms. Specifically, we use it to investigate the electron-induced dissociation of borazine, a common precursor for Boron Nitride deposition. Thanks to the inert character of graphene, we can discern the dissociation due to the interaction with the electron beam from any surface-induced dissociation processes. Moreover, graphene can be used as an adsorption template for studying reactions between adsorbates and gas phase molecules. Using hydrogen adsorbates, we analyze the stability of different H-structures under mbar pressures of oxygen. We show that graphene acts as a catalyst for water formation by providing the required adsorption configuration that promotes the reaction. This finding paves the way for future research using graphene as an adsorption template for fundamental catalysis studies.

Graphene can also be employed as a confining agent to study undercover reactions, a trending topic in the catalysis field due to the reported higher performance of catalysts when placed in confined environments. We use graphene to investigate copper oxidation undercover, revealing that its presence stabilizes a Cu_2O phase undercover, delaying the evolution toward complete oxidation (CuO). Graphene is also an ideal model system for studying more fundamental aspects of undercover reactions, such as the coexistence of different molecules undercover or their intercalation kinetics. Specifically, we use graphene to investigate the coexistence of hydrogen and CO with already intercalated oxygen while following the intercalation process *in situ* with APXPS.

Altogether this thesis provides several examples of how graphene can be integrated into surface science studies and paves the way for its implementation in the surface science field.

Key words Graphene, Surface Science, EBID, Catalysis, Undercover Catalysis, XPS, APXPS, STM

Classification system and/or index terms (if any)

Supplementary bibliographical information	**Language** English
ISSN and key title	**ISBN** 978-91-8039-447-5 (print) 978-91-8039-448-2 (electronic)
Recipient's notes	**Number of pages** 96 / Price
	Security classification

Graphene: Applications in Surface Science Studies

Virgínia Boix de la Cruz

LUND
UNIVERSITY

Cover illustration: “Surface changes reflected on an hexagonal structure” by Giulio D’Acunto

Division of Synchrotron Radiation Research

Department of Physics, Faculty of Science

Lund University

ISBN

978-91-8039-447-5 (print)

978-91-8039-448-2 (electronic)

Printed in Sweden by Media-Tryck, Lund University

Lund 2022

To Kali,

who taught me to always be ready for an adventure

Acknowledgements

They say that a PhD is a lonely journey, however that has not been the case for me. During these years I have found two new families, one in science and another one in my heart. I want to thank everyone that has been part of my life during this process, thank you for being there and supporting me, you are all part of my success.

This thesis would not have been possible without the relentless support and encouragement of my main supervisor, Jan Knudsen. You always helped me believe in myself, sharing your excitement for research and making me feel welcome to share my thoughts. I have learned so much working with you, thank you for your time and guidance. I also want to thank my other supervisors, Joachim Schnadt for his valuable feedback and all the spectroscopy knowledge, and Anders Mikkelsen for always making time for me when I needed an additional perspective into my work.

This work wouldn't have been possible without all the beamtimes at MaxIV, Astrid and Elettra. Beamtimes are hard work and crazy hours, but with the right people they are also great fun. The APXPS crew, Mattia, Suyun, Andrey, Rob, Calley, Rosie, and Esko, what a pleasure it is to work with you. Thank you for all the laughs and all the learning. I want to specially thank Mattia, my beamtime dream team and, together with Calley, the co-masters of the plasma source ;)

I also want to thank the people at SLJUS for making the department feel like home, we forget how privileged we are to work surrounded by friends. I want to specially thank Giulio, for all the discussions, igor help, and beamtimes with the best cooking! Sanna, for being the best office mate, the ten times per year we managed to be in the office together! Yen-Po, my Hercules co-conspirator. Giuseppe, Sandra, and Lukas, and, by extension, Monica, Veronika, Valeria, and Konstantin, thank you for being much more than my friends, but my family, I can't wait for the next weekend

getaway! Finally, I want to specially thank Hanna, for being there when I most needed you and supporting me through the hardships of writing a thesis.

The department wouldn't be the same without Patrik, thank you for the humor, the *skånska* lessons, and the bureaucracy help! I also want to thank the STM crew, thanks for all the cake every Wednesday, and special thanks to Estephania, for always being available to throw a helping hand.

I also want to thank my family and friends in Barcelona. *Gràcies per seguir aprop encara que estiguem lluny. Gràcies per creure en mi i pel coratge que sempre m'heu donat. Sense saber-ho, formeu una xarxa que m'empenta a aconseguir objectius que mai m'hagués imaginat.*

And finally, I want to thank Jack, my love, my family, my best friend. Thank you for being here for me, I couldn't have done this without you.

Table of Contents

Abstract

This thesis addresses how graphene can be a valuable asset for surface science studies. Using a combination of X-ray photoelectron spectroscopy, scanning tunneling microscopy, and low-energy electron diffraction, we take advantage of graphene's sensitivity to changes in its chemical environment to obtain an atomic scale understanding of different reactions occurring above and below the film.

As a substrate, graphene provides an inert base for studying growth mechanisms. Specifically, we use it to investigate the electron-induced dissociation of borazine, a common precursor for Boron Nitride deposition. Thanks to the inert character of graphene, we can discern the dissociation due to the interaction with the electron beam from any surface-induced dissociation processes. Moreover, graphene can be used as an adsorption template for studying reactions between adsorbates and gas phase molecules. Using hydrogen adsorbates, we analyze the stability of different H-structures under mbar pressures of oxygen. We show that graphene acts as a catalyst for water formation by providing the required adsorption configuration that promotes the reaction. This finding paves the way for future research using graphene as an adsorption template for fundamental catalysis studies.

Graphene can also be employed as a confining agent to study undercover reactions, a trending topic in the catalysis field due to the reported higher performance of catalysts when placed in confined environments. We use graphene to investigate copper oxidation undercover, revealing that its presence stabilizes a Cu_2O phase undercover, delaying the evolution toward complete oxidation (CuO). Graphene is also an ideal model system for studying more fundamental aspects of undercover reactions, such as the coexistence of different molecules undercover or their intercalation kinetics. Specifically, we use graphene to investigate the coexistence of hydrogen and CO with already intercalated oxygen while following the intercalation process *in situ* with ambient pressure XPS.

Altogether this thesis provides several examples of how graphene can be integrated into surface science studies and paves the way for its implementation in the surface science field.

Popular abstract

When one thinks about reactions, one maybe remembers the experiments performed in chemistry labs in high school or thinks about the reactions involved when cooking a meal: we mix some ingredients, something happens and we get a result (let's be honest, we all hope it's a cake!). However, to make better desserts or more useful reactions in the lab, it is necessary to understand what happens *during* the reaction, and, ideally, with a LOT of detail. Following with the cake example, we want to know what each molecule of gluten is doing in an oven while the cake is baking.

The problem is that these reactions can be very complex, there are multiple ingredients all doing things at the same time and at different places, and all can happen very fast! A way that scientists have found to tackle this is what we call "the surface science approach". The idea is simple: break down the system in small simple pieces until we can actually follow a specific part of the reaction. We do that by simplifying either the number of ingredients, their conditions, or both. It would be to study, for example, what happens to flour when we heat it up. And, the next day, study what happen to eggs where they get whisked. And so on. Understanding reactions in terms of these simple steps allows us to imagine what could happen in the oven when we put everything together.

But of course things are not that simple, and we know that reactions can behave differently when we increase their complexity. Because of that, the surface science field have been developing new techniques that allow us to investigate systems in more complex conditions. This is not an easy task. For example, looking at the chemical composition of the surface of a material *in air* is a much more complex endeavor that one could expect. For once, atoms and molecules stick on a surface when is exposed to air, making it very hard to distinguish what is underneath. On the other hand, the electrons that we usually use to determine the elemental composition of a material cannot travel very far in air, making them very hard to detect in those

conditions (electrons are nice and like to remember which atom they came from, so when we detect them, we know too). You can probably see now where I am going... studying reactions in realistic conditions is hard. Specially if you want to do that with atomic detail! Therefore, any additional information we can get is extremely welcome. Ideally one would like to have something like a news reporter in the middle of the reaction telling us what is *really* going on. Live. On site. Well, this thesis is centered around how we can do that.

Who is the news reporter? We find our answer in Graphene. You might have heard about this material. It is made of carbon, and what makes it unique is that it has only two dimensions. Imagine a sheet of paper made of carbon but only one atom thick (as a reference, a sheet of normal paper is about 1 million atoms thick). Graphene is used in a lot of different fields because of its exotic properties, such as its strength or its conductivity. However here we are interested in it because of its sensitivity. Because of low dimensionality, graphene's electronical properties are easily affected by anything happening around it. So much that, for example, its conductivity changes when atoms are weakly attached to it.

The work included in this thesis is centered around showing how graphene can be the ideal "news reporter" to study surface reactions. For example, I have used graphene to understand better how materials grow on top of it. Another of the projects in this work uses graphene to understand how hydrogen and oxygen react on top of it. Finally, I also show how graphene can *report* on reactions happening underneath it. I used it to follow in real time how copper oxides underneath it, or even how different molecules move in and out the space covered by graphene.

There is still a lot of work to do, other reactions to investigate and multiple systems to explore. However, with my experiments I aim to show how graphene can be an excellent news correspondent for future surface reaction studies.

Resum de divulgació científica

Si pensem en reaccions químiques, potser recordem els experiments que fèiem a l'institut, o les reaccions que tenen lloc en el menjar quan el cuinem: els ingredients es barregen, succeeix alguna cosa i obtenim un resultat (com ara un pastís!). El problema és que, per fer millors postres o reaccions químiques mes útils al laboratori, necessitem entendre el que passa durant la reacció química, i si és de manera detallada millor. Un exemple seria saber què fa cada una de les molècules de gluten mentre es cou el pastís al forn.

En aquest sentit, una de les dificultats amb què ens trobem és que aquestes reaccions són molt complexes: hi ha molts ingredients, fent diversos processos, en llocs diferents i de forma simultània. Per aquest motiu, la comunitat científica ha desenvolupat una estratègia per intentar entendre amb detall el que passa durant una reacció química anomenada "Estratègia de la ciència de superfícies". La idea és simple: descomponem el problema general en una sèrie de petits problemes que podrem entendre individualment. Seguint l'exemple del pastís, en comptes d'intentar entendre com es forma el pastís sencer, estudiem primer el que li passa a la farina quan s'escalfa; després, com es combinen la farina i la mantega, o què els hi passa als ous quan els batem. I d'aquesta manera, podem anar avançant fins que tenim prou informació per intentar reconstruir el que succeeix al llarg del procés de manera global.

Desafortunadament, les coses no són tan simples com semblen i podem afirmar que no es el mateix investigar un sistema per parts que investigar-ho tot de forma conjunta. Per aquest motiu, i amb l'objectiu de resoldre la discrepància entre estudis simples i els sistemes reals, la comunitat científica ha posat un gran esforç en desenvolupar tècniques experimentals que ens permetin estudiar reaccions complicades en directe. Malauradament, ens hem trobat amb algunes dificultats tècniques, com ara la impossibilitat de determinar els elements en la superfície d'un material exposat a l'aire: d'una banda, les molècules de l'aire cobreixen la superfície

del material en menys d'un segon d'exposició, emmascarant la part de la superfície que ens interessava. D'altra banda, els electrons que normalment utilitzem per determinar la composició d'un material no poden viatjar llargues distàncies a través de l'aire, per la qual cosa són molt difícils de detectar (els electrons recorden de quin àtom provenen, de manera que quan els detectem podem saber quins àtoms hi ha al material). Arribats aquest punt, estem arribant a la clau de volta de tot plegat: estudiar reaccions reals és una tasca difícil i encara més si ho volem fer amb precisió atòmica. En aquestes circumstàncies, qualsevol font d'informació addicional és més que benvinguda. I posats a pensar en un món ideal, ens interessaria tenir un corresponsal enmig de la reacció informant-nos en directe del que està passant. Doncs bé, precisament aquesta tesis està centrada de forma específica en aquesta qüestió.

En aquest sentit, la primera pregunta que ens hauríem de fer és qui és el corresponsal? La resposta la trobem en el grafè, del qual segurament ja n'has sentit a parlar. El grafè és un material fet de carbó amb una característica que el fa únic: té nomes dues dimensions. Imagina un full de paper fet de carbó, només amb un àtom de gruix (perquè et facis una idea, un full de paper normal té al voltant d'un milió d'àtoms de gruix). El grafé s'ha fet famós per que té unes propietats molt exòtiques, per exemple, pot conduir electricitat gairebé sense resistència. En tot cas, el que ens interessa a nosaltres d'aquest material és la seva sensibilitat. Com que només té dues dimensions, el grafé es molt sensible al que passa al seu voltant, per exemple, les seves propietats electròniques canvien només amb molècules movent-se al seu voltant!

Aquesta tesis explica com podem utilitzar la sensibilitat del grafé com a "corresponsal de notícies" per estudiar reaccions químiques en directe. En aquest sentit, hem fet servir el grafé per entendre com altres materials es formen damunt seu. En un altre dels projectes inclosos, utilitzem el grafé per estudiar com molècules d'oxigen interaccionen amb àtoms d'hidrogen a sobre el grafé. Finalment, mostrem com el grafé és el corresponsal idoni per estudiar reaccions químiques encapsulades (nano reactors químics!). En aquesta línia, hem utilitzat el grafé per entendre millor com s'oxida el coure a sota seu, o per seguir en directe com diferents molècules entren i surten d'aquests mini reactors. En definitiva, amb els estudis presentats en aquesta tesis s'intentarà demostrar com el grafé és el corresponsal ideal per seguir en directe reaccions complexes.

List of Publications

This thesis is based on the following papers, referred in the text by their roman numerals.

I. Area-selective Electron-Beam induced deposition of a-BN_x on Graphene

V. Boix, C. Struzzi, T. Gallo, N. Johanssona, G. D'Acunto, Z. Yong, A. Zakharov, Z. Li, J. Schnadt, A. Mikkelsen, and J. Knudsen

Applied Surface Science 557, 149806 (2021)

I was the main responsible for the project, including planning and performing the experiments (STM, XPS, and LEEM), data analysis, and writing the manuscript.

II. Graphene as an adsorption template for studying double bond activation in catalysis

V. Boix, W. Xu, G. D'Acunto, J. Stubbe, T. Gallo, M. D. Strømsheim, S. Zhu, M. Scardamaglia, A. Shavorskiy, K. Reuter, M. Andersen, J. Knudsen

The Journal of Physical Chemistry C 126, 33, 14116–14124 (2022)

I was the main responsible for the planning and experimental part of the project, including performing the experiments (APXPS and STM), and the data analysis. W.X. and I contributed equally to writing the manuscript.

III. Comparative study of copper oxidation protection with graphene and hexagonal boron nitride

M. Scardamaglia, **V. Boix**, G. D'Acunto, C. Struzzi, N. Reckinger, X. Chen, A. Shivayogimath, T. Booth, and J. Knudsen

Carbon 171, 610-617 (2021)

I participated in the APXPS experiments and took part in the discussion of the manuscript.

IV. Following the kinetics of undercover catalysis with APXPS and the role of hydrogen as an intercalation promoter

V. Boix, M. Scardamaglia, T. Gallo, G. D'Acunto, M. D. Strømsheim, F. Cavalca, S. Zhu, A. Shavorskiy, J. Schnadt, J. Knudsen

ACS Catalysis 12, 9897-9907 (2022)

I was the main responsible for the data analysis and writing the manuscript. Since the project started before the start of my PhD, I was not the main responsible for planning and performing the initial experiments (inherited from T.G.). I was responsible for planning and executing later beamtimes.

V. HIPPIE: a new platform for ambient-pressure X-ray photoelectron spectroscopy at the MAX IV Laboratory

S. Zhu, M. Scardamaglia, J. Kundsen, R. Sankari, H. Tarawneh, R. Temperton, L. Pickworth, F. Cavalca, C. Wang, H. Tissot, J. Weissenrieder, B. Hagman, J. Gustafson, S. Kaya, F. Lindgren, I. Källquist, J. Maibach, M. Hahlin, **V. Boix**, T. Gallo, F. Rehman, G. d'Acunto, J. Schnadt, A. Shavorskiy

Journal of synchrotron radiation 28, 624-636 (2021)

I contributed with one of my projects performed at HIPPIE (now published as paper IV) as a case study for this paper.

Other publications in which I have participated and are related to the topic of this thesis. However, in order to limit the scope of this work, they have not been included. Nevertheless, these papers will be referenced in the thesis:

VI. Stroboscopic operando spectroscopy of the dynamics in heterogeneous catalysis by event-averaging

J. Knudsen, T. Gallo, **V. Boix**, M. D. Strømsheim, G. D'Acunto, C. Goodwin, H. Wallander, S. Zhu, M. Soldemo, P. Lömker, F. Cavalca, M. Scardamaglia, D. Degerman, A. Nilsson, P. Amann, A. Shavorskiy, J. Schnadt

Nature communications 12, 6117 (2021)

I participated in the APXPS experiments and contributed in the editing of the manuscript.

VII. Gas Pulse–X-Ray Probe Ambient Pressure Photoelectron Spectroscopy with Submillisecond Time Resolution

A. Shavorskiy, G. D'Acunto, **V. Boix**, M. Scardamaglia, S. Zhu, R. H Temperton, J. Schnadt, J. Knudsen

ACS applied materials & interfaces 13, 47629-47641 (2021)

I participated in the APXPS experiments and contributed in the editing of the manuscript.

VIII. Cluster Superlattice Membranes

T. Hartl, M. Will, D. Capeta, R. Singh, D. Scheinecker, **V. Boix**, S. Dellmann, P. Lacovig, S. Lizzit, B. V Senkovskiy, A. Gruneis, M. Kralj, J. Knudsen, J. Kotakoski, T. Michely, P. Bampoulis

ACS nano 14, 13629-13637 (2020)

I participated in the XPS experiments as expert support and contributed in the editing of the manuscript

IX. Growth, stability, and electronic decoupling of Pt clusters on h-BN/Ir (111)

M. Will, T, Hartl, **V. Boix**, P. Lacovig, S. Lizzit, J. Knudsen, T. Michely, P. Bampoulis

The Journal of Physical Chemistry C 125, 3880-3889 (2021)

I participated in the XPS experiments as expert support and contributed in the editing of the manuscript.

X. Carbon Embedding of Pt Cluster Superlattices Templated by Hexagonal Boron Nitride on Ir (111)

T. Hartl, M. Will, P. Bampoulis, D. Herrmann, P. Valerius, C. Herbig, **V. Boix**, P. Lacovig, V. Vonk, S. Chung, A. Stierle, S. Lizzit, J. Knudsen, T. Michely

The Journal of Physical Chemistry C 125, 23435-23444 (2021)

I participated in the XPS experiments as expert support and contributed in the editing of the manuscript.

XI. Segregation dynamics of a Pd-Ag surface during CO oxidation investigated by NAP-XPS

M. D Strømsheim, I-H. Svenum, M. Mahmoodinia, **V. Boix**, J. Knudsen, H. J Venvik

Catalysis Today 384, 265-273 (2022)

I participated in the APXPS experiments and contributed in the editing of the manuscript.

Publications in which I have contributed but are not included in this thesis

XII. Oxygen relocation during HfO_2 ALD on InAs

G. D'Acunto, E. Kokkonen, P. Shayesteh, **V. Boix**, F. Rehman, Z. Mosahebfard, E. Lind, J. Schnadt, R. Timm

Faraday Discussions 236, 71-85 (2022)

I contributed in the discussion of the data analysis.

List of Abbreviations

0D, 1D, 2D, 3D	Zero-, One-, Two-, and Three-dimensional
AFM	Atomic Force Microscope
CB	Conduction Band
CLS	Core-Level Shift
CVD	Chemical Vapor Deposition
DFT	Density Functional Theory
(L)DOS	(Local) Density of States
DLD	Delay Line Detector
EBID	Electron Beam Induced Deposition
FCC	Face Centered Cubic
FWHM	Full Width Half Maximum
Gr	Graphene
h-BN	hexagonal Boron Nitride
HCP	Hexagonal Close Packing
IMFP	Inelastic Mean Free Path
LEED	Low Energy Electron Diffraction
LEEM	Low Energy Electron Microscope
LINAC	Linear Accelerator
MCP	Multi-Channel Plate

MFC	Mass Flow Controller
ML / MLE	Monolayer / Monolayer Equivalent
PE	Pass Energy
(AP)PEEM	(Ambient Pressure) Photoemission Electron Microscope
SEM	Scanning Electron Microscope
(HP)STM	(High Pressure) Scanning Tunneling Microscope
STS	Scanning Tunneling Spectroscopy
TEM	Transmission Electron Microscope
TMDC	Transition Metal Dichalcogenide
TPG	Temperature Programmed Growth
UHV	Ultra-High Vacuum
VB	Valence Band
VdW	Van der Waals
(AP)XPS	(Ambient Pressure) X-Ray Photoemission Spectroscopy

1. Introduction

Detailed knowledge of surface reactions helps us understand better how materials interact with their surroundings. Almost every technological application benefits from studying the processes occurring on the surfaces of their components. From determining the stability of a material under different conditions, to designing valuable combinations of materials for electronic applications, all require understanding how the different materials interact with each other or with their environment, and those interactions occur at the surface. Altogether, the study of surfaces and surface reactions is deeply embedded in our technology.

The importance of surface studies is such that the field of surface science has expanded dramatically over the last century. The "surface science approach" was introduced by I. Langmuir in 1922,[1] who suggested using model systems (i.e., well-characterized single crystalline surfaces) in highly controlled environments (ultra-high vacuum, or "UHV") to study the elementary processes underlying chemical reactions at surfaces.

Nowadays, the same approach is used to study a variety of complex systems (heterogeneous structures, nanoparticles, alloys, etc.) in much more intricated environments (high pressures, high temperatures, under reaction conditions, in liquid environments, etc.). To do so, many new techniques have been developed together with imaginative ways to disentangle experimental data from those complex systems. In this work, I present one of these new approaches to surface science studies: Specifically, I have incorporated graphene (Gr), a two-dimensional carbon-based material, in our studies of various surface reactions. In the following chapters, I will show in detail how graphene can be a powerful tool for surface science studies, as a substrate, as a cover, and, most of all, as a chemically sensitive probe.

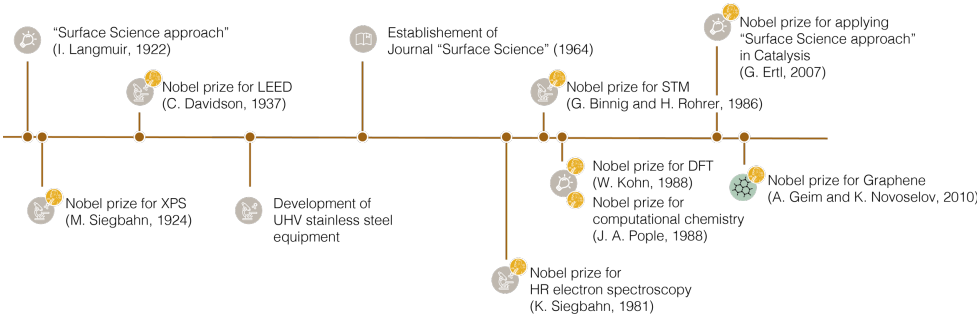

Figure 1.1: Basic timeline illustrating the early development of the surface science field. Includes related Nobel prizes, most relevant technical developments, and relevant journals.

Starting from the beginning, why would anyone want to study highly simplified surfaces under un-realistic conditions? What Langmuir's intuition suggested is that studies of reactions on well-defined surfaces would become appropriate models for more "real" surfaces under more realistic conditions.[2] However, the difficulty of building vacuum apparatus (at the time using glass enclosures) greatly limited the implementation of Langmuir's vision. It was not until the 1960's when, thanks to the development of stainless steel vacuum hardware, the surface science approach became possible.[3]

At that point, the field of surface science experienced a rapid development. Experimental methods for compositional surface analysis increased from none in the 60's to more than twenty in a period of only 10 years,[3] and continue increasing today.

The surface science approach have had such an impact on the scientific community that several Nobel prizes were awarded in relation to the development or application of surface science techniques; in 1981 it was awarded to K. Siegbahn for "his contribution to the development of high-resolution electron spectroscopy",[4] hereby making X-Ray spectroscopy (a technique his own father, M. Siegbahn, was awarded the Nobel prize for discovering in 1924)[5] suitable for surface science studies. In the following years Nobel prizes were also awarded to G. Binnig and H. Rohrer for "their design of the scanning tunneling microscope" (STM) (1986),[6] to W. Kohn for "his development of the density-functional theory" and J. A. Pople for "his development of computational methods in quantum chemistry" (1998),[7] and, more recently in 2007, to G. Ertl for "his studies of chemical processes on solid surfaces".[8]

Today, surface science can be considered an established field providing fundamental understanding to other fields such as catalysis, nanofabrication, etc.

Over the last 30 years, the development of new instrumentation has allowed the surface science community to push the limits of the surfaces and environments studied, essentially closing the so-called "material gap" and "pressure gap". The material gap refers to increasing the complexity of the surfaces studied in order to approach more realistic systems used in industrial applications, while the pressure gap refers to the complexity of the system's environment.

We find multiple examples in the literature where surface science techniques are now applied to, for example, complex 3D structures, such as nanowires or nano-devices, even during operando conditions.[9] In catalysis, the use of faceted surfaces is sometimes replacing the traditional flat single crystals,[10,11] and complex alloys (see , for example, **paper XI**),[12] or even nanoparticles,[13] can now be characterized in *in situ* reaction studies.

The experimental conditions are also becoming more complex. Initially, many of the *in situ* work focused on surfaces at steady state conditions. However, thanks to instrumental improvements, time-resolved studies in changing conditions are now possible.[14,15] We can find examples of this in material deposition studies, such as *in situ* Atomic Layer Deposition studies.[16]

All this advances have been possible by the development of techniques and methods by surface scientists, which allowed us to keep obtaining fundamental knowledge on systems of increased complexity.[17,18] Some of the advances seemingly small have had huge implications, for example the implementation of differential pumping systems and electrostatic focusing[19–21] allowed electron-based techniques (TEM, SEM, XPS) to bridge the gap between UHV to measurements up to the mbar regime. In the case of Ambient Pressure XPS (APXPS), even higher pressures have been recently achieved by implementing advances such as swift potential to maximize the number of photoemitted electrons that make it to the detector,[22] or the introduction of small reaction chambers combined with micro-perforated analyzer cones that allow high local pressures of the order of tens of bars.[23]

Not all developments have been exclusively technical, new approaches to data analysis have also allowed to access insights of surfaces under reaction conditions not accessible otherwise: For example a recent study in our group presented an averaging technique that can be used to extract information from noisy datasets (**paper VI**). Or the implementation of pulsing conditions (either by changing the gas composition or for example the temperature of the system) and synchronized measurements allow for detailed measuring at specific moments of a surface transition (see also **paper VII**).[15]

It is within this context of technical and analytical advances in the surface science field that the work included in this thesis takes place. In my case, the additional perspective into surface science studies is related to graphene.

Graphene can be defined as a two-dimensional carbon structure, the building block for other graphitic compounds such as graphite (3D), carbon nanotubes (1D) and fullerenes (0D). Graphene was theoretically predicted in the 1940s,[24] and synthetizing efforts already stared on the 1960s.[25,26] However, it wasn't until 2004 that Geim and Novoselov managed to measure its unique properties,[27] which awarded them the Nobel prize in 2010.[28] Since then, the interest in graphene has been shifting from fundamental studies of its exotic properties (high strength,[29] stiffness, and low density, combined with a very high electron mobility – 15.000 cm^2/Vs –,[30] a high thermal conductivity,[31] and high opacity,[32] to mention some) to applications is a vast number of fields. Graphene's versatility and popularity is reflected in a recent editorial of the journal *ACS Applied Nanomaterials*, which reviewed almost 200 papers related to graphene published in their journal in a span of 2 years and concluded that "*graphene based nanomaterials are pervading all domains of modern technology, from environmental remediation, sensing and catalysis, to functional materials, electronic devices, and energy-related technologies. Graphene will undoubtably be intimately linked to the technological progress of our era.*".[33]

1.1 Motivation for this work

In my case I explored how graphene can be used as a tool to enhance the possibilities of surface science studies. Graphene's implementation in surface science techniques is already a reality, an excellent example of which is the use of graphene as a membrane able to hold several orders of magnitude of pressure difference for spectroscopy studies.[34–36] In my case I made use of the strength and stability of graphene for a more fundamental approach to surface science studies: to gain understanding of different surface reactions. Moreover, I exploited the fact that graphene is highly sensitive to its chemical environment, therefore it can be used as an additional probe to monitor adsorbates or reactions happening atop or below the film.

The results presented are separated in two sections: first I address the capabilities of graphene as a substrate to study molecular decomposition by other means than surface-mediated reactions (which include the results of **paper I**), followed by the discussion of graphene's potential as an adsorption template for fundamental catalysis studies (**paper II**). The second part of this thesis continues with catalysis applications, however, this time, graphene is used as an inert cover to study confined heterogeneous reactions (**papers III, IV** and **V**).

This thesis is organized as follow: chapter 2 includes a general introduction to surfaces, adsorbates, and surface reactions, chapter 3 presents the experimental techniques used in my work, with special focus on XPS and STM, and chapter 4 presents the system employed in my studies, iridium-supported graphene. The results of my research are then presented in two separate chapters: chapter 5, and chapter 6, each of which also includes a dedicated introduction to the field, a brief discussion of the results, and an outlook. Finally, chapter 7 provides a general outlook to future research.

2. Surfaces, adsorbates, and reactions

The work included in this thesis revolves around molecular processes occurring at the interface between a solid surface and different gas environments. This chapter will give a short introduction to crystalline surfaces and their interaction with gas-phase molecules, focusing on adsorbate-substrate and adsorbate-adsorbate interactions, diffusion, and surface catalyzed reactions.

2.1 Crystals and surfaces

Crystals are solids whose atomic structure can be defined by a periodic translation of the smallest repeating atomic arrangement within the material, its unit cell. A crystal can be truncated in any arbitrary direction, however there are specific orientations that represent the flattest, lowest energy, and most fundamental planes, the so-called low index planes. The direction of the crystal truncation is defined by the Miller indices, (*hkl*), which are the values of the unit vectors that define the crystal unit cell in reciprocal space (**a***, **b***, **c***):

$$\boldsymbol{g}^*_{hkl} = h\boldsymbol{a}^* + k\boldsymbol{b}^* + l\boldsymbol{c}^* \tag{2.1}$$

As an example, the real space unit cell of a *face-centered cubic* (fcc) crystal is shown in figure 2.1a, together with the (111) low index plane in the unit cell and a top and side view of the resulting surface. Note that, for orthogonal vectors, the reciprocal unit vectors (**a***, **b***, **c***) will be parallel to the ones defining the crystal in real space (**a**, **b**, **c**), as it is the case in the fcc crystal structure represented in figure 2.1a.

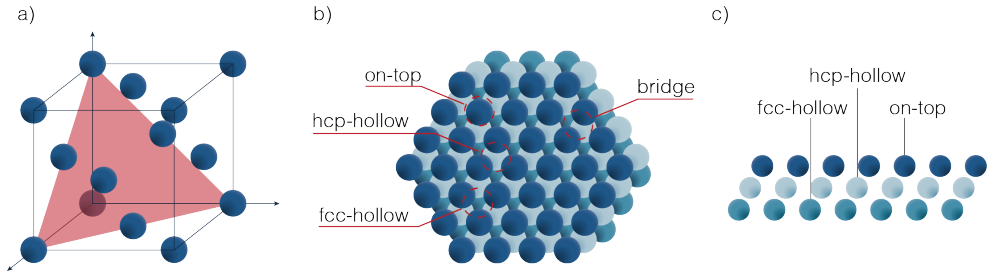

Figure 2.1 a) Unit cell of a fcc crystal with the (111) plane higlighted in red. b) Top view of the fcc crystal cut in the (111) plane. The unique geometrical sites (or high symmetry sites) are marked with red circles (on-top, hcp-hollow, fcc-hollow, and bridge). c) lateral view of the fcc crystal cut in the (111) plane showing also the high symmetry sites.

It is important realize that even though high-symmetry surfaces have a single plane of atoms which can be considered as *flat*, the surface as such is not *homogeneous*. Instead it contains several different sites that are geometrically unique. See for example how we can identify the so-called bridge, fcc-hollow, hcp-hollow, and on-top sites on the (111) surface of an fcc crystal in figure 2.1 (panels b and c).

This variation of solid surfaces is extremely relevant for surface-adsorbate interactions. From an electron point of view, the surface's atomic arrangement will be reflected as undulations in the surface electron density. These changes or *undulations* will be even more pronounced in the presence of defects such as surface steps, vacancies or impurities. The variations in electron density along a surface effectively mean that different sites will have different ability to exchange electrons with adsorbates and, hereby, form (or not) chemical bonds.

2.2 Adsorbate surface interaction

Depending on the strength of the substrate-adsorbate interaction, we can distinguish between two types of adsorption: physisorption and chemisorption. Physisorption is characterized for weaker interaction forces, such as Van der Waals, which result in small binding energies and large surface-adsorbate equilibrium distances. Because of this weak interaction, physisorbed adsorbates are not so sensitive to the surface

potential and can therefore diffuse more easily across the surface. Ordered structures are rarely formed unless the temperature is very low.

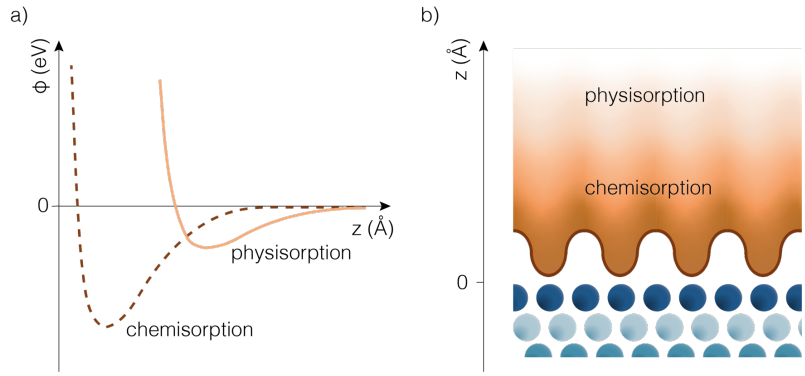

Figure 2.2 a) One-dimensional potential energy diagram comparing physisorption and chemisorption. b) Example for a surface potential an adsorbate encounters on its way to the surface and along the surface.

On the other hand, we can talk about chemisorption when there is an exchange of electrons between the surface and the adsorbate, meaning that a chemical bond is formed. Chemisorption potentials result in stronger binding energies and smaller adsorbate-equilibrium distances, meaning that the adsorbate "feels" strongly the variations of the surface's density of states i.e. its adsorption sites (schematically shown in figure 2.2b). As a result of this, the positions of adsorbed species tend to be more rigidly related to the available surface adsorption sites and commensurate structures tend to form (2D adsorbate layers with ordered structures related to the surface atomic structure). Such adsorbate overlayers are commonly described in Wood's Notation:

$$\left(\frac{a_o}{a_s} \times \frac{b_o}{b_s}\right) \mathrm{R}\gamma^\circ - \mathrm{X} \qquad (2.2)$$

Where $\mathbf{a}_s$ and $\mathbf{b}_s$ are the substrate lattice vectors and $\mathbf{a}_o$ and $\mathbf{b}_o$ are the overlayer lattice vectors, $\gamma°$ is the angle between the substrate and adsorbate structures, and X is the chemical symbol of the adsorbate species. In this thesis, this notation has been used to describe different adsorption structures on Ir(111). See an example in figure 2.3.

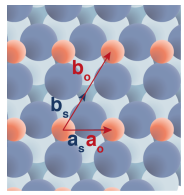

Figure 2.3 Atomic oxygen (red) adsorbed on an Ir(111) substrate (blue) forming a (2×1)-O adsorption structure.

Intuitively, one can expect that possible adsorbate structures forming on a surface will depend on the density of adsorption sites and the nature of the adsorbates. However, the most stable structures also depend heavily on the pressure and the temperature of the system, with the pressure determining the density of adsorbates on the surface, and the temperature determining their mobility (i.e. ability to rearrange to more energetically favorable adsorption structures). Because adsorbates also interact with each other (directly or by affecting the surface potential of their neighboring adsorption sites), higher densities will result on different configurations. For example, the most energetically favorable CO structure on Ir(111) is a $(\sqrt{3} \times \sqrt{3})30°$-CO configuration when exposed at low pressures,[37,38] but it evolves into a $(3\sqrt{3} \times 3\sqrt{3})30°$-CO structure at higher pressures.[38,39]

2.3 Diffusion

As mentioned above, the temperature of the system influences the mobility of adsorbates on the surface and, therefore, their residence time on the surface or their ability to organize in the most energetically favorable configurations. The process of migration of atoms or molecules on a surface is referred as *diffusion* and it depends on the ratio between the thermal energy ($k_B T$) and the energy barrier between adsorption sites (E_{act}).

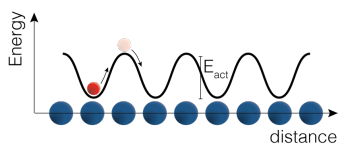

Figure 2.4 Potential energy diagram of the diffusion of an adsorbate between adsorption sites on a surface.

In the simple case of one adsorbate on a surface, illustrated in figure 2.4, the diffusion rate (D) can be described as

$$D = D_0 \, e^{-E_{act}/k_B T} \tag{2.3}$$

where D_0 is the diffusion constant, sometimes also referred as "diffusivity" (cm^2/s).[40]

If we focus on the extreme cases, $E_{act} << k_B T$ describes a situation where all molecules on a surface can move freely. This is the case of physisorbed molecules (small activation energies) or chemisorbed molecules on a system at very high temperatures. The other extreme case ($E_{act} >> k_B T$) results in immobile adsorbates, which is the case of strongly chemisorbed adsorbates or physisorbed molecules at very low temperatures. Indeed, liquid nitrogen temperatures or liquid helium temperatures are usually employed to immobilize physisorbed molecules on a surface on which they would have a residence time too small to be measured with standard surface science techniques otherwise. In recent experiments, not included in this thesis but briefly discussed in the outlook of chapter 5 (see section 5.3), we made use of low temperature to immobilize physisorbed borazine molecules on a graphene surface long enough to measure them with XPS.

2.4 Surface Reactions: Heterogeneous Catalysis

In some cases, the electronic exchange between a surface and an adsorbed molecule is so strong that it weakens the molecular bonds resulting in dissociative chemisorption. In this case, the energy barrier for dissociation can be easily overcome just by thermal or vibrational excitations. This is the simplest example of surface-mediated reactions or, in other words, heterogeneous catalysis, as interaction with the surface is what lowers the energy barrier towards molecular dissociation.

We can define a catalyst as an active chemical spectator, as it takes part in a reaction but it's not consumed. Or, as stated by W. Ostwald in his Nobel prize lecture,[41,42]

"catalysis is a chemical acceleration brought about by the presence of substances which do not appear in the reaction product"

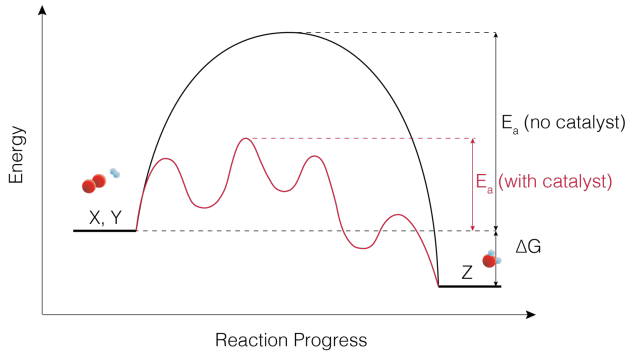

Figure 2.5 Schematic representation of the reaction paths with and without a catalyst for a generic reaction between molecules X and Y, and their reaction product Z (red and black lines, respectively).

A catalyst produces its effect by changing the height of an activation barrier, usually speeding up the reaction but not changing the energetics of reactants and products. Often catalysts are also designed to be selective, i.e. the formation of a specific reaction product out of several possibilities is the only one promoted/accelerated.

The effect of a catalyst is illustrated in figure 2.5, where the energy diagram of a simple reaction between two molecules is shown. The figure compares the mechanism and energy required for the reaction to occur in the gas phase, with the mechanism and energetics of the surface mediated reaction.

The gas phase reaction is straightforward, the molecules meet in the gas phase and combine to form the product (X + Y => Z). However, as shown in figure 2.5, the activation energy for this reaction is prohibitable large. The surface-mediated reaction, on the other hand, has lower activation barriers, but requires additional steps. From this simple scenario we can visualize how the free energy (ΔG) is the same for the gas-phase reaction and the surface-mediated route. Therefore the catalyst does not affect the equilibrium constant of the overall reaction (X + Y => Z). Instead, the catalyst works by offering an alternative reaction path with lower activation barriers, so the reaction can proceed faster.

We talk about heterogeneous catalysis when the reaction occur in systems with two or more phases are present. Liquid/solid and gas/solid interphases are of special interest because the solid surface provides a way to immobilize a catalytic substance, avoiding the catalytic site to be washed out with the products. There are several examples of

surface-mediated reactions (or heterogeneous catalysis) in this thesis; from the growth of graphene on Ir(111) (see chapter 4) and classic CO oxidation and hydrogen oxidation reactions (chapter 6), to more unusual approaches to catalytic reactions, such as the "geometrical" catalytical influence of graphene for the activation of oxygen's double bond (chapter 5).

3. Characterization Methods

To fully characterize a surface one would like to know a) what type of atoms are present and what are their concentrations, b) Where are these atoms located, and c) what are these atoms binding to?

No single technique is capable of providing detailed answers to all these questions. Therefore, usually several techniques are used in combination to provide all the relevant information. For the studies presented in this thesis, I used the combination of chemically sensitive techniques such as X-Ray Photoemission Spectroscopy (XPS) and structural characterization via microscopy and diffraction techniques such as Scanning Tunnelling Microscopy (STM) and Low Energy Electron Diffraction (LEED). In the papers included in this thesis, other techniques such as Low Energy Electron Microscopy (LEEM) and Density functional Theory (DFT) were also employed. However, this section will be limited XPS, STM and LEED as they are the main techniques I have used in my work.

All the experimental techniques mentioned above are electron-based, a common feature among many surface science techniques. Using electrons for surface characterization is advantageous because a) Electrons are easy to generate, steer and detect, and b) Electrons interact strongly with their surroundings, limiting the depth they can travel through matter, making electron-based techniques intrinsically very surface sensitive.

The distance an electron beam with energy E can travel through a medium before its intensity is reduced by a factor of 1/e is defined by what we call the inelastic mean free path (IMFP, λ). When traveling, electrons loose energy via plasmon excitations, electron hole pair formation, or vibrational excitations, each process being the predominant one depending on the energy of the electrons.

Figure 3.1 shows how the mean free path of an electron as a function of its kinetic energy follows a "universal curve", apparently independent of the material its traveling through. The reason is that, for the energies of interest here, the electrons in a solid can be approximated as a free-electron gas. As a result, the energy loss of the traveling electron will be determined by the mean electron-electron distance, which can be considered roughly equal for all materials. A more in-depth discussion of the IMFP and the efforts into its quantification can be found in Hüfner (chapter 1 and the references herein).[43]

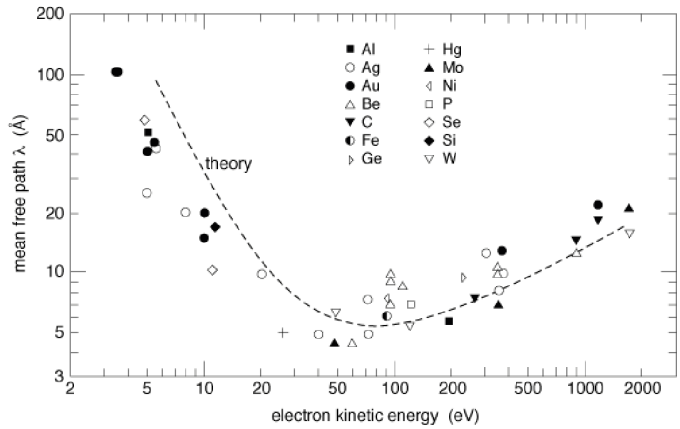

Figure 3.1 The inelastic mean free path of electrons with kinetic energies between 2 and 2000 eV. The markers represent values determined experimentally for some solids, and the dashed line the theoretical universal curve. Reproduced with permission from ref. 44. Copyright © 2006 GlobalSino.

However, the use of electrons for surface characterization also poses some limitations. Due to their short mean free path, only electrons from the upmost atomic layers will escape the material. Moreover, the ones that escape must then travel relatively long distances to the detector. Here the short mean free path of electrons becomes a problem. As a reference value, in a pressure of 1 mbar, the electron mean free path will be of the order of only 1 mm[a]. Therefore, in order to maximize the number of

[a] The electron mean-free path in a gas atmosphere can be obtained from $\lambda_e = k_B \cdot T/P \cdot \sigma_e$, where σ_e is the electron–molecule scattering cross-section.[20]

electrons reaching the detector, electron-based techniques often shorten the traveling distance, or they are used in vacuum conditions.

The need for vacuum conditions is also relevant so the surface of the material of interest remains clean of adsorbates. This requires the use of ultra-high vacuum (UHV) conditions (between 10^{-8} and 10^{-10} mbar).[45] Such extreme consideration can be illustrated with a simple example: if we consider a gas phase molecule with a sticking coefficient of 1 (i.e. every molecule impinging on the surface will stick there), at a pressure of 10^{-6} mbar (normal vacuum conditions), it would take only few seconds for the surface to be fully covered of adsorbates. This time increases to around 1 hour when the pressure decreases to 10^{-9} mbar. Therefore, in order to characterize clean surfaces, UHV pressures are usually required.

All experimental work included in this thesis was carried out in vacuum or ultra-high vacuum conditions, with the notable exception of ambient pressure XPS (AP-XPS) experiments, which will be discussed in more detail at the end of section 3.1.

3.1 X-Ray Photoemission Spectroscopy

X-Ray photoemission Spectroscopy can be considered one of the basic working horses within the surface science field, because of its versatility for surface analysis.

Basic operational principles

XPS is based on the photoelectric effect: where photons can induce electron emission from a solid as long as the photon energy ($h\nu$) is larger than the work function of the material. The *work function* (Φ), illustrated in the energy diagram of figure 3.2, is defined as the minimum energy required to remove an electron from the highest occupied level in the solid to the *vacuum level*. When the incident photon beam is energetic enough, it can also induce the photoemission of more strongly bounded electrons: i.e. inner valence electrons or core electrons. In my work, I used core-level spectroscopy (**papers I-XI**) and auger spectroscopy (**paper III**) extensively.

The core-level photoemission process is illustrated in figure 3.2, where the XP spectrum of iridium is correlated to the photoemission from different core levels of the material. Referring to the photoelectron emission from the Ir 4d level illustrated in figure 3.2, energy conservation gives a direct relation between the kinetic energy of the emitted electron leaving the sample (E_K), the binding energy of the core level (E_B) (measured with respect to the highest occupied level of the solid), the work function of the material (Φ), and the energy of the incident photon beam ($h\nu$):

$$h\nu = E_K + E_B + \Phi \;\rightarrow\; E_B = h\nu - (E_K + \Phi) \tag{3.1}$$

While expression 3.1 helps understand the photoemission process, it does not reflect the values that we experimentally measure with XPS. This is because expression 3.1 does not consider the influence of the electron analyzer on the measured kinetic energy of the photoemitted electron.

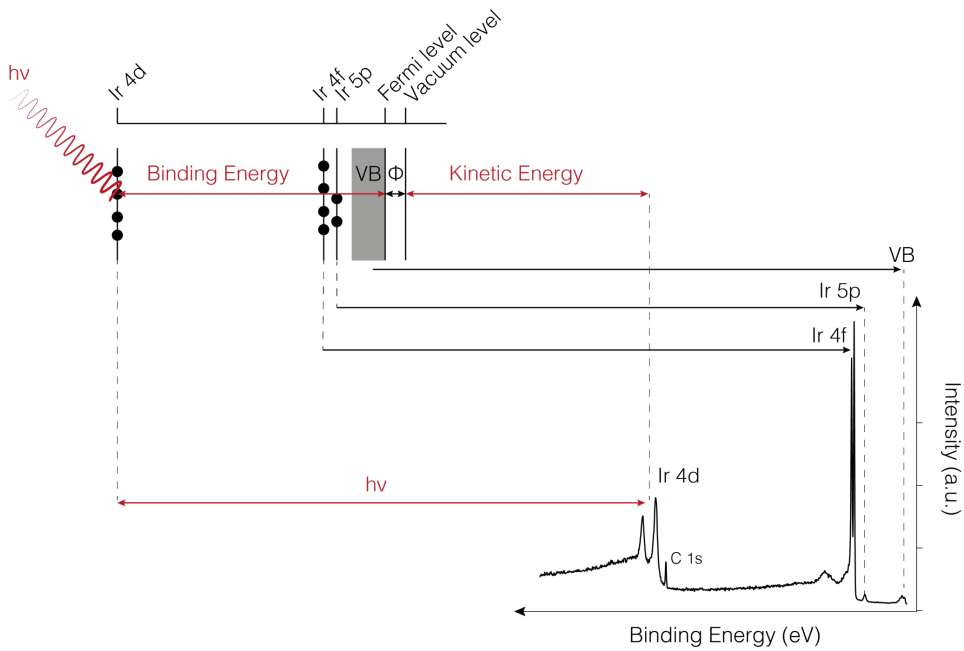

Figure 3.2 The energetics of an x-ray photoemission spectrum. Features from an iridium spectrum (right) are correlated to the different energy levels of the material (left). Note that only the levels distinguishable in the spectrum have been included in the sketch of the electronic configuration. The relationship between the kinetic energy and the binding energy of a photoemitted electron is illustrated for the Ir 4d level.

In reality, the sample and the electron analyzer are in electrical contact, therefore, the *measured* kinetic energy (E_K') is relative to the work function of the analyzer (Φ'), not of the sample.

$$E_B = h\nu - (E'_K + \Phi') \tag{3.2}$$

Core electrons do not actively participate in chemical bonding, therefore, their spectral signature act as a fingerprint of the elements present on the surface. For example, in the spectrum in Figure 3.2, measured on a graphene-covered iridium substrate, we can identify the core levels corresponding to iridium and carbon (see C 1s peak near the Ir 4d doublet).

In XPS measurements we can also observe Auger transitions. The two-step process for the generation of an Auger photoelectron is schematically shown in Figure 3.3 below. First, the direct photoemission of a core electron leaves a core whole, which is then filled by a higher lying electron (core or valence) in a *radiationless* transition. The excess energy is then released by the ejection of a second electron, the Auger electron. From figure 3.3 it becomes apparent that Auger electrons will have a fixed kinetic energy, independent of the photon energy used to create the initial core hole.

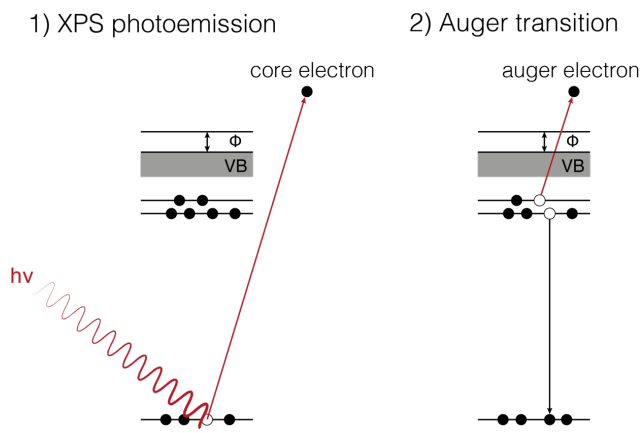

Figure 3.3 Schematic representation of the two step process for the generation of an auger electron: 1) ionization via, in this case, X-Ray photoemission and 2) auger transition between core levels.

Like core-level spectroscopy, Auger spectroscopy can be used for qualitative elemental analysis of a surface. However, because auger electrons are usually generated at higher levels (i.e. much closer to electrons involved in bonding to other atoms), they can be more sensitive to changes in the chemical environment compared to the core-level electrons. This is the case of the LMM[b] auger of copper, which is commonly used to follow the surface oxidation process, instead of other core-levels (see for example **paper II** in this work).

XPS analysis

Peak position

To extract more details from an XP spectrum besides the elemental configuration of the surface we need to first understand better the concept of the binding energy (E_B). We can define the binding energy of a photoelectron to be equal to the difference between the initial and final states of the atom (before and after photoemission):

$$E_B = E_f - E_i = E(n-1) - E(n) \tag{3.3}$$

Where *E(n-1)* and *E(n)* are the energy of the atom with *n-1* and *n* electrons, respectively. From equation 3.3, one can intuitively see that anything that affects the energy of the system before or after the photoemission process, will influence the binding energy of the photoemitted electron. Everything that affect the system before and after photoemission (E(n) and E(n-1)) can be referred as *initial state effects* and *final state effects,* respectively.

[b] Auger transitions are labelled using X-Ray notation of the levels involved. In the Cu LMM transition the first photoemitted electron originates in the 2nd electronic shell (L), which is then filled by an electron from the 3rd shell (M), and the auger emitted electron also originates from the 3rd shell (M). Note that the subshells involved (s, p, d, …) are not specified in this case, as multiple transitions are included in the LMM signal.

Alternatively, if we consider that the energy and spatial distribution of the remaining electrons after photoemission is *exactly the same* as in the initial state[c], the binding energy can be considered equal to the negative orbital energy of the emitted electron, ε.

$$E_B{}^{Koop} = -\varepsilon \tag{3.4}$$

This is the so-called *Koopmans' approximation*, and is one of the simplest approaches for calculating the binding energy of a photoemitted electron. We can also define initial and final states effects using Koopmans' definition of binding energy, where *initial state effects* are any phenomena that influence the epsilon in equation 3.4, and everything else being *final state effects*.

Within Koopmans framework, a straightforward example of initial state effects are the chemical shifts or core-level shifts (CLS). The CLS reflect the differences in the electronic configuration of an atom due to their specific chemical bonding.

To visualize better how changes in the bonding configuration affect the binding energy of a core electron, we can focus on the case of graphene. Graphene core levels are especially sensitive to doping effects due to the small density of states (DOS) around graphene's charge neutrality point. Very small charge transfers (due to adsorption, intercalation, etc.) will have a pronounced effect in the DOS, as illustrated in figure 3.4a. Here we introduce yet another approximation, the *rigid band model*, which assumes that the binding energy of the core levels is not influenced by the changes in the valence band (VB).

[c] This approximation is usually referred as *frozen orbital approximation.*

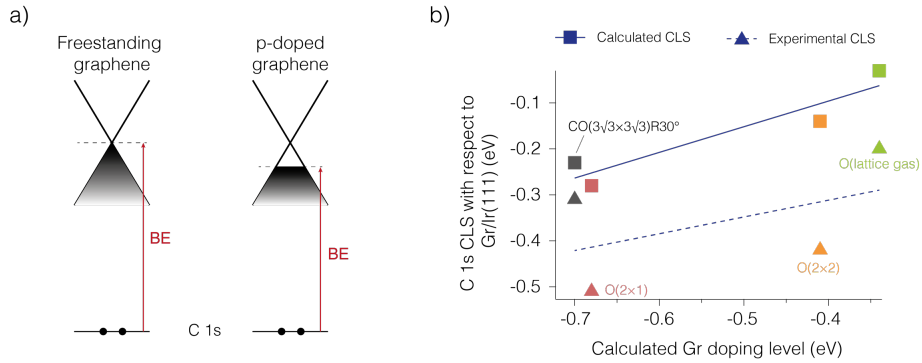

Figure 3.4 a) Schematic representation of the CLS of graphene due to doping as per the rigid model. b) C 1s core level shifts measured on graphene as a function of the graphene doping level (due to intercalation). Comparison between values calculated with the rigid band model reported in ref. 38, and experimental values (**Paper IV**). The plot highlights the sensitivity of graphene, as some the CLS included are due to the intercalation of the same element (oxygen) just with different intercalation structures.

Based on the rigid band model we can predict that the E_B of a core-level (C 1s of graphene in this case) will become smaller for a depleted VB (p-doped) and larger for a n-doped material. This general rule holds in the case of graphene, however, as discussed by Schröder *et al.* in ref. 46, the quantity of the CLS are usually smaller than the VB shift. This is illustrated in the comparison included in figure 3.4b. The discrepancy observed is due to additional screening effects not included in the rigid band model, and final state effects that will be discussed now.

In reality, the binding energy of a core electron is never equal to its original orbital energy (before photoemission), and we must consider effects not included in Koopmans' approximation, the *final state effect*s. They influence the binding energy of the main photoemission signal and generate additional features in the XP spectra, known as *satellite features.*

For example, *after* photoemission the remaining electrons of the atom relax to a different configuration, so the presence of the core hole influences the final state of the emitted photoelectron. Figure 3.5 illustrates other examples of characteristic satellite features often observed in the XPS data included in this thesis: a) the multiplet splitting in the O 1s spectra of an oxygen molecule (in the gas phase), and b) a shake-up feature at the high binding energy side of the intense Ir 4f doublet.

This multiplet splitting results from spin-spin interactions when un-paired electrons are present in the outer shells of the atom/molecule. Molecular oxygen, in this case, has a total valence electron spin of S = 1. After photoionization of the 1s shell, the photo-hole's spin (s = 1/2) can couple to the valence band spin and produce two final states whose energy depend on whether the spins are aligned parallel or anti-parallel to one another (J = 1/2 or 3/2), resulting in the split of the direct photoemission peak visible in Figure 3.5a. The intensity of each peak reflects the 2J+1 degeneracy of the total angular momentum of the states.

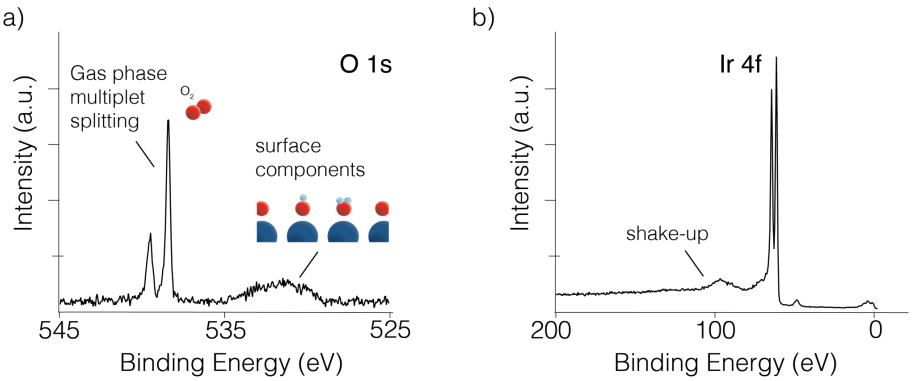

Figure 3.5 a) O 1s spectrum measured on an Ir(111) crystal at 1 mbar O_2 pressure. The multiplet splitting of the gas phase componets is visible at the high binding energy side of the spectrum. b) Survey spectrum measured on a clean Ir(111) crystal showing shake-up at the high binding energy side of the Ir 4f doublet.

Shake-up features, such as the one in figure 3.5b, occur when the photoemitted electrons excite a valence electron to a previously un-occupied state. In a very simplified picture, we can understand that the photoelectrons must give up some of their kinetic energy in order to excite the shake-up transition, therefore shake-up features are always at the high binding energy (or low kinetic energy) side of the main photoemission peak.

Spectral Background

Similar to the shake-up features, all photoemitted electrons can also lose energy while escaping from the material due to inelastic scattering interactions. Unlike the specific feature of a shake-up, which involves a specific transition in the valence

band/conduction band of the material, this energy loss involves multiple possible excitations, resulting in the characteristic, broad, staircase-like background observed in XPS spectra. Figure 3.6 compares the XP spectrum of Gr/Ir(111), with a color representation of the origin of each background step.

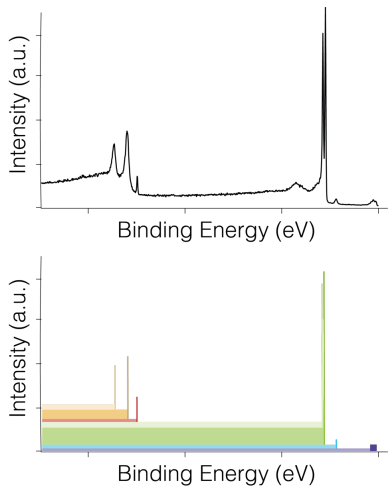

Figure 3.6 Schematic representation of the origin of the background (bottom) of an XP spectra of graphene-covered Ir(111)(top). Adapted with permission from ref. 16.

This characteristic background shape can be modeled by a Shirley function.[47] However, sometimes, the Shirley background, although phenomenological in nature, does not apply. This is the case of components located on the tail of other (more intense) core-levels, or when detector sensitivity changes affect the intensity of the spectra (when measuring in snapshot mode, see page 32). In these instances a polynomial background can be a more accurate fit.

Overall, there is no standard way to model an XPS background, and it is usually left at the scientist discretion. However, as a rule of thumb, one must prioritize being consistent, i.e. use the same background function when comparing different measurements of a specific core level.

Lineshapes

The intrinsic width of an x-ray photoemission peak, Γ, is related to the core-hole lifetime, τ, via the Heisenberg uncertainty relation as follows:

$$\Gamma = h/\tau \tag{3.5}$$

Where h is Planck´s constant. The lifetime generally decreases (and the intrinsic width increases) the deeper the core-hole, as there are more electrons available in higher levels to fill it, thus lowering the lifetime. The intrinsic width of an XPS peak is homogeneous (i.e. symmetric) and it can be described by a Lorentzian line shape. In reality however, XP spectra are often asymmetric, specially metallic peaks. For highly asymmetric peaks, an intrinsic asymmetric function as the Doniach-Šunjić lineshape[48] can be employed instead of a Lorentzian function.

Besides that, XPS peaks are broadened by other effects, such as un-resolved components, broadening due to the energy distribution of the incident photon beam, or the limited energy resolution of the detector. This additional broadening is described by a Gaussian line shape.

To take all these effects in consideration, XP peaks are thus fitted by the convolution of a Gaussian with a Lorentzian or the convolution of a Gaussian with a Doniach-Šunjić function. The Gaussian and Lorentzian convolution is usually approximated by a Pseudo *Voigt* function (see for example ref. 49), due to the high computation cost of doing the convolution numerically. Each fit will describe the photoemission peak using the following parameters: peak position (i.e. binding energy), intensity, Lorentzian full width half maximum (LFWHM), Gaussian FWHM, and, in some cases, a so-called asymmetry parameter.

Note that, in reality, the Lorentzian contribution of the fit is meaningless when measuring on solids. This is because of un-resolved small chemical shifts originating from the vibrational components of all kinds of different chemical environments on the material. This means that the *intrinsic* width of the measured peak can rarely be determined. In most fits of spectra originating from solids, the Lorentzian contribution just gives a better result, but does not correspond to any physical quantity.

Quantification of XPS signal: coverage determination

XP spectra can also be used to quantify the elemental configuration of a surface as the intensity of the photoemission peak depends, among other factors, on the concentration of the photoemitting element on the surface. In more detail, the intensity of a peak is a function of the number of photoemitting species in the volume probed by the beam (can be expressed as coverage in monolayers equivalent (MLE), Θ), the probability of photoemission (i.e. cross section, σ), the flux of the incident photon beam (F), the escape depth of the photoemitted electrons (λ, which includes the IMPF and elastic scattering effects), and, finally, an umbrella term that describes the instrumental response (i.e. the efficiency of the detector for detecting electrons with a specific kinetic energy, T):

$$I = \Theta \cdot \sigma \cdot F \cdot \lambda \cdot T \tag{3.6}$$

While all these terms can be calculated (cross-section[50] and the escape depth[51,52]) or determined experimentally (Intensity, Flux, and instrumental response), it can be an arduous and time consuming task. Instead, one can quickly obtain a rough estimation of the coverage by comparing intensities of a known and unknown surface.

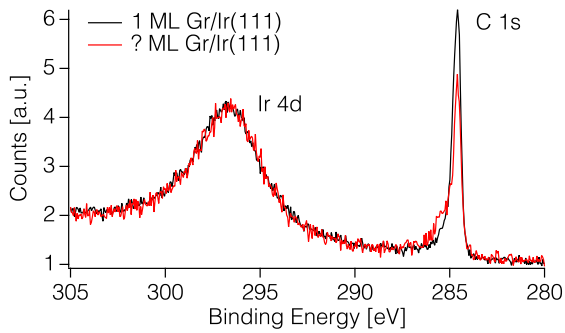

Figure 3.7 XP spectra of C 1s and Ir $4d_{5/2}$ measured at the same incident photon energy (800 eV) on a known sample (1 ML Gr/Ir(111)) and an unknown sample. Both signals are normalised to the intensity of the Ir $4d_{5/2}$ component.

I routinely used this method to, for example, determine the coverage of graphene on an iridium substrate. As shown in figure 3.7, one can compare the intensity of C 1s

measured on a known surface (a closed 1 ML graphene on Ir(111)[d]), with the intensity of C 1s measured on the surface of interest (in this case, graphene flakes not fully covering the surface). To account for changes in the incoming photon flux (F), we normalize the signal to the intensity of the core-level from an element that will not change during the experiment. In the case illustrated in figure 3.7, the C 1s was measured together with the Ir 4d core-level, and its area was normalized to the Ir $4d_{5/2}$ component[e]. By comparing the normalized intensities, one obtains the coverage in ML of the graphene flakes (~0.8 ML in figure 3.7).

Experimental setup

Light sources

Nowadays, the most common sources of x-rays are *synchrotron light sources* and *x-ray tubes*. The way each source generates x-rays is quite different: X-ray tubes use the radiation resulting from the interaction of an electron beam with a metal target. The impinging electrons create electron vacancies in the target material. X-rays with discrete energies are then emitted when those vacancies are filled with electrons from outer shells. Synchrotron light sources, on the other hand, make use of the *bremsstrahlung radiation* that is emitted by electrons when they are de-accelerated[f]. This approach offers several advantages. First of all, one can tune the electron trajectory and hereby, in principle, all photon energies in the x-ray spectrum can be generated at synchrotrons. Modern synchrotron sources are also much more *brilliant*[g], around ten orders of magnitude higher than a standard x-ray tube.

---

[d] The competition of the graphene film can be checked by exposing the Gr/Ir(111) to CO. As CO will adsorb only on bare iridium patches, the lack of CO signal in the C 1s spectra confirms the full coverage.

[e] Because the graphene will be maximum one atomic layer covering the whole surface, we neglect any attenuation effects on the iridium signal due to the presence of the graphene, or any photoelectron diffraction effects.

[f] Note that bremsstrahlung radiation is also generated in x-ray tubes as a result of the de-acceleration of the impinging electrons once they hit the target material.

[g] Brilliance is defined as the number of photons per unit of time, area, angle, and 0.1% of the energy bandwidth.

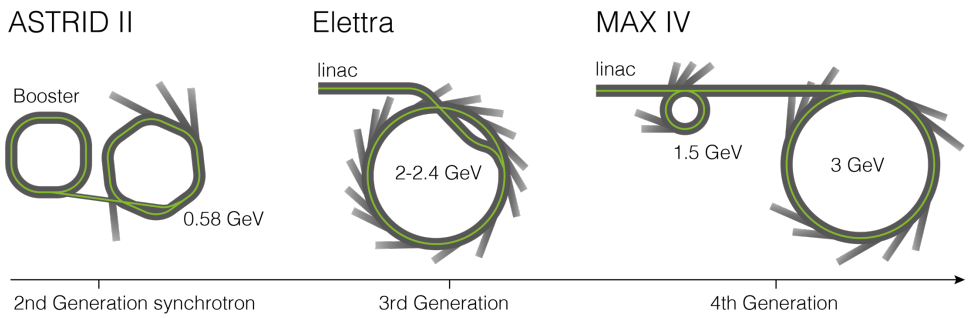

Figure 3.8 Schematic representation of the synchrotron sources used in this thesis work. Drawings not to scale.

Higher brilliance and energy tunability are crucial requirements for the work included in this thesis: Adjusting the photon energy allows us to maximize the surface sensitivity and/or the cross section of a specific element. Moreover, a more brilliant x-ray beam generates a stronger photoemission signal, increasing the feasibility of spectroscopy measurements under high pressure conditions.

All the XPS studies discussed in this thesis have been done using synchrotron light at three different light sources: The MAX IV laboratory in Sweden,[53] Elettra sincrotrone in Italy,[54] and ASTRID II synchrotron in Denmark.[55] While each source belongs to a different generation of synchrotron facilities, they all follow similar working principles:

1) electrons are accelerated to the desired energy, either by a booster electron ring (ASTRID II) or by a linear accelerator or LINAC (MAX IV, and Elettra).

2) the electrons are injected in the storage ring, where they travel close to the speed of light. In the storage ring, the electron trajectory is controlled and stabilized by a combination of magnetic devices. This is illustrated by a section of the MAX IV storage ring displayed in figure 3.9. Already at this stage, bremsstrahlung radiation is emitted at the *dipoles* or *bending magnets*, where the electrons are forced to turn to follow the trajectory of the storage ring. Indeed, this is how synchrotron radiation was first observed in early accelerators used for nuclear research.[56] This radiation, which is a continuous

and broad spectra over several eV (see figure 3.10), is used in some beamlines at Astrid II and Elettra as the source of light[h].

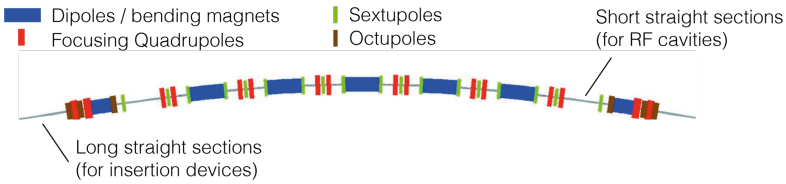

Figure 3.9 Schematic representation of the magnets conforming one of the sections (achromat) of the MAX IV 3 GeV storage ring. Adapted from ref. 53.

3) Alternatively, x-rays can be generated in insertion devices, such as undulators or wigglers. Both devices consist in a carefully arranged array of magnets with alternating polarity that make the electrons oscillate in a sinusoidal path, as illustrated in figure 3.10. Due to the high speed of the electrons and the consequential relativistic effects, the bremsstrahlung radiation is emitted as a narrow cone in the forward direction at each turn of the electron beam. The energy of the emitted radiation can be tuned by adjusting the separation between the magnetic structures, which modifies electron's trajectory. As sketched in figure 3.10, the spectrum emitted by undulators is not continuous, instead it consists of narrow and intense emission peaks.

4) to compensate for the energy loss due to radiation (while traveling in the storage ring and in the insertion devices), radio frequency cavities are placed along the ring to maintain the electrons' original energy.

[h] The radiation originating from bending magnets can be advantageous for experimental techniques that, for example, require a continuous change of photon energy for their measurements (such as X-ray absorption spectroscopy).

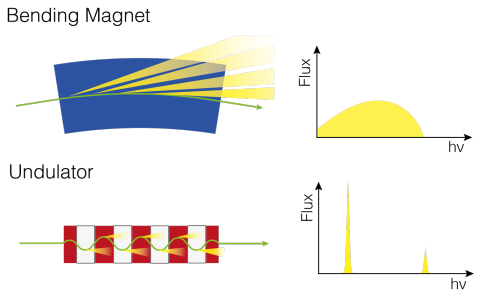

Figure 3.10 Schematic representation of the radiation emitted by the electron beam in a bending magnet (top) compared with the one emitted in an undulator (bottom).

Anatomy of a beamline

All beamlines I have used can be described with three different parts: 1) the optics, 2) analysis chamber, and 3) preparation chamber. The following description is loosely based on the HIPPIE beamline, but applies to all the beamlines I used.

The optics hutch is placed outside the storage ring, immediately after the insertion device that generates the x-ray beam. There, the x-rays are collimated, further monochromated, and focused by a set of specialized mirrors. The elements in the optics hutch basically define what portion of the light from the undulator is taken into the rest of the beamline. All elements on the x-ray path are kept in UHV conditions to avoid contamination of the mirrors[i].

All analysis chambers contain a manipulator for sample positioning (usually equipped with thermocouples to monitor the sample temperature and a heating setup such as a laser or an e-beam heater) and an electron analyzer.

The hemispherical electron analyzer is used to measure the number of photoemitted electrons as a functions of their kinetic energy and the emission angle ($N(E_k,\theta)$). It consists of two electrically isolated concentric hemispheres to which a potential difference is applied.

[i] A common problem of beamlines is the accumulation of carbon on the mirrors surface, which adsorbs x-rays at the carbon K-edge (around 290 eV) causing less flux at those energies. This is usually referred as "the carbon dip".

As illustrated in figure 3.11, the electrostatic field separates the electrons entering the space between the hemispheres and allows only the electrons with a specific kinetic energy (the "pass energy" or PE, green line in figure 3.11) to pass through to the detector. In the case of HIPPIE, the detector consists in a multi-channel plate (MCP) that acts like a spatially-resolved electron multiplier, coupled to a phosphorous screen and a CCD camera. Other beamlines, such as SuperESCA at Elettra, are equipped with delay line detectors (DLD).

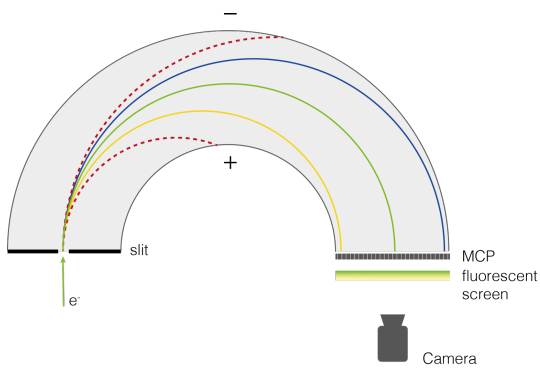

Figure 3.11 Schematic representation of an electron energy analyser (EEA) illustrating the energy separation of the photoelectrons.

For a specific pass energy, electrons with a kinetic energy E_k = PE ± ΔE_k will be detected (yellow and blue lines in figure 3.11). This helps us illustrate how much the pass energy affect the resolution of a measurement: the higher the pass energy, the higher the energy spread (i.e. the range in E_k measured by the detector), but the lower the resolution (i.e. the less channels per eV).

We can measure XP spectra in two different modes:

1) The *scanning* or *Swept* mode uses a negative electrode at the entrance of the analyzer that slows down the electrons to the desired PE. By changing the relative voltage of this retarding element, we can scan the kinetic energy scale to produce a spectrum in the desired region. The scanning of the retarding voltage is done so that each kinetic energy is measured by all the detector channels, thus averaging out the non-uniform detector sensitivity. This measuring mode allows for high resolution spectra.

2) Alternatively, one can measure in *Snapshot* or *fixed* mode. In this case, the retarding voltage is fixed so a specific kinetic energy range is measured (from PE - ΔE_k to PE + ΔE_k) This mode allows for fast measuring over a specific region of the spectrum, only limited by the frame rate of the camera and the processing time of the acquisition software. However, this mode also has its limitations. On one hand, it is much more sensitive to the non-uniformity of the detector, affecting the apparent intensity of components. On the other hand, fast measurement also implies short acquisition times. Photoemission signals with low intensities can be hard to measure in snapshot mode. This can be addressed by increasing the intensity of the signal, either by increasing the pass energy, opening the analyzer slit, or increasing the photon flux onto the sample. However, all these approaches result in a reduction of the resolution of the spectra and, in the latter case, can also increase the probability of beam induced damage. At the end, one needs to find a compromise for each measurement, maximizing the resolution or the measuring frequency depending on the goal of the experiment.

Finally, most beamlines will have a preparation chamber with in-vacuum connection to the analysis chamber. The preparation chambers on beamlines are highly tunable to adapt to the needs of a variety of users, however, they usually provide standard surface science equipment. For example, most setups include e-beam and/or resistive sample heating, a sputtering gun, leak valves to dose the required gases, and standard surface characterization tools such as LEED.

Ambient Pressure XPS

Ambient pressure XPS beamlines can be described by the same elements introduced above but with a few additional considerations regarding the electron analyzer and the sample environment.

First of all, hemispherical electron analyzers cannot operate in ambient pressure conditions. In the 1970s the group of Kai Siegbahn in Uppsala University developed the first APXPS analyzer by including a differential pumping system before the hemispherical analyzer combined with a small aperture nozzle positioned very close to the sample (typically within a millimeter), so the photoemitted electrons travel the

shortest possible distances through the gas.[57,58] This clever design, makes it possible to measure in near ambient pressure conditions while keeping the analyzer in vacuum. Since then, the design of APXPS analyzers has been improved by including additional elements. For example, modern analyzers include differentially pumped electrostatic lenses, which improve the electron transmission inside the analyzer.[19] The HIPP-3 analyzer[59] used at HIPPE beamline, also includes a so called *swift* potential at the entrance of the analyzer which increases the kinetic energy of the photoemitted electrons, reducing their cross section while traveling through the ambient pressure conditions from the sample to the analyzer.[22]

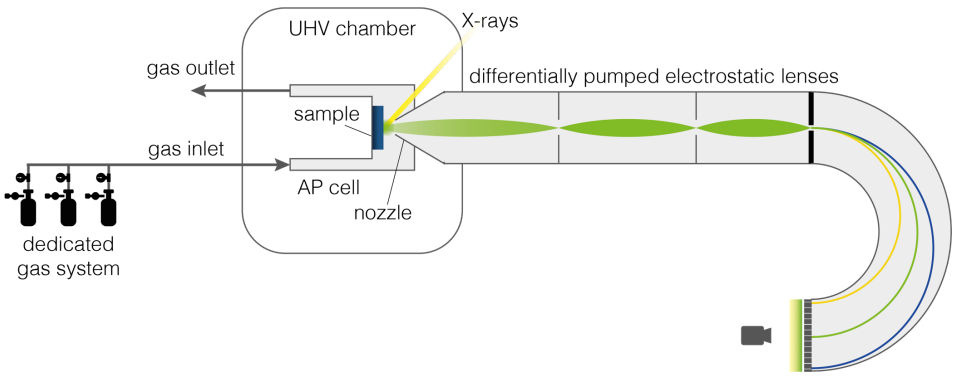

Figure 3.12 Schematic representation of an APXPS analysis chamber based on the setup of HIPPIE beamline. Adapted from ref. 60.

The sample environment on APXPS beamlines is also adapted. A simple solution is to install an APXPS analyzer to an XPS chamber and perform ambient pressure experiments. The HIPPIE beamline uses another approach (so-called "Lund" or in-cell approach, illustrated in figure 3.12), which consist of a small reaction cell inside the main vacuum system that can be attached to the analyzer for APXPS measurements.[60,61]

As shown schematically in figure 3.12, the reaction cell at HIPPIE also includes a dedicated gas delivery system. This system consists of multiple gas lines, each one equipped with individual mass flow controllers (MFCs), coupled to the inlet line to the reaction cell. This unique gas setup, coupled with the small reaction volume of the cell, allows very fast switching between gas mixtures (of the order of seconds), as

demonstrated in recent publications (see **paper V**). Moreover, the work included in **papers IV, VI**, and **VII** was only possible thanks to this unique feature.

3.2 Scanning tunnelling Microscopy

STM is also considered a standard tool in surface science, the strength of which is its capability to provide real space images of surfaces with atomic resolution. This poses a great advantage over other standard surface science tools, which provide averaged information (see XPS and LEED in sections 3.1 and 3.3, for example).

Basic operational principles

STM relies on the phenomenon of electron tunneling, meaning the ability of electrons to penetrate a potential barrier even though their kinetic energy is lower than the height of the barrier. In this specific case, it means the ability of electrons to propagate from a sharp metallic tip to a conductive sample (or vice versa) through a vacuum barrier.

Figure 3.13 illustrates the energy level diagram for the tunneling process in an STM setup. In panel a, a schematic representation of the energy diagram of a tip and a sample is shown. Because they are physically separated, the energy levels are aligned to the vacuum level (E_{vac}) and no current flows through the system. When brought close together (i.e. within a few nanometers, panel b), the energy levels of the tip and the sample align to the fermi level. Due to the small separation, the barrier between the tip and the sample is now finite, meaning that electrons can tunnel from the sample to the tip and vice-versa. To generate a net current, an additional bias voltage (V_{bias}) is applied to the sample. This bias results in the further shifting of the sample's electronic energy levels, so that electrons can tunnel from filled to empty states. This results in a small, yet measurable, tunnelling current, I_t.

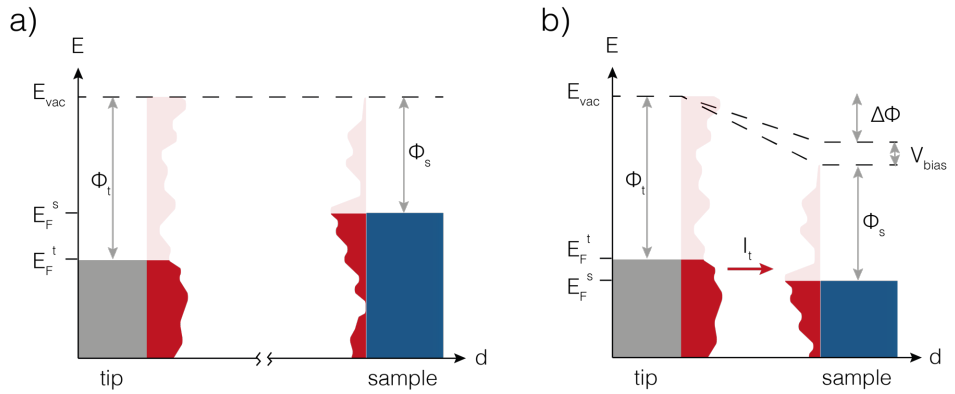

Figure 3.13 STM energy diagram (schematic representation). A) tip and surface not in contact. B) tip and surface in contact (including an additional bias applied, V_{bias}).

According to the Tersoff and Hamman approximation,[62] the value of the tunneling current will be proportional to the bias voltage (V_{bias}), and the energy-integrated local density of states (LDOS) projected to the position of the tip above the surface (r_0):

$$I_t \propto V_{bias} \cdot LDOS\,(E_F, r_0) \tag{3.6}$$

Because of the confinement of the electron densities around each atomic nuclei, STM can achieve atomic resolution. The tunneling current will also strongly depend on the separation distance between the tip and the sample. To a good approximation, for sample-tip separation change of 1 Å, the tunneling current will vary an order of magnitude, giving STM its extreme height resolution.

Experimental setup

Figure 3.14 illustrates schematically the components of an STM. An atomically sharp tip (usually made of Tungsten or of a Pt/Ir allow) is mounted in the STM head on a piezoelectric tripod. Tips are usually manufactured by electrochemical etching. They can also be sharpened while scanning, by controllably crashing them onto a surface or a step edge, or by applying voltage pulses.

The piezoelectric tripod controls the movement of the tip along the surface. Piezoelectric materials expand/contract very precisely with an applied current (around

1 Å/mV),[40] allowing a very accurate positioning of the tip. However, piezoelectric rods have several limitations such as non-linearity at high voltages (resulting in the curved appearance of straight features), the slow response upon pronounced voltage changes (usually referred as *creep*, very pronounced at the edges of large STM images or after substantial tip repositioning on the surface), or thermal variations leading to changes on the scan area[j].

There are two modes of scanning a surface, constant current mode and constant height mode. In the constant current mode (the one I used in my work), the tip is scanned across the x-y plane of the surface while the tunneling current (I_t) is maintained constant. At each step, a feedback unit (see figure 3.14) monitors and corrects the tip-sample distance (z) in order to maintain the tunneling current value. The resulting image is a 2D plot of the tip-sample distance, z, as a function of the surface position, which *reflects*[k] the topography of the surface.

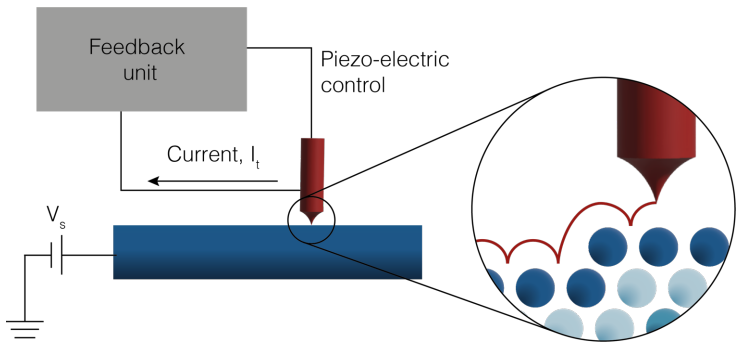

Figure 3.14 Schematic representation of an STM setup operating in constant current mode as described in the text above. Zoom in of the tip movement reflecting the surface topography is included on the right side.

In order prevent high frequency vibrations while scanning, which could lead to distortions in the STM image, the STM head is usually built on a rigid platform

[j] Note that thermal variations can also originate from the sample, resulting in the same effect.

[k] A more accurate way to interpret an STM image is to consider it a contour of constant surface charge density

which includes the tip and the sample. At the same time, it is of outmost importance to shelter the entire microscope from any external vibrations, as they could result in a collision between the tip and the sample. In the microscope employed in my work (ScientaOmicron STM1), this is achieved by suspending the microscope by soft springs. The goal is to achieve a maximum mismatch between the mechanical modes of the soft suspension system and the high resonance of the stiff microscope head. Moreover, additional vibration damping is achieved by an eddy current damping system. Altogether, these precautions effectively shield the STM against outside vibrations.

3.3 Low Energy Electron Diffraction

Low Energy Electron Diffraction (LEED) is based on the mapping of low-energy electrons diffracted on a surface. In my work, we have mainly used LEED as a complementary technique to quickly and reliably check the surface order (or lack of it). In this section I briefly describe the main theory behind LEED and the experimental setup necessary for its measurements.

Basic operational principles

LEED uses electrons elastically back scattered from a surface to obtain structural information of it. The energy of the incident electrons is between 20 – 1000 eV which has two main advantages for probing surfaces: on one hand, electrons with energies in this range have an IMFP around 10 Å (see Figure 3.1), meaning that the information the backscattered electrons provide is mostly from the surface. On the other hand, the de Broglie wavelength of electrons with this energy (equation 3.7) is of the same order as the interatomic spacing of a solid or between atoms/molecules on a surface, and can therefore diffract on it if the atoms are arranged periodically.

Below, the modified de Broglie equation is included, resulting in electron wavelengths between 0.39 – 2.74 Å for kinetic energies in the range of 20 – 1000 eV.

$$\lambda(\text{Å}) = \sqrt{\frac{150.6}{E(eV)}} \tag{3.7}$$

In practical terms, every real space 2D lattice defined by lattice unit vectors **a** and **b** will generate an associated *reciprocal lattice* upon diffraction (defined by reciprocal lattice unit vectors **a*** and **b***). Both lattices are related as follow:

$$\boldsymbol{a}^* = 2\pi \frac{\boldsymbol{b}\times\boldsymbol{c}}{\boldsymbol{a}\cdot\boldsymbol{b}\times\boldsymbol{c}}$$

$$\boldsymbol{b}^* = 2\pi \frac{\boldsymbol{c}\times\boldsymbol{a}}{\boldsymbol{a}\cdot\boldsymbol{b}\times\boldsymbol{c}} \tag{3.8}$$

Where **c** is a unit vector normal to the surface in real space. Therefore, from the position of the diffracted electrons we can easily obtain the two-dimensional periodicity of the surface unit cell. See in figure 3.15 a schematic representation of an Ir(111) surface with the lattice vectors **a** and **b**, and the correspondent LEED image of the same surface, with the reciprocal lattice vectors **a*** and **b***.

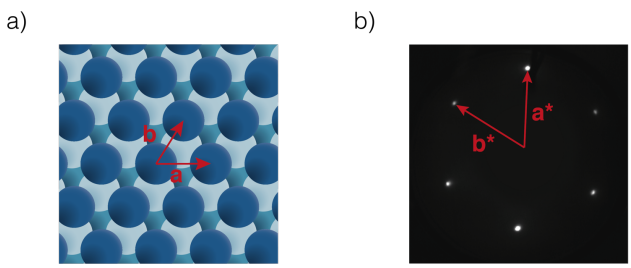

Figure 3.15 Lattice vectors of Ir(111) in real space (a) vs reciprocal space (b). a) schematic representation of the atomic configuration of the Ir(111) surface with the corresponding surface lattice vectors. b) LEED image of an Ir(111) surface with the reciprocal lattice vectors included (incident electron energy 70.9 eV).

Finally, LEED can also be used to obtain a more complete picture of the surface geometry, including bond lengths and angles, if a detailed analysis of the relative intensities of the different diffraction spots is performed. However, in this work we restricted our use of LEED only for monitoring surface periodicity.

Experimental setup

Figure 3.16 illustrates schematically a standard LEED setup. A monochromatic electron beam with energy E_i (adjustable from 0 – 1000 eV, typically) is generated by the electron gun. The beam interacts with the sample (which must be of a conductive material and connected to the ground to prevent charging) and diffracts. The backscattered electrons travel through a series of concentric grids which ensure that only the desired electrons reach the detector:

- G1 and G4 are connected to the ground and ensure that the electrons travel in a field-free region. The grounding of G1 also screens out the high voltages of the phosphorous screen.
- G2 and G3 ensure that only elastically scattered electrons reach the detector by being held at a negative potential - E_i + V, with V being adjustable (0 - 10 V)

Finally, the electrons reach a fluorescent screen biased at a high positive voltage (typically 6 keV). The high voltage is to accelerate the electrons to a kinetic energy high enough to trigger light emission in the phosphorous screen, which is then captured with a camera or by the scientist eye.

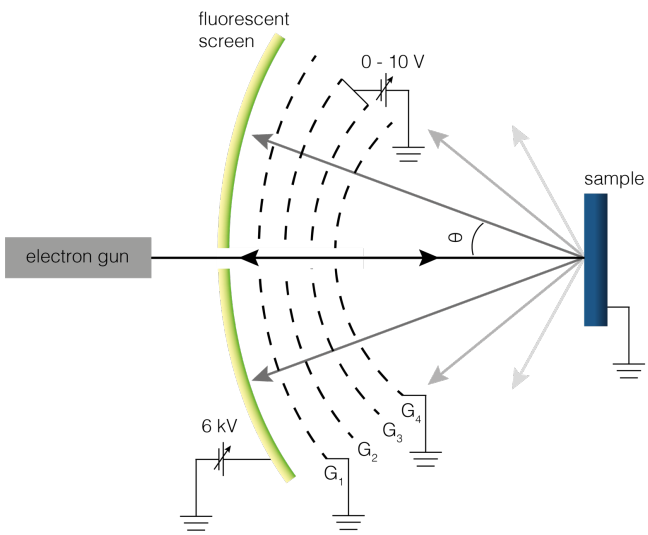

Figure 3.16 Schematic representation of a LEED setup. The elements included are described in the text above.

4. Graphene on Ir(111): model system

The focus of this section is on graphene grown on iridium (111) (Gr/Ir(111)), as this system was used in many of the papers included in this thesis (**I, II, IV**, and **V**).

4.1 Iridium

Iridium is a transition metal that crystallizes in a face-centred cubic (fcc) structure (figure 2.1). Its (111) surface has an hexagonal lattice defined by a cell parameter of 2.715 Å.[63] It has been shown that this (111) surface of Ir can be used to synthesize high-quality graphene films with almost perfect alignment to the iridium substrate via thermal decomposition of hydrocarbons.[64,65] This is because iridium is a very active catalyst for a number of reactions, including oxidation reactions,[66] hydrogenation,[67] or carbon-carbon bond formation.[68] In addition, iridium has a very low carbon solubility (preventing double layer growth) and a very high melting point of 2700 K, ideal for the high temperatures needed for graphene formation.

Before the graphene synthesis, a well-defined, clean iridium surface has to be produced. This can be achieved by several cycles of noble-gas ion sputtering (usually Ar^+ ions with ion energies in the range of 0.6 – 2 keV, either at room temperature or at elevated temperatures (~ 900 K)), followed by oxygen glowing and annealing. For the oxygen glowing step, the crystal is exposed to oxygen atmospheres (of the order of 10^{-7} mbar) at elevated temperatures (~ 1120 K). This ensures that the majority of contaminants on the surface are oxidized and subsequently removed. The final annealing step at UHV conditions (~ 1300 K) ensures the recovery of the surface consisting in large terraces of the specified crystal orientation with the absence of any adsorbates.

4.2 Graphene growth

As mentioned above, excellent graphene flakes or films can be obtained by chemical vapor deposition (CVD) on Ir(111). CVD is an umbrella term for a vast number of techniques that make use of the catalytic properties of a substrate to grow materials with atomic precision.[69]

CVD is based on the thermal decomposition of volatile molecules (precursors) on a catalytically active substrate, where they dissociate and recombine into the desired structure. Since the layer grown is usually inert for precursor adsorption, the reaction stops when the catalytic substrate is covered. This growth mode is what we call a *self-limiting reaction* and one can intuitively guess that is of special interest for the growth of 2D materials.

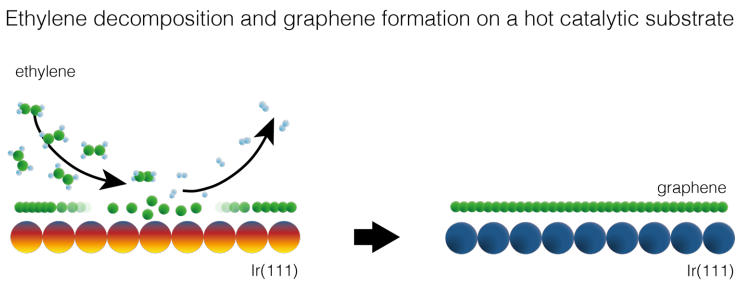

Figure 4.1 Schematic representation of graphene growth by Chemical Vapour Deposition on a metal substrate.

Figure 4.1 illustrates the particular case of CVD growth of graphene on an iridium surface. The most common precursors for graphene are hydrocarbon molecules, such as ethylene (C_2H_4), or propene (C_3H_6), although any volatile molecule containing carbon atoms could, in principle, be used.[70]

Graphene on Ir(111) seems to have been already inadvertently grown in the 1970s by Nieuwenhuys *et al.* when studying the thermal desorption of chemisorbed hydrocarbons on (111) iridium crystal surfaces.[71] However, it was not until the 2000s that dedicated studies on the growth of graphene on iridium started to appear. Among them, I want to highlight the work done in the group of Thomas Michely.

They thoroughly investigated variations on the graphene growth recipes and their effects on the graphene morphology.[63–65,72–75]

For example, together with the group of M. Horn-von Hoegen, they showed that graphene grown at temperatures below 1200 K is highly disordered and the surface is covered by randomly rotated graphene domains instead. Only CVD growth temperatures higher than 1500 K resulted in high quality and single orientation graphene films.[74] Other projects focused in comparing variations of the CVD growth mechanism. In particular, the study by Coraux *et al.* show that high quality flakes can be obtained with a variation CVD named Temperature Programmed Growth (TPG). [65] TPG is also based on the thermal decomposition of hydrocarbons on a catalytically active surface. However, differently than CVD, TPG is a step-wise process, where the surface is first saturated by hydrocarbons at room temperature, and then flash annealed to high temperatures for the substrate-mediated decomposition, as illustrated in figure 4.2.

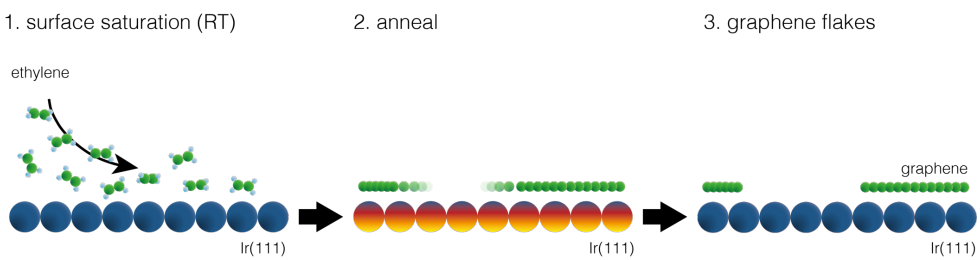

Figure 4.2 Schematic representation of the steps involved in Temperature Programmed Growth.

A clear advantage of TPG is that the growth can be done at very high temperatures without compromising the experimental setup, as the high temperature does not have to be kept for long period of time (as would be the case of CVD growth). Moreover, the high-quality TPG graphene flakes can then act as nucleation seeds for lower temperature CVD growth if one wants to obtain a complete graphene film.

In my work (**Papers I, II**, and **IV**) I have used either TPG to obtain graphene flakes (3 cycles of TPG for a 0.5 ML coverage), or I have combined TPG (1 cycle) with 30 minutes of CVD growth to obtain highly oriented graphene films covering the whole surface (1 ML).

4.3 Characterization

Because of the different lattice constants of iridium and graphene (2.715 Å and 2.458 Å,[63] respectively), iridium-supported graphene film has a characteristic a moiré pattern. As illustrated in figure 4.3, moiré patterns originate from the superposition of two lattices generating a third one.

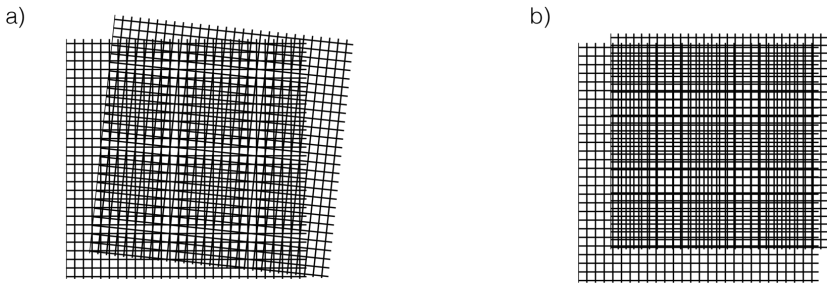

Figure 4.3 Examples of moiré patterns using a square lattice base. a) Moiré pattern from the superposition of two misaligned lattices. b) Moiré pattern originating from the superposition of two lattices with different lattice constants (10% difference).

In the case of Gr/Ir(111) the moiré lattice is defined by a (9.32 × 9.32) unit cell with R0° rotation (i.e. having parallel rows of graphene and Ir(111)), and a periodicity of 25.3 Å when the graphene is grown at optimal conditions.[63,64] A Gr/Ir(111) moiré unit cell is shown in figure 4.4a.

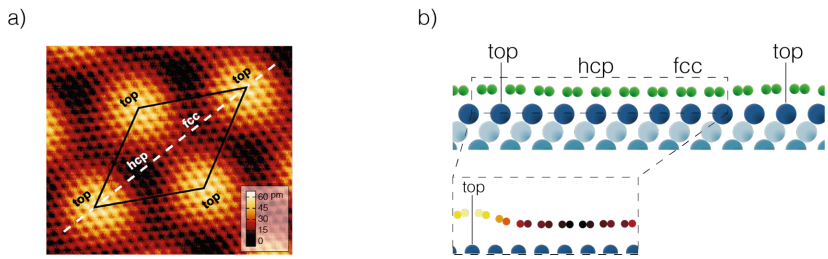

Figure 4.4 a) Constant frequency shift AFM image of the graphene moiré. Reprinted with permission from ref. 76. Copyright © 2013 by the American Physical Society. b) Cross section through the moiré unit cell along the white dashed line in (a). Inset: Magnification of the area marked with the dashed box to better illustrate the corrugation of the graphene layer. Adapted with permission also from ref. 76.

There one can distinguish three different high-symmetry domains: atop, hcp, and fcc. The difference between the domains arise from the relative position between the C-atoms and the Ir-atoms below. In figure 4.4b it can be seen how in the atop region the Gr ring is centered on top an iridium atom, while in the hcp and fcc regions of the moiré, the Gr ring is centered above the hcp and fcc high-symmetry domains of the iridium substrate, respectively. The interaction between the substrate and the graphene will vary in the high-symmetry domains, giving rise to a slight corrugation of the film. The theoretical mean height and corrugation of the graphene film is 3.41 Å and 0.35 Å, respectively, in agreement with X-ray standing wave experiments[73] and Atomic Force Microscopy (AFM) measurements.[76]

Figure 4.5 summarizes the characterization of 1ML Gr/Ir(111) with STM and LEED. The moiré pattern is visible in the STM image in figure 4.5a, as well as reflected in the LEED pattern in figure 4.5b. The LEED pattern also reflects the orientation of the graphene with respect to the iridium substrate, as seen by the alignment between the main iridium and Gr diffraction spots.

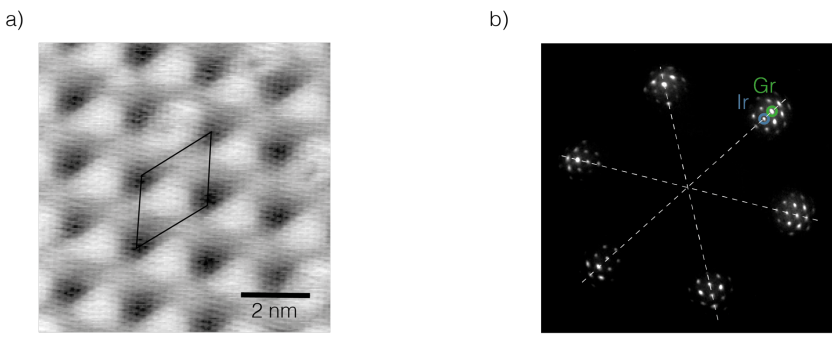

Figure 4.5 a) STM image of 1 ML Gr/Ir(111) with a moiré unit cell highligted in black. b) LEED pattern measured from 1 ML Gr/Ir(111) (MaxPEEM beamline). Iridium and graphene diffraction spots higlighted in blue and green, respectively. Dashed lines included to higlight the alignment between the two materials.

The moiré pattern is extremely sensitive to the presence of atomic defects or to variations in the orientation of the graphene film with respect to the surface. At the same time, easily visible at larger STM images, even when atomic resolution cannot be achieved. Therefore, one use graphene's moiré as a *magnifying glass* for detecting small changes or defects in the graphene structure.[74,77,78]

In the projects included in this thesis, the Gr/Ir(111) moiré pattern has been used as a characteristic STM fingerprint for assessing the quality of graphene on Ir(111). For example, in figure 4.6 we can see how a small defect in the graphene structure (at the top center of the image) can be easily identified due to its effect on the periodicity of the moiré (changes highlighted in green lines).

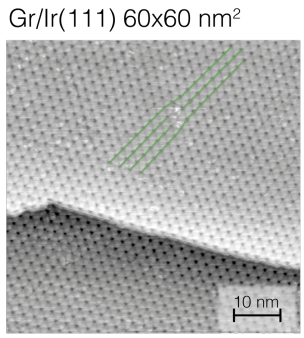

Figure 4.6 Example of the moiré pattern magnifying atomic defects on the graphene film. STM image obtained from 1 ML Gr/Ir(111).

Finally, Gr/Ir(111) has been also characterized extensively via XPS. The fingerprint of graphene in X-ray photoelectron spectroscopy is a single C 1s peak located at 284.1 eV,[79–81] with the different components caused by the corrugation not usually resolved.[80,82] However, these unresolved components are reflected in the C 1s FWHM, so changes on the corrugation of the film can, in principle, be detected by monitoring the width of the C 1s photoemission peak. For example, Grånäs *et al.* found a smaller FWHM on oxygen intercalated graphene than on iridium supported graphene. The difference was ascribed to the fact that, upon oxygen intercalation, graphene can be considered almost freestanding and, therefore, flat[83]. This conclusion was corroborated by STM measurements. A C 1s spectrum measured on 1ML Gr/Ir(111) is shown in figure 4.7a.

Graphene interacts only weakly with the iridium substrate, which is reflected by the almost identical Ir $4f_{7/2}$ spectra with and without graphene included in Figure 4.7b. Only a small variation in the FWHM of the Ir 4f surface component has been observed in detailed measurements by Lacovig *et al.* in ref. 82. More drastic changes

can be observed in the iridium spectrum when the interaction with the substrate is stronger. For example, in the case of graphene flakes[82] or when adsorbates are present on the graphene film,[80] part of the Ir 4f surface component shifts to different binding energies due to the substrate-graphene interaction, resulting in a different surface-bulk ratio (see **papers I** and **II**, for example).

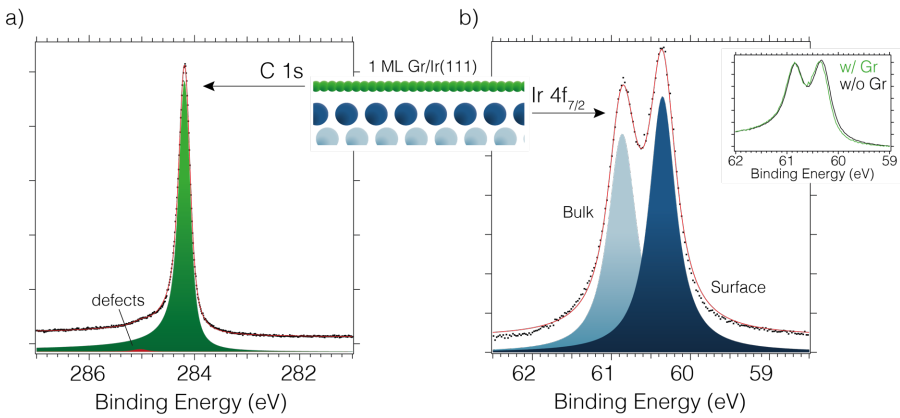

Figure 4.7 XPS fingerprint of 1 ML Gr/Ir (111). a) C1s measured on 1 ML Gr with 390 eV photon energy and fitted with a Doniach-Šunjić convoluted with a gaussian. The small component at 285 eV originates from defects. B) Ir $4f_{7/2}$ measured on 1 ML Gr using 130 eV incident photon energy and fitted with an asymmetric Pseudo Voight. Inset: comparison of Ir $4f_{7/2}$ measured 1 ML Gr (green line) and Ir $4f_{7/2}$ measured on a clean iridium substrate (black line).

In conclusion, iridium is an excellent substrate that allows the growth of high quality graphene films. The resulting Gr/Ir(111) system has been extensively characterized with multiple techniques, thus making it an excellent base for our Gr-based surface science studies.

5. Graphene as a substrate

Parallel to the development of novel 2D materials and the research of their fundamental properties, great research efforts have been directed into implementing the existing 2D materials in a variety of technological applications. Many of these applications require combining different 2D materials with each other (such as 2D stacked heterostructures),[84,85] or the integration of 2D-materials with organic interfaces,[86,87] or in mixed-dimensional structures.[88]

If we focus on graphene as a substrate (as the most established 2D material at the moment), extensive research has been devoted in understanding the adsorption of different atoms or molecules on a graphene film, as a way to obtain 0D(1D)-Gr mixed structures,[89,90] but also as a first step for growing other materials on top.[91]

This chapter is dedicated to review these uses of graphene as a substrate, including the results of **papers I** and **II**. **Papers VIII - X** are also included in the discussion as additional examples.

5.1 Van der Waals substrate

Besides the possible applications mentioned above, graphene is intrinsically interesting to be employed as a substrate. For example, graphene's strong in-plane bonding structure makes it inert to chemisorption, due to the lack of available out-of-plane dangling bonds. This is of particular interest when the substrate-adsorbate interaction must be minimized, for example, to facilitate adsorbate mobility in growth processes.

In the literature, growth on such inert substrates can be referred as Van der Waals (VdW) growth, due to the nature of the interaction forces between the substrate and

the overlayer. This term was coined by Koma in 1992,[92] and has been adapted to any growth technique used on inert substrates (i.e. VdW epitaxy, VdW molecular beam epitaxy, etc.).

We can find multiple examples of growth on graphene or graphite as a VdW substrate, especially in the field of 2D materials growth.[93–96] CVD-grown graphene on transition metals can also be used as an inert substrate for 2D materials, as shown for example by Shi *et al.*[97] who grew molybdenum di-sulfide (MoS_2) on copper-supported graphene, or by Hall and colleagues,[98] who showed how iridium-supported graphene is an excellent substrate for clean, well oriented, and almost defect-free islands and monolayers (ML) of different transition metal dichalcogenides or TMDCs (MoS_2, TaS_2, and WS_2).

Graphene substrates can also be of interest due to their screening effects of the substrate underneath. This has been shown in a recent study by Murray *et al.*,[99] where they showed how Gr/Ir(111) can be a reliable substrate for MoS_2 band-gap characterization by scanning tunneling spectroscopy (STS), due to graphene's unique combination of conductive nature (necessary for the STS measurements) and minimal influence on gating, band re-hybridization and strain effects on the MoS_2 overlayer. Other groups have used this same substrate to facilitate the characterization and transfer of MoS_2 to other substrates,[100,101] or to even investigate in detail the growth mechanism of MoS_2 on Gr/Ir(111) and the stability of the heterostructure.[102]

In the work included in **paper I**, I explored the role of iridium-supported graphene as a VdW or inert substrate to investigate the dissociation of molecules via external processes. Specifically I investigated the electron-induced dissociation of borazine, a common precursor for Boron Nitride deposition. Thanks to the inert character of graphene, I was able to discern the dissociation due to the interaction with the electron beam from any surface-induced dissociation processes, and therefore shine some light onto the structure and composition of the first stages of electron-beam-induced deposition.

Electron Beam Induced Deposition (EBID) is a widely used technique, specially very well established for thin film growth.[103] However, the electron-precursor interaction is rather complex, and the number of studies addressing it from a surface science perspective are limited.[104] In the case of borazine, previous work assumed that the

reaction mechanism consisted in the beam-induced de-protonation of the borazine molecule, allowing an intact BN ring to adsorb on the surface, while the hydrogen recombined and desorbed.[105,106] However, this picture might be too simplistic, as it assumes that only the incident electrons interact with the precursor molecules. When an electron beam impinges on a surface, not only the incident electrons will affect the molecules in their path, but the cloud of back-scattered secondary electrons will also interact with molecules close to the surface[l]. Moreover, it is not known if the adsorption of the precursor molecules on the substrate (prior to the e-beam irradiation) has an effect in their decomposition under the beam.

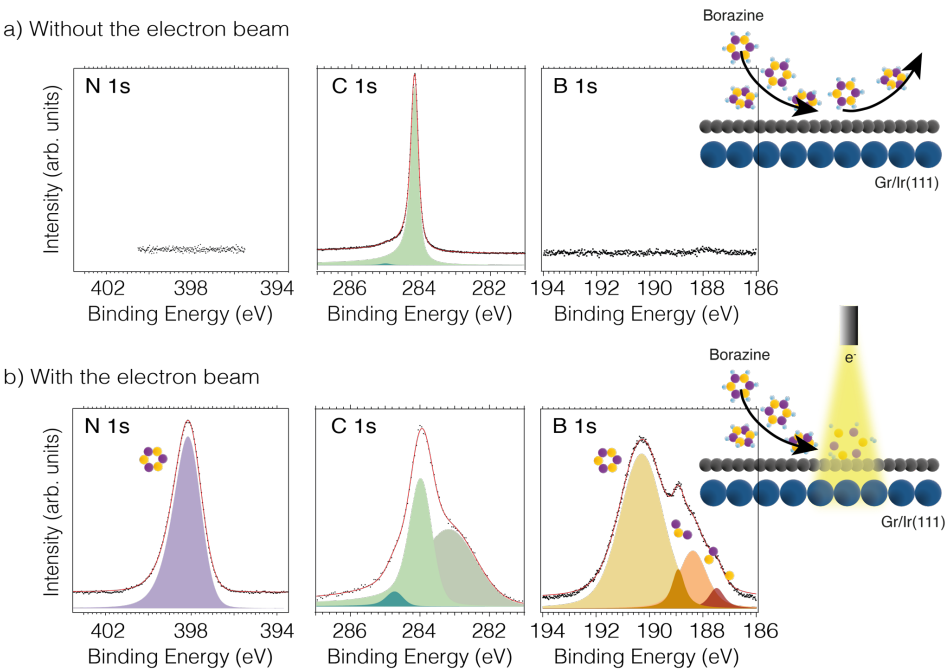

Figure 5.1 XPS characterization of a Gr/Ir(111) film exposed to borazine without (a) and with (b) an electron beam. On the right side of each panel, a schematic representation of each experiment is included. Adapted from **paper I**.

[l] A similar effect to what we observe in XPS, usually referred as *beam damage*.

As shown in figure 5.1a, our experiments confirm that graphene is inert to borazine adsorption, as no boron and nitrogen can be detected on the surface after borazine exposure without the electron beam. On the other hand, in figure 5.2b we can see how a combined exposure to borazine and the e-beam results in the accumulation of boron and nitrogen on the surface. This means that, by focusing the electron beam we can control where the BN is deposited on the surface. We performed such experiment at the MaxPEEM beamline (MAX IV) using the focused electron beam of the beamline's electron microscope to deposit BN on a confined area on the surface (see figure 5.2).

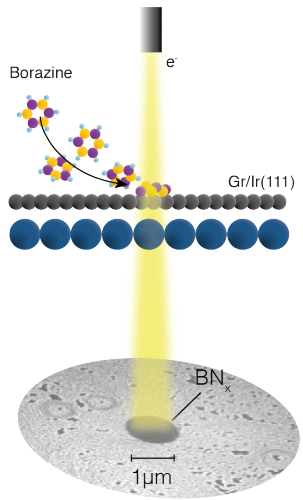

Figure 5.2 Low Energy Electron Microscope (LEEM) image of a Gr/Ir(111) surface after EBID of boron nitride with the focused electron beam of the electron microscope. Schematic representation of the deposition included on top.

Moreover, the fact that graphene is inert to borazine adsorption allows us to analyze the decomposition by the electron beam knowing that the substrate does not play an active role. With the setup employed in the XPS experiments (figure 5.1), where the electron beam was generated by a tungsten filament placed in front of the sample and biased to the desired voltage, we found that borazine decomposes under the beam, resulting in the deposition of an non-stoichiometric and amorphous BN thin layer. This decomposition is reflected by the multiple B 1s components measured after the electron-induced deposition and shown in figure 5.1b.

However, recent follow-up experiments in our group suggest that this high decomposition could be due to the presence of the tungsten filament in the chamber. These follow-up experiments, which were the result of our efforts to follow the EBID *in situ* and will be further discussed in the outlook section of this chapter, are an excellent example of the need of detailed experiments on the electron beam induced deposition process. Regardless of those results, the work in **paper I** illustrates already the advantages of using graphene as a substrate: we can study the electron beam decomposition of a precursor molecule without any additional substrate effects.

5.2 Adjustable adsorption template

Another very important feature of using 2D materials as substrates is that one can tune the adsorbate-substrate interaction by modulating the electronic states of the 2D material itself. The electronic and geometric properties of a 2D material are known to be influenced by its underlying substrate.[107–110] Therefore one can easily tune those properties by changing the graphene-substrate interaction via, for example, intercalation.

The work of Schumacher *et al.* illustrates this idea, as they showed that the adsorption of ionic adsorbates (Cs and Eu) could be prevented by p-doping of the graphene film, which they achieved by intercalation of Cs or Eu.[111] Similarly, Huttmann *et al.* used Eu intercalation to govern the adsorption of naphthalene on iridium supported graphene.[112] Other intercalants can be used, as demonstrated by Sutter *et al.* who showed that oxygen intercalation under Gr/Ru(0001) removes the strong metal–carbon coupling and restores the characteristic Dirac cones of freestanding graphene.[113]

If de-coupling a graphene film from a substrate can be used to prevent the adsorption of some motifs, increasing the film modulation by using a stronger interacting substrate can be used to promote adsorption on specific sites. When there is a lattice mismatch between a 2D material and its substrate, a long-range periodic superposition known as moiré pattern forms, as presented for the Gr/Ir(111) case in chapter 4 (see figure 4.2). This pattern does not only cause a geometric interference

(with corrugations up to 1 Å), but it also changes the local electronic state and structure of the 2D material.[79] The stronger the substrate-graphene interaction, the more pronounced these changes can be. In practice, this modulation generates a periodic array of different adsorption sites, presenting different electronic configurations, essentially making the graphene a 2D nano template for adsorbates.

One application for such a template is to build (and support for characterization) highly ordered arrays of metal nanoparticles or clusters. The fabrication of cluster arrays on a flat substrate is highly interesting in the field of nanotechnology. Due to their limited size, clusters exhibit unique chemical and physical properties, different from their corresponding bulk materials.[114]

The moiré superstructure of graphene on an underlying densely-packed metal offers the perfect template for exceptionally well-ordered cluster lattices, as illustrated in figure 5.3. Initial work by N'Diaye *et al.* in 2006 showed how the Gr/Ir(111) moiré could be used for highly ordered arrays of Ir nanoparticles with a narrow size distribution.[72] From there, the suitability of the moiré superstructure as a cluster template has been shown for multiple materials (such as Pt, W and Re),[89] and for other 2D films besides graphene (like h-BN).[115] Nowadays, research efforts are focused on stabilizing these cluster superstructures so they can endure different temperature and pressure conditions (including **papers VIII, IX**, and **X**).[116,117]

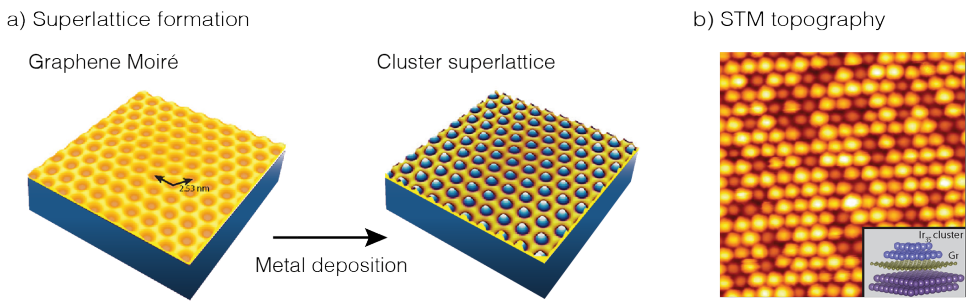

Figure 5.3 a) Schematic representation of cluster lattice formation on graphene on Ir(111). b) STM topograph of iridium clusters on Gr/Ir(111). Adapted with permission from **paper VIII**. Copyright © 2020 American Chemical Society.

Besides forming metal-cluster superstructures, the moiré structure of graphene can also be a template for the adsorption of other atomic or molecular structures. This is usually studied as *graphene functionalization*, due to the influence of the adsorbates on the electronic structure of graphene[118].

The modification of graphene is necessary to integrate graphene in micro- and nano-electronics, as, ironically, the zero-bandgap of graphene is not as interesting as an adjustable bandgap would be for these applications. The electronic structure of graphene can be affected by weaker (physisorbed) adsorbates, as well as for covalently bonded (chemisorbed) species. The latter case, chemisorption, has a more drastic effect on the electronic structure of graphene, as it involves the re-hybridization of the C-C bonds from sp^2 to a sp^3 configuration, losing the double bond character of the pristine graphene C-C configuration.[119] We find examples of such modification in the work by Schulte *et al.*,[120] who showed how the controlled adsorption of oxygen on graphene resulted in a pronounced energy bandgap (0.35 eV) at saturation coverage. Similarly, Balog *et al.* and Jørgensen *et al.*,[121,122] showed that the chemisorption of an ordered array of hydrogen clusters also resulted in a bandgap opening in graphene.

Different adsorption structures are expected to be more or less robust, and therefore should be stable under different conditions. However, opposite to the metal cluster superlattices introduced earlier, not many studies can be found that directly address the stability of chemisorbed structures under ambient pressure conditions, even though such knowledge is highly relevant for the implementation of adsorbate-functionalized graphene on (nano)devices that operate in ambient conditions. At the time of writing this thesis, I am aware of only two studies that address this problem, however indirectly. The work by Yamamoto *et al.* addresses the enhanced adsorption of CO_2 on O-functionalized graphene at ambient pressures,[123] and a study by Khyl *et al.* who exposed H-functionalized graphene to mbar pressures of CO in order to study the enhanced protection against CO intercalation.[124]

The work included in **paper II** addresses this issue. Focusing on the hydrogen functionalized graphene case, we performed a dedicated study on the stability of different H-structures on graphene exposed to near ambient pressure conditions (mbar pressures).

Previous studies have identified two different adsorption structures for hydrogen atoms on iridium-supported graphene:[81,121,122,125] H-clusters that preferentially adsorb on either the fcc or hcp regions of the Gr/Ir(111) moiré structure[m], and less stable H-dimers adsorbed on the atop regions. Both structures are showed schematically in figure 5.4.

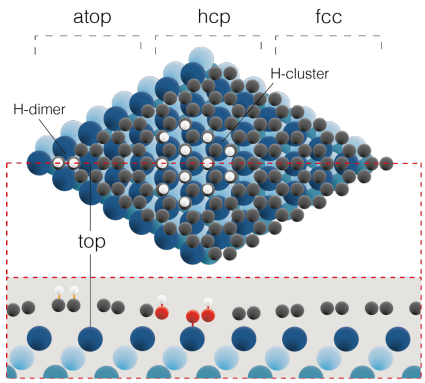

Figure 5.4 Structure of graphene on Ir(111) functionalized by a 12- atom graphane-like H cluster in the hcp region. The structure of an H dimer in the ortho configuration (here placed in the atop region) is also icluded in the sketch. Below, the lateral view across the red dashed line is included. The bonding configuration of the C and H atoms is shown for the clusters vs the dimers: H-atoms in clusters involve the re-hybridization of the C-C bonds from sp^2 to a sp^3 configuration (re-hybridized C atoms are shown in red), losing the double bond character of the pristine graphene C-C. Adapted from **paper II**.

From their bonding configuration illustrated there, H-dimers are expected to be much less stable than the cluster structures. Indeed, we found that only H-dimers were removed after exposing H-saturated graphene to mbar pressures of oxygen at room temperature. This is illustrated in Figure 5.5, which includes STM images of a 1 ML graphene film on Ir(111) after graphene growth (a), after hydrogenation (b), and after exposure to oxygen at room temperature (c).

[m] Jørgensen *et al.* showed that the hcp region is slightly more favorable. At high enough coverages, both the fcc and hcp regions can be occupied.[121]

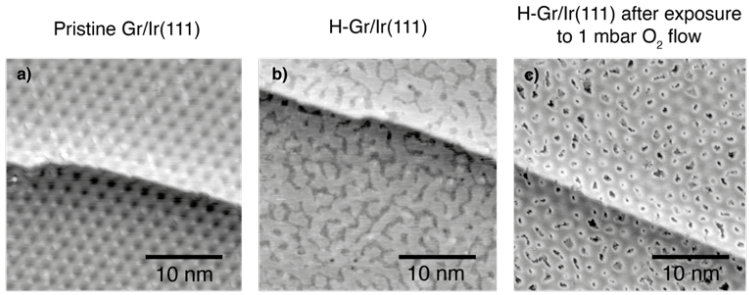

Figure 5.5 STM images of a 1 ML Gr/Ir(111) illustrating the H-dimers removal by molecular oxygen exposure. a) Pristine Gr/Ir(111) with the characteristic Moiré superstructure. b) 1 ML Gr after hydrogen saturation. Elongated structures cover the whole surface, indicating that all hcp, fcc and top regions of the moiré have H adsorbates (as clusters in the fcc and hcp regions, and as dimers in the top regions). c) same sample after 60 s exposure to oxygen (1 mbar). Most H adsorbates are removed, leaving only the most stable H-clusters behind. Reproduced from **paper II**.

This result itself is highly interesting for the functionalized graphene applications suggested earlier, as one can extrapolate that any hydrogenated graphene film will consist of only H-clusters after being exposed to air. However, it also opens up for more fundamental questions about the adsorbate-gas phase interaction. Specifically about the H-dimers removal mechanism as well as the role of graphene as support.

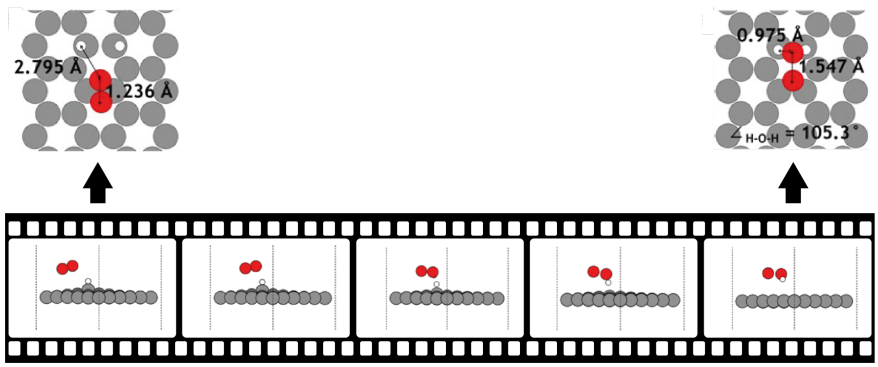

Figure 5.6 Illustration of the reaction path for water formation atop graphene. The top views of the initial and final configurations are included above. Note that when a molecular oxygen picks up the hydrogen atoms, they are already in a geometrical configuration very similar to water (105.3° compared to 104.5° on a water molecule). Adapted from **paper II**.

Additional density functional theory (DFT) calculations by Wenbin Xu in the group of M. Andersen and K. Reuter showed that hydrogen dimers are able to activate the unsaturated double bond of molecular oxygen, already at room temperature, resulting in the formation of water or hydrogen peroxide. In other words, the hydrogen is reacted away from the surface, as illustrated in figure 5.6. This is not the case for the most stable hydrogen structures, which are too tightly bound to the surface.

Interestingly though, it seems that the reason for such low temperature activation relies not only on the low binding energy of the H-dimer adsorbates, but also on the geometrical configuration of those H-atoms. As shown in the top view of the first reaction step in figure 5.6, the closed-packed structure of graphene allows for hydrogen atoms to adsorb in a very close configuration, which facilitates their reaction with oxygen. Moreover, we found that the energetics of the reaction pathway are almost unchanged by the removal of graphene. Therefore, in a way, the graphene acts like a catalyst for water formation just by providing the adsorption configuration necessary for the H adsorbates that promotes the reaction. This finding paves the way for future research using graphene as an adsorption template for fundamental catalysis studies.

5.3 Conclusions and outlook

This chapter summarized my research on the adsorption of atoms and molecules on graphene. As I have tried to convey, graphene is an interesting and versatile substrate for such studies, as it can provide both an inert base for studying growth mechanisms, as well as an adsorption template for studying reactions between adsorbates and gas phase molecules.

The work in **paper I** falls into the first application: using graphene as an inert substrate. My results illustrate the advantages of using graphene to investigate an electron beam induced deposition processes. However, the complex electron beam-precursor interaction is far from being completely understood.[104] For this reason, *in situ* characterization of the electron beam deposition is the natural following step for this project.

Indeed, initial efforts in this direction have been taken by our group and the beamline staff at SuperESCA beamline at Elettra. Together we implemented an electron-beam pulsed setup that allowed us to monitor the surface with XPS in between short e-beam pulses. This setup, combined with graphene's inert substrate and liquid nitrogen temperatures, provided us a way to *slow down* the electron beam deposition process (i.e. lower the probability of interaction between the e-beam and the precursor molecule) enough to be able to follow it *in situ* with XPS.

Figure 5.7 illustrates the initial results measured at SuperESCA. Using B 1s core level, we follow the deposition of borazine on different substrates as well as compare them with the electron beam induced deposition. Panels a and b compare the deposition of borazine on Ir(111) without (a) and with (b) the electron beam. Without the beam, borazine adsorbs and dissociates on the iridium substrate (as reflected by the three distinct boron components) and the deposition stops once the iridium substrate is fully saturated. With the electron beam, on the other hand, decomposition can be observed only at the beginning of the deposition (see several boron component in the bottom 2D plot in panel b), and the coverage does not reach saturation. Instead, it increases linearly with the combined borazine and e-beam exposure.

Panel c reproduces this last e-beam deposition but on a graphene substrate. Again, it is clear that no adsorption occurs without the e-beam, as no boron can be detected on the surface while the e-beam is off. Once the deposition starts, we observe only one boron component, the intensity of which increases only during the combined e-beam borazine exposure. Further analysis will allow us to compare the initial stages of EBID in both active (Ir(111)) and inert (Gr/Ir(111)) substrates, as well as determine the e-beam deposition rate. These results will be compiled in an forthcoming manuscript, which, unfortunately, could not be included in this thesis due to lack of time.

Further work within the EBID field could include the deposition different materials or of complex vertically stacked heterostructures by alternating precursors. Moreover, the same setup can be used to study precursor decomposition within different background pressures of other gases, such borazine in a background of nitrogen gas in order to obtain a stoichiometric BN film.

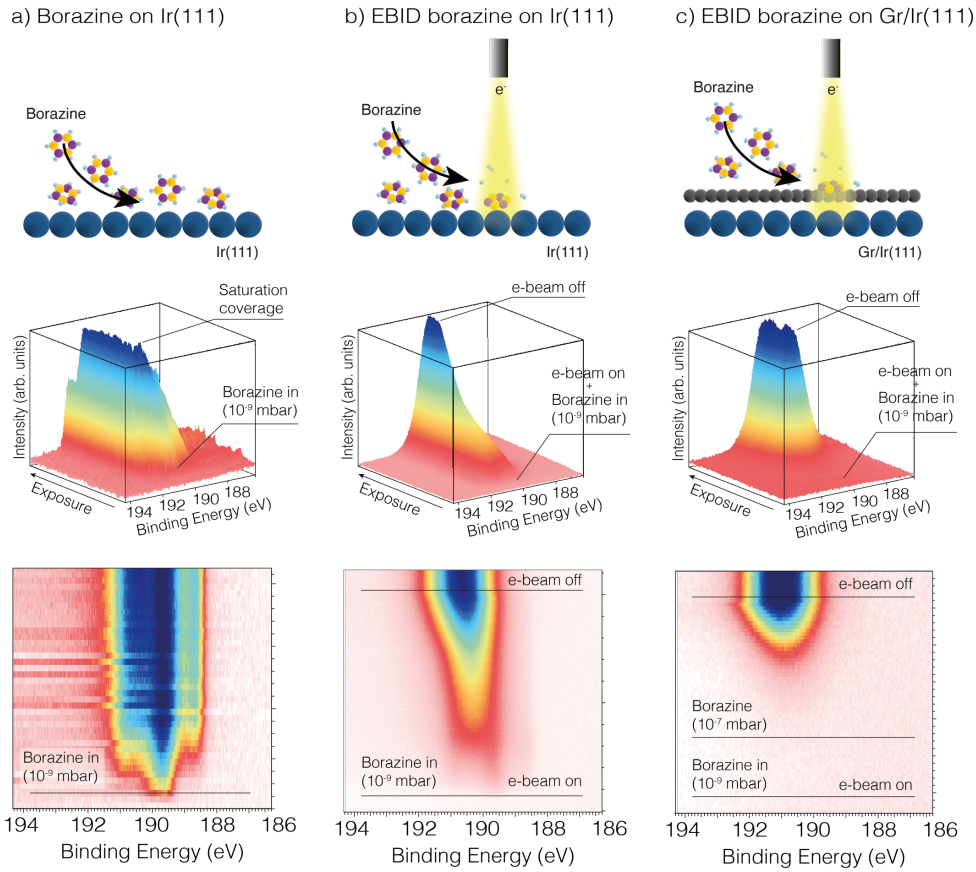

Figure 5.7 Comparison of *in situ* deposition of borazine with and without electron beam, and on an active (Ir(111)) and an inert (Gr/Ir(111)) substrate. Each panel contains a sketch of the experiment (top), a 3D plot (middle) and a top view (bottom) of the B 1s core level measured during the borazine deposition.

The work in **paper II**, on the other hand, looked more closely to different adsorption structures on Gr/Ir(111) and their stability and reactivity under ambient pressure conditions. In this chapter, I have discussed how adsorption of molecules can be used to modify graphene's properties. However the application of such functionalization in real devices is not feasible until their stability is tested. Future work could thus focus on studying the effects of ambient pressure conditions on other 0D/1D-Gr heterostructures[126]. Strong interacting molecules that open a bandgap on the graphene electronic structure would be interesting initial candidates for such studies.[127,128]

Moreover, our project proposes a new role for graphene in catalysis: as a adsorption template for fundamental reaction studies. Future work could focus on modifying graphene's structure (via, for example, changing the substrate interaction) to promote the adsorption of different motifs of interest, which can then be studied under ambient pressure conditions. Examples could be the adsorption of hydrogen or oxygen atoms on freestanding graphene, to cluster or 1D structures in highly corrugated graphene. The adsorption of molecules on the edges of graphene nano ribbons (edge decoration) could also offer interesting possibilities for reactivity studies.

6. Graphene as a cover

The previous chapter was dedicated to reactions occurring atop of a graphene film. In this chapter I change perspective and focus on phenomena that occurs *under* graphene. This is the realm of *undercover catalysis*. I will present how graphene's role here is not just as confining agent but also as a chemically sensitive probe that allows us to follow the reactions underneath.

In Section 2.4 a catalytic site was defined as a chemical center that takes part in a reaction but is not consumed. However, catalytic centers do not exist in a void, they are supported by a surrounding environment. While the catalytic center is understood as the main actor in catalysis, the environment has an indispensable role as modulator of its electronic and geometric structure.

In this context, confinement in catalysis can be understood as a way to modulate the environment of a catalytic site.[129] A specific case of confined catalysis is undercover catalysis, which takes advantage of nano-confined environments that provide favorable intermolecular interactions between the adsorbates or between the adsorbate and the substrate. This effect results in chemical reactions behaving different in confined environments than on uncovered surfaces.[130–132]

The interest in undercover catalysis arises from the reported higher performance of catalysts when placed in such unique confined environments.[133–136] Moreover, well-defined 2D materials such as graphene or hexagonal boron nitride, directly grown on catalytic metal substrates can be directly employed as model systems to understand this chemistry undercover.[130,131]

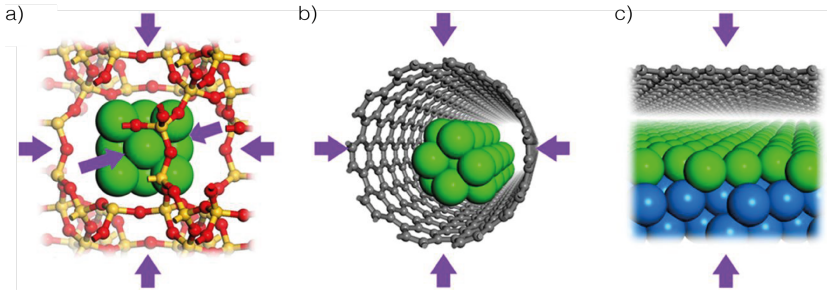

Figure 6.1 Schemes for confined catalysis in different environments: a) 0D pores, b) 1D carbon nanotubes and c) 2D space under 2D materials. Reproduced from ref. 131. Copyright © 2017 National Academy of Sciences.

As illustrated in figure 6.1, various configurations have been reported so far to provide this confinement: from the void spaces in between van der Waals materials or 2D van der Waals heterostructures,[137,138] to nanotubes,[139] and porous surfaces.[140]

Here, I focus on simple reactions occurring in the confined space between 2D films (graphene and hexagonal boron nitride, h-BN) and a catalytic metal surface (Ir(111) or polycrystalline Cu films) which includes and contextualizes the results of **papers III** and **IV**. The goal of this chapter is to better understand how graphene can assist in the research of undercover reactions.

6.1 Intercalation

The first step for an undercover reaction is the intercalation of the reactants. Extensive research efforts have been dedicated to understand the intercalation mechanism of small molecules such as oxygen, hydrogen or CO under graphene.[38,113,130,133,141–143]

To understand the intercalation of different atoms and molecules and their stable adsorption configurations, we can take a step back and look at the adsorption of molecules onto a bare surface. A useful approach here is to compare adsorption potentials for different adsorption and intercalation structures.[38] The adsorption potential is the energy gained per molecule when an adsorbate moves from a gas or solution phase to the surface.

For adsorbates on a clean surface it can be expressed as

$$E_{ads,pot} = \left(E_{s,ads} - (E_s + n \cdot \mathrm{E}_{ads})\right)/n \quad (6.1)$$

The two main terms in equation 6.1, describe the chemical potential of the adsorbate structure on the surface ($E_{s,ads}$) minus the chemical potential of the surface (E_s) and the isolated adsorbate (E_{ads}) independently. The term *n* refers to the number of adsorbates. When $E_{s,ads}$ is smaller than (E_s + n·E_{ads}), meaning that the adsorption on the surface is more favorable, the resulting adsorption potential is negative.

If we now add graphene in the picture, the adsorbates must intercalate the film in order to adsorb on the surface. In terms of the adsorption potential we can now write

$$E_{ads,int,pot} = \left(E_{s,ads,int} - \left(E_{s,Gr} + n \cdot \mathrm{E}_{ads}\right)\right)/n \quad (6.2)$$

Where $E_{s,ads,int}$ refers to adsorbates on the surface (below graphene) and $E_{s,Gr}$ is the chemical potential of the surface with graphene. Similarly to the previous expression, if the $E_{ads,int,pot}$ is negative, means that the adsorption on the substrate *via intercalation* will occur. We can then obtain the energy necessary to intercalate from the difference between these two adsorption potentials[n].

From the adsorption potential expressions above, because $E_{s,Gr}$ is not the same as E_s, one can intuitively understand that some adsorption structures stable on bare surfaces, will not occur undercover. To illustrate this, table 6.1 summarizes the different stable adsorption structures experimentally found for oxygen and CO on bare Ir(111) and intercalated under iridium-supported graphene flakes.

[n] Note that any additional kinetic barriers are not considered in this statement.

Oxygen[38,83,144–149]			Carbon Monoxide[37–39,149–151]		
Coverage	Ir(111)	Under Gr	Coverage	Ir(111)	Under Gr
0.08 ML	-	lattice gas	0.33 ML	(√3×√3)R30°	-
0.25 ML	(2x2)	(2x2)	0.58 ML	(2√3×2√3)R30°	-
0.50 ML	(2x1)	(2x1)	0.70 ML	(3√3×3√3)R30°	(3√3×3√3)R30°

Table 6.1 Reported adsorption structures of oxygen and CO at different coverages on bare Ir(111) and graphene-covered Ir(111) surfaces (underlined structures only stable at high pressure conditions). The references for the coverages and structures reported are included in the table.

Comparing adsorption potentials helps us understand why intercalation occurs, but we need a kinetics point of view to describe how. Different 2D materials result in different intercalation mechanisms. In porous structures, such as, for example, 2D silica[o], big molecules like CO, CO_2,[152] or H_2O [153] can diffuse in and out the confined space through the 2D film pores[132]. This is not the case for the more densely packed structures of graphene and h-BN, which are impermeable to most gases.[154] For those systems it has been shown that intercalation occurs mostly through defects or via the film edges.[130,141,143]

In general, we can summarize the intercalation process in the following steps (schematically shown in figure 6.2):

1) (Dissociative) adsorption on the bare metal patches
2) Accumulation on the bare metal patches
3) Attack of the graphene edge: delamination of the 2D film
4) Diffusion into the covered surface

[o] 2D silica refers to a bilayer SiO_2 structure containing two parallel Si-O sheets connected by oxygen atoms, resulting in hexagonal open facing pore sites with a width of ~ 5 Å. [152]

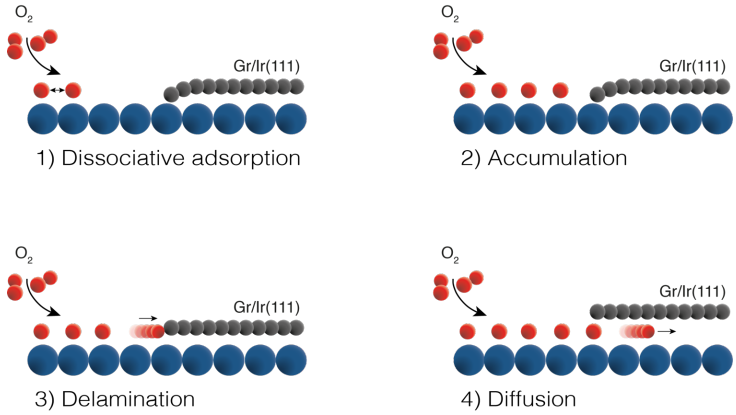

Figure 6.2 Schematic representation of the steps involved in oxygen intercalation under iridium-supported graphene flakes.

There are of course differences depending on the molecule intercalating. For example, CO does not dissociate on Ir(111), instead it remains strongly bound to the substrate. Moreover, because only high coverage structures are energetically favorable under graphene on Ir(111) (see table 6.1), pressures of the order of mbar are usually required for CO intercalation at room temperature.[151] This is not the case of oxygen, which dissociates on the bare iridium and diffuse under the graphene flakes forming adsorption structures with increasing coverage.[83] Hydrogen also dissociates prior to intercalation, however only high coverage structures are observed under graphene.[155]

Graphene: an additional probe

As already introduced in the methods chapter, the core-level shifts (CLSs) of the C 1s photoelectrons from graphene are frequently used to study adsorption and intercalation due to graphene's sensitivity to changes in the surrounding environment. Indeed, most of the experimental intercalation studies mentioned earlier characterized the different undercover species by measuring the core level shift of the C 1s signal from graphene with XPS. Altogether, their reported results conform a library of intercalation fingerprints, whose values have been also corroborated by theoretical models.[38,46,109]

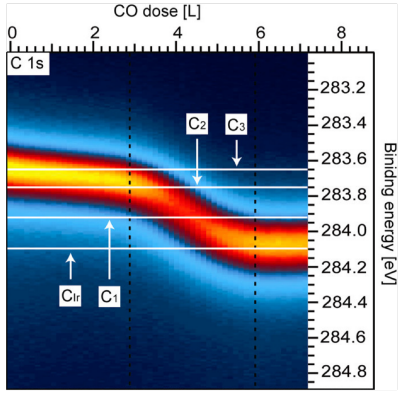

Figure 6.3 CLS of graphene measured on an oxygen intercalated Gr film exposed to CO (10^{-7}mbar pressures). We can follow the slow de-intercalation of the film over accumulated CO exposure due to CO reacting with oxygen on the bare iridium patches which allow oxygen to diffuse out of the flake. The smooth change in C 1s BE reflects the different adsorption structures under the graphene film, which change from p(2x1) (C_3) to p(2x2) (C_2) and O-lattice gas (C_1) with the decreasing oxygen coverage under the flake. The component C_{Ir} refers to un-intercalated Gr/Ir(111). Reproduced from ref. 83. Copyright © 2012 American Chemical Society.

The sensitivity of graphene, combined with these known intercalation fingerprints and the intensity of the C 1s photoemission signal, make graphene the perfect cover for intercalation studies. Several groups have already used graphene to follow intercalation processes *in situ,* however under UHV conditions. An example of such work can be seen in figure 6.3 which shows the evolution of C 1s upon oxygen de-intercalation and the different undercover structures that can be deduced from it. Moreover, the high intensity of the C 1s signal allows us to bridge the pressure gap in intercalation studies and investigate undercover processes *in situ* and under reaction conditions.

6.2 Undercover reactions

Undercover reactions can include reactions with the substrate or between multiple intercalating molecules or atoms present in the confined space.

In **paper III** we studied the first case, copper oxidation under graphene. Copper oxidation is a well-studied process that proceeds in three steps: 1) the dissociative adsorption of oxygen, 2) the formation of a Cu_2O layer, and 3) the formation of highly corrugated CuO islands.[156]

It is known that the presence of a 2D cover delays the oxidation of the copper,[157–161] but by following the oxidation process *in situ* with APXPS, we were able to understand more about the protection mechanism. This work shows that, h-BN protection is very straightforward: the oxidation of the substrate is delayed until the coating layer is etched away. Since the barrier for oxygen diffusion under h-BN and graphene is similar,[162] this behavior should not be ascribed to the absence of intercalated oxygen, but to the absence of galvanic corrosion due to the insulating nature of h-BN,[163] which prevents further oxidation of copper.

Graphene, on the other hand, has a more complex protection mechanism. We can follow the system's evolution by monitoring the C 1s of graphene and the O 1s signal from the surface oxide. Figure 6.4a shows the intensities of these core levels, together with the binding energy of C 1s, as a function of temperature.

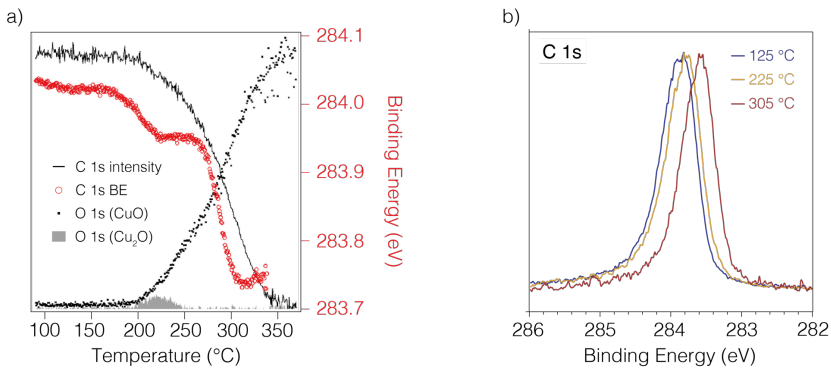

Figure 6.4 Following the undercover oxidation of copper using the C 1s CLS and O 1s intensities. a) Fitting results for graphene/Cu in 2 mbar O_2. b) C 1s spectra at increasing temperatures (intensity normalized). Adapted from **Paper III**.

The graphene cover allows oxygen intercalation and the beginning of copper oxidation to Cu_2O at lower temperatures than in the h-BN case. This is because, opposite to h-BN, the highly conductive graphene provides a path for galvanic corrosion, acting as the cathode in the electrochemical circuit which results in an increasing of the Cu_2O area.

For un-covered copper, the evolution towards CuO would immediately proceed, however, we found that the presence of graphene stabilizes the Cu_2O phase delaying the evolution towards CuO. This is shown by the shift of C 1s (shown in more detail in figure 6.4b), which reflects the presence of oxygen underneath the film. Such protection mechanism can be explained as a simple mass limitation issue, i.e. the presence of the graphene slows the access of oxygen to the undercover space, as it must intercalate the film through defects and then diffuse around the surface. In other words, the presence of the graphene cover stabilizes a Cu_2O phase at temperatures in which otherwise would already be transformed into CuO.

The work in **paper IV** focused on reactions between multiple intercalating molecules or atoms present in the confined space. Simultaneous intercalation of multiple reactants can be an experimental challenge. When exposed to gas mixtures, usually the intercalation of one of the species will be more energetically favorable, limiting the intercalation of any other species. In other words, resulting in the poisoning of the undercover space.

Because of that, most undercover catalysis studies employ stepwise exposures, i.e. exposing the 2D/metal system to first one reactant and then the other.[130,131] Extensive research efforts have been dedicated to research the step-wise intercalation (and sometimes subsequent reaction) of molecules on graphene-covered metal surfaces. Published studies include, for example, CO oxidation on Gr/Pt(111),[133,164,165] and on Gr/Ir(111),[83] H_2 oxidation on Gr/Pt(111),[130] and on Gr/Ir(111),[166] and water decomposition on Gr/Ni(111).[167]

However, we must ask ourselves if, in all of those cases we are really studying the undercover reaction or just the substitution of one intercalating species by another. **Paper IV** addresses this problem explicitly: can we intercalate another atom/molecule when the undercover space is already occupied? Will they substitute each other? Or can they co-exist (and even react) in the confined space?

As in the previously mentioned intercalation studies, we must add an external driving force to push different species into the confined space. In our study we made use of a recently developed methodology for studying fast surface changes during catalytic reactions (see **paper VI**). The method is based on gas pulses of varying compositions that oscillate a catalytically active surface between active and inactive phases. In our case, the gas pulses create an artificial driving force for pushing the reactants (oxygen, hydrogen, or CO) under the graphene flakes, avoiding poisoning the undercover space by one reactant or product molecule.

Specifically, I investigated the coexistence of hydrogen and CO with already intercalated oxygen. In all our experiments we used the CLS of C 1s as a main source of information, complemented, it in some cases, with the information from other core levels such as O 1s. Figure 6.5 shows a schematic representation of the three studied undercover reactions, while Figure 6.6 compares the C 1s measurements *in situ* for the three cases of interest.

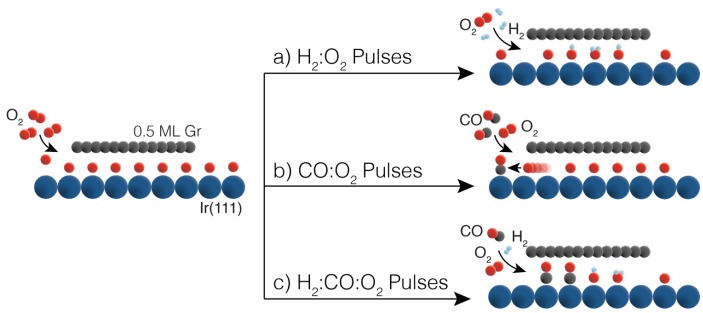

Figure 6.5 Sketch of the undercover reactions studied testing the coexistence of hydrogen and CO with oxygen under iridium-supported graphene flakes. Reproduced from paper IV.

Based on previous UHV intercalation studies,[38,46,83,151,166] we used five components for the C 1s curve-fitting-analysis: pristine graphene (C_{Gr}), graphene with an oxygen lattice gas below ($C_{O\text{-}gas}$), graphene with a p(2×2)-O phase below ($C_{O\text{-}2\times2}$), graphene with a p(2×1)-O phase below ($C_{O\text{-}2\times1}$), and finally graphene with a dense OH-H_2O phase below ($C_{OH\text{-}H2O}$). Note that the $C_{O\text{-}gas}$ component also corresponds to graphene intercalated with CO (see figure 6.6c). The results of the fit are included in figure 6.6, which illustrate the sensitivity of the C 1s from graphene to changes in the undercover structures.

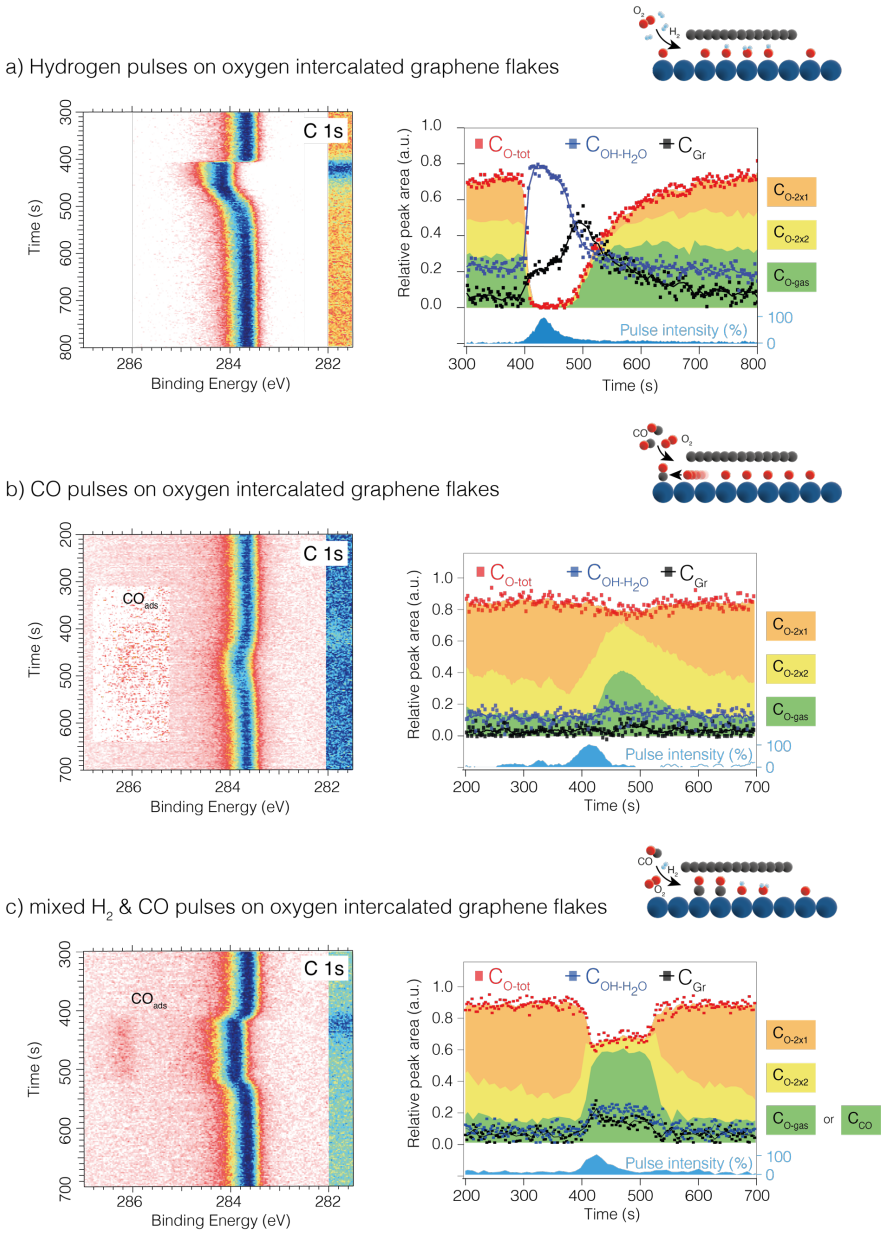

Figure 6.6 2D image plots of C 1s measured on oxygen-intercalated 0.5ML Gr/Ir(111) during a) one hydrogen rich pulse (50 s of a hydrogen rich mixture H_2:O_2 9:1 sccm), b) one CO rich pulse (50 s of a CO rich mixture CO:O_2 9:1 sccm), and c) one combined CO and hydrogen pulse (50 s of H_2:CO:O_2 4.5:4.5:1 sccm). A slice of non-normalized background data is shown on the low-binding energy side in each panel, which marks the arrival and extension of each gas pulse. Besides each plot, the integrated intensities of the C 1s fitting components are included (components: pristine graphene (C_{Gr}), oxygen intercalated graphene ($C_{O\text{-}tot}$, deconvoluted in the three intercalated oxygen phases ($C_{O\text{-}2\times1}$, $C_{O\text{-}2\times2}$, and $C_{O\text{-}gas}$), and water intercalated graphene ($C_{OH\text{-}H2O}$). Adapted from **paper III**.

In our study we found that the presence of oxygen does not affect the diffusion of hydrogen in any way. This is reflected by the rapid CLS of C 1s at around 400 s in figure 6.6a. If anything, the fact that the graphene flakes are already intercalated facilitates hydrogen intercalation, because it removes the energy barrier related to de-laminate the graphene film from the substrate (usually the limiting factor for hydrogen intercalation).[155] Once intercalated, hydrogen rapidly reacts with the available oxygen and forms a dense mixed OH-H_2O structure under graphene, as reflected by the fit in figure 6.6a. This intercalation structure was also observed in previous stepwise intercalation experiments.[166]

On the other hand, we found that CO is unable to intercalate a graphene flake already intercalated by oxygen, as visible by the minimal change of the C 1s from graphene in figure 6.6b, as well as in the associated fit. Instead, CO would adsorb on the bare patches, and react with oxygen available there. This would result in the increase of available adsorption sites on the un-covered space, which, as we know from previous studies,[83,151] accelerates the removal from undercover oxygen. Based on this previous work, we speculate that CO would be able to intercalate the graphene flakes only once all oxygen is removed from the undercover space. This finding greatly limits the applications of undercover catalysis for CO oxidation.

Finally we investigated if hydrogen can promote CO intercalation on the Gr/O/Ir(111) system. Our experiments showed that indeed that was the case. By mixing hydrogen on the CO pulse, we were able to intercalate CO on an already oxygen intercalated graphene flake. The intercalation is shown in figure 6.6c with the combined CLS of C 1s from graphene and the clear component at 286 eV originating from CO adsorbed on iridium (CO_{ads}). The way that hydrogen facilitates the intercalation is by immediately reacting with the undercover oxygen, effectively generating free undercover space for the CO to diffuse to.

Moreover, we found that a less dense CO structure was stable under graphene when co-existing with OH and water. Specifically, we proposed a $(2\sqrt{3} \times 2\sqrt{3})30°$-CO structure with a 0.6 ML coverage, known to form only on bare iridium under vacuum conditions.[38] Nevertheless, XPS is an averaging technique, therefore the assumption that less dense CO phases can stabilize under graphene with the presence of OH-H_2O structures should be corroborated by imaging techniques, such as STM.

6.3 Conclusions and outlook

This chapter focused on the study of simple reactions underneath graphene. The discussed literature together with the results presented (**papers III** and **IV**) illustrate how graphene can be a valuable asset for these studies, both as a confining agent but also as an extremely sensitive probe to the undercover species and the kinetics of their intercalation.

With applications of graphene as a coating agent in mind (**paper III**), future research could focus on limiting intercalation by functionalization of the graphene film. In chapter 5, I have reviewed how the graphene-substrate interaction can be easily modified by functionalization. However, so far, not many studies have used this characteristic of graphene in coating applications,[160] and much less have addressed the stability of these structures under ambient pressure conditions.[124]

Research efforts could thus be focused on finding functionalization structures that are stable under ambient pressure conditions and not removed by the intercalation process. Initial work in this direction has started in our group: Inspired by the adsorbate structures covered in chapter 5, and using the gas pulses approach employed in **paper IV**, we started to explore carbon-clusters as a stable (and inert) way to increase the graphene-substrate interaction, effectively limiting the access to the undercover space.

We tested these structures using the hydrogen rich pulses described in section 6.2 (figure 6.6a). Figure 6.7 compares hydrogen intercalation under oxygen intercalated Gr flakes with and without carbon clusters. As in **paper IV**, we follow the undercover process by monitoring the CLS of C 1s. We have already discussed that, without carbon clusters, hydrogen intercalates and reacts with the oxygen already present undercover, forming a dense OH-H_2O structure in the confined space (panel a). On the other hand, the graphene sample decorated with carbon clusters show a different CLS upon hydrogen exposure, which corresponds to pristine graphene on Ir(111) (panel b). This suggests that the presence of the carbon clusters modify the energetics of the system, making unfavorable the formation of water undercover. We speculate that in this system, the oxygen is removed from the confined space to react with hydrogen on the bare iridium patches.

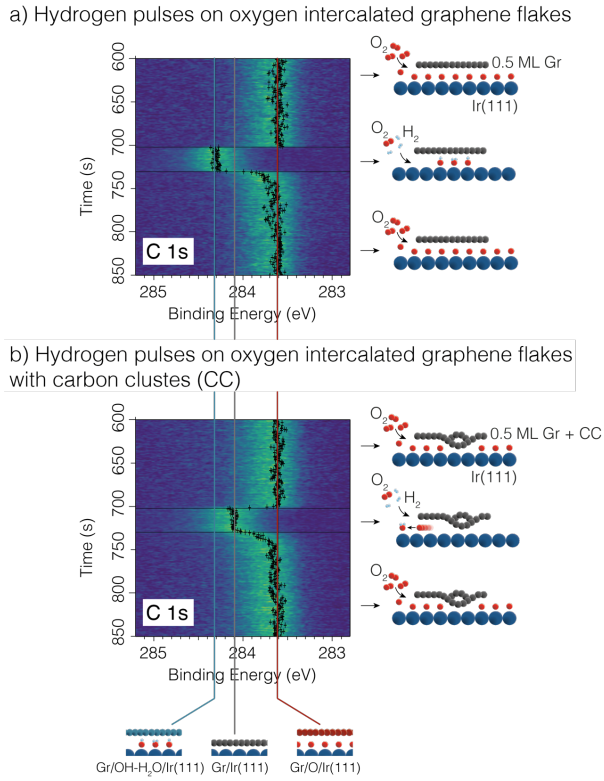

Figure 6.7 a) C 1s spectra measured on 0.5 ML graphene and b) C 1s spectra measured on 0.5 ML C-functionalized graphene during a hydrogen rich pulse. Vertical lines show the characteristic binding energies of graphene intercalated by oxygen (red), pristine (grey), and intercalated by a mixed OH-H_2O structure (blue). Schematic representations of the intercalation structures are included below the spectra. Sketches of the system before, during, and after the pulse are included on the right side. Adapted with permission from ref. 168.

Altogether, these preliminary results confirm that carbon functionalization can affect the undercover chemistry, however it does not prevent the intercalation of oxygen. Further work should investigate in more detail the intercalation resistance mechanism that carbon clusters offer for different molecules, and under different temperature and pressure conditions.

Future research could also take advantage of our "gas-pulses approach" to test other gas compositions, pressures, or pulse structures and their effect to the intercalation of metal-supported graphene. Alternatively the same gas pulse setup can be employed to study intercalation of other 2D materials. Hexagonal Boron Nitride would be an

interesting first candidate due to its relevance in multiple catalysis studies,[130] as well as its strong boron and nitrogen signals, suitable for APXPS. Furthermore, in future projects it would be of interest to study confined reactions in more "exotic" 2D materials configurations, such as vertically stacked heterostructures.[169]

Finally, the undercover CO adsorption structures suggested in **paper IV** should be further corroborated by structural sensitive techniques. Movies of the intercalation and de-intercalation process recorded with STM, PEEM or LEEM (as in ref. 133) would be the natural follow-up to the experiments presented in **paper IV**. Special focus should be given to techniques that can be performed at similar pressure and temperature conditions as our work. This is the case of high pressure STM (HP-STM),[170] which, coupled with recent advances in spiral high-speed scanning modes,[171] would help us to obtain a detailed *in situ* picture of the undercover reactions. Furthermore, different confining systems such as bigger graphene flakes could be investigated thanks to the recent development of near ambient pressure PEEM (NAP-PEEM).[172] This technique would even allow us to study the effect of larger scale graphene deformations (such as wrinkles) on the diffusion and coexistence of species undercover.

7. Future prospects

With this thesis I set out to show how graphene can be a versatile tool for surface science studies. Chapters 5 and 6 provided an overview of the uses of graphene in two different ways: as a substrate to study reactions above, and as a cover to study reactions below. In this chapter I want to discuss how one could use graphene in future studies.

Future projects can use **graphene as a substrate** to investigate multiple material deposition processes, such as MBE, plasma-assisted MBE, or even Atomic Layer Deposition (ALD). Furthermore, as discussed in the conclusion of chapter 5, electron beam deposition should be further studied. With the e-beam setup described in section 5.3, one could investigate *in situ* the electron beam decomposition of other precursor materials.[173] Organic compounds for carbon deposition would be interesting candidates, as a wide range of materials are claimed to be deposited with these precursors: from amorphous carbon to graphene, and, in some cases, diamond-like carbon structures.[103] Moreover, carbon deposition is a common, undesired, byproduct of EBID processes that would benefit from being further studied with a surface science approach.

The e-beam setup together with a graphene substrate could also be used to investigate other phenomena. For example, we can use the e-beam to functionalize graphene or other 2D films, either by generating defects,[174,175] or by adsorption of other molecules.[176] Such functionalization can be of interest to modify the graphene's properties, but also to generate adsorption sites for further adsorption,[177] also referred as *anchor sites*.

Other deposition techniques can make use of these adsorption or anchor sites. A clear example would be Atomic Layer Deposition, already mentioned above. ALD is a widely used method to grow a variety of materials with atomic precision.[178] Graphene

could be an interesting substrate for ALD films for applications in (nano)electronics,[179,180] or for easy transfer to other substrates [181,182]. ALD requires active sites on the surface for the first precursor molecule to adsorb, which could be generated by e-beam functionalization of the graphene. Moreover, one could even employ a focused e-beam to functionalize only specific areas of a graphene substrate This would allow the growth of patterned ALD structures, as ALD precursors would nucleate only on the pre-treated areas.

Note that the e-beam deposition of anchor sites on graphene could also be of interest for catalysis studies. For example, one could study the stability (and the reactivity!) of the e-beam deposited molecules under ambient pressure conditions. Such studies would contribute in the field of *single molecule catalysis* or *single atom catalysis*.[183]

The field of undercover catalysis would also greatly benefit to further study undercover reactions using **graphene as a cover**. On one hand, graphene is widely employed as a coating agent, for metals (as in **paper III**), but also for other substrates and structures, such as semiconductors or nanowires. Understanding the intercalation of molecules under graphene on these other systems would be of great interest for extending the applications of graphene as a coating agent.

On the other hand, multiple studies (including **paper IV**) have shown that graphene can be an excellent model system for fundamental undercover chemistry studies. In this field of catalysis, a better understanding of the undercover reactions will ultimately help to design high-performance confined nano-catalysts. However, in order to do that, future studies should address the intrinsic mass transfer issues of confined catalysis. While it might be interesting to confine a catalyst to promote or facilitate a specific reaction, the overall production of the catalyst will be limited by the access of the reactants into the undercover space. With this problem in mind, it would be of great interest to explore the capabilities of undercover OH-H_2O formation to change the kinetics of intercalation.

Furthermore, undercover OH-H_2O could also be employed to promote the intercalation of bigger molecules.[136] This would open an avenue of possibilities for undercover catalysis applications, as now they are just limited to small molecules such as the ones discussed in chapter 6. Moreover, if we think of realistic catalytic environments, hydrogen and oxygen are a very abundant elements, usually present on

reactors or generated as by-products of the reaction. Studying how their intercalation and undercover reaction can affect the access of different molecules to the undercover space is of great importance, especially if selectivity to smaller compounds is assumed for confined catalysts.

Altogether, all these research prospects highlight the versatility of graphene for surface science studies, usually with both an active role in the system (as substrate or confining agent) and, simultaneously, a passive role as additional chemically sensitive probe.

As wisely stated by Ferrand, Siaj, and Claverie in their 2020 ACS Applied Nano Materials editorial, "*Graphene will undoubtably be intimately linked to the technological progress of our era".*[33] Following their spirit, I hope the work included in this thesis will inspire future research of reactions around graphene, embedding this unique material in the technological progress of the surface science field.

References

(1) Langmuir, I. Chemical Reactions on Surfaces. *Trans. Faraday Soc.* **1922**, *17*, 607–620.

(2) Ertl, G. Reactions at Well-Defined Surfaces. *Surf. Sci.* **1994**, *299–300* (C), 742–754.

(3) Palmberg, P. W. Ultrahigh Vacuum and Surface Science. *J. Vac. Sci. Technol. A Vacuum, Surfaces, Film.* **1994**, *12* (4), 946–952.

(4) Nobel Prize Outreach AB. The Nobel Prize in Physics 1981. NobelPrize.org https://www.nobelprize.org/prizes/physics/1981/summary/ (accessed Oct 13, 2022).

(5) Nobel Prize Outreach AB. The Nobel Prize in Physics 1924. NobelPrize.org https://www.nobelprize.org/prizes/physics/1924/summary/ (accessed Oct 13, 2022).

(6) Nobel Prize Outreach AB. The Nobel Prize in Physics 1986. NobelPrize.org https://www.nobelprize.org/prizes/physics/1986/summary/ (accessed Oct 13, 2022).

(7) Nobel Prize Outreach AB. The Nobel Prize in Chemistry 1998. NobelPrize.org https://www.nobelprize.org/prizes/physics/1998/summary/ (accessed Oct 13, 2022).

(8) Nobel Prize Outreach AB. The Nobel Prize in Chemistry 2007. NobelPrize.org https://www.nobelprize.org/prizes/physics/2007/summary/ (accessed Oct 13, 2022).

(9) Liu, Y. P. Surfaces and Interfaces of Low Dimensional III-V Semiconductor Devices | Lund University Publications, Lund University, 2022.

(10) Walter, A. L.; Schiller, F.; Corso, M.; Merte, L. R.; Bertram, F.; Lobo-Checa, J.; Shipilin, M.; Gustafson, J.; Lundgren, E.; Brión-Ríos, A. X.; Cabrera-Sanfelix, P.; Sánchez-Portal, D.; Ortega, J. E. X-Ray Photoemission Analysis of Clean and Carbon Monoxide-Chemisorbed Platinum(111) Stepped Surfaces Using a Curved Crystal. *Nat. Commun. 2015 61* **2015**, *6* (1), 1–7.

(11) Schiller, F.; Ilyn, M.; Pérez-Dieste, V.; Escudero, C.; Huck-Iriart, C.; Ruiz Del Arbol, N.; Hagman, B.; Merte, L. R.; Bertram, F.; Shipilin, M.; Blomberg, S.; Gustafson, J.; Lundgren, E.; Ortega, J. E. Catalytic Oxidation of Carbon Monoxide on a Curved Pd Crystal: Spatial Variation of Active and Poisoning Phases in Stationary Conditions. *J. Am. Chem. Soc.* **2018**, *140* (47), 16245–16252.

(12) Abdel-Mageed, A. M.; Klyushin, A.; Rezvani, A.; Knop-Gericke, A.; Schlçgl, R.; Jürgen Behm, R.; MAbdel-Mageed, D.; Rezvani, A.; JBehm, D.; Klyushin, D.; Knop-Gericke, D.; Schlögl, D. Negative Charging of Au Nanoparticles during Methanol Synthesis from CO_2/H_2 on a Au/ZnO Catalyst: Insights from Operando IR and Near-Ambient-Pressure XPS and XAS Measurements. *Angew. Chemie Int. Ed.* **2019**, *58* (30), 10325–10329.

(13) Ferrah, D.; Haines, A. R.; Galhenage, R. P.; Bruce, J. P.; Babore, A. D.; Hunt, A.; Waluyo, I.; Hemminger, J. C. Wet Chemical Growth and Thermocatalytic Activity of Cu-Based Nanoparticles Supported on TiO_2 Nanoparticles/HOPG: In Situ Ambient Pressure XPS Study of the CO2 Hydrogenation Reaction. *ACS Catal.* **2019**, *9* (8), 6783–6802.

(14) Lundgren, E.; Zhang, C.; Merte, L. R.; Shipilin, M.; Blomberg, S.; Hejral, U.; Zhou, J.; Zetterberg, J.; Gustafson, J. Novel in Situ Techniques for Studies of Model Catalysts. *Acc. Chem. Res.* **2017**, *50* (9), 2326–2333.

(15) Schnadt, J.; Knudsen, J.; Johansson, N. Present and New Frontiers in Materials Research by Ambient Pressure X-Ray Photoelectron Spectroscopy. *J. Phys. Condens. Matter* **2020**, *32*, 413003 (29pp).

(16) D'Acunto, G. Reaction Mechanisms and Dynamics in the Early Stage of High-κ Oxide Atomic Layer Deposition: Investigations by In Situ and Operando X-Ray Photoemission Spectroscopy | Lund University Publications, Lund University, 2022.

(17) Flavell, W. R. Spiers Memorial Lecture: Prospects for Photoelectron Spectroscopy. *Faraday Discuss.* **2022**, *236* (0), 9–57.

(18) Trotochaud, L.; Head, A. R.; Karslioğlu, O.; Kyhl, L.; Bluhm, H. Ambient Pressure Photoelectron Spectroscopy: Practical Considerations and Experimental Frontiers. *J. Phys. Condens. Matter* **2017**, *29* (5), 053002.

(19) Ogletree, D. F.; Bluhm, H.; Lebedev, G.; Fadley, C. S.; Hussain, Z.; Salmeron, M. A Differentially Pumped Electrostatic Lens System for Photoemission Studies in the Millibar Range. *Rev. Sci. Instrum.* **2002**, *73* (11), 3872.

(20) Frank Ogletree, D.; Bluhm, H.; Hebenstreit, E. D.; Salmeron, M. Photoelectron Spectroscopy under Ambient Pressure and Temperature Conditions. *Nucl. Instruments Methods Phys. Res. Sect. A Accel. Spectrometers, Detect. Assoc. Equip.* **2009**, *601* (1–2), 151–160. https://doi.org/10.1016/J.NIMA.2008.12.155.

(21) Kolmakov, A.; Gregoratti, L.; Kiskinova, M.; Günther, S. Recent Approaches for Bridging the Pressure Gap in Photoelectron Microspectroscopy. *Top. Catal.* **2016**, *59* (5–7), 448–468.

(22) Edwards, M. O. M.; Karlsson, P. G.; Eriksson, S. K.; Hahlin, M.; Siegbahn, H.; Rensmo, H.; Kahk, J. M.; Villar-Garcia, I. J.; Payne, D. J.; Åhlund, J. Increased Photoelectron Transmission in High-Pressure Photoelectron Spectrometers Using "Swift Acceleration." *Nucl. Instruments Methods Phys. Res. Sect. A Accel. Spectrometers, Detect. Assoc. Equip.* **2015**, *785*, 191–196.

(23) Amann, P.; Degerman, D.; Lee, M. T.; Alexander, J. D.; Shipilin, M.; Wang, H. Y.; Cavalca, F.; Weston, M.; Gladh, J.; Blom, M.; Björkhage, M.; Löfgren, P.; Schlueter, C.; Loemker, P.; Ederer, K.; Drube, W.; Noei, H.; Zehetner, J.; Wentzel, H.; Åhlund, J.; Nilsson, A. A High-Pressure x-Ray Photoelectron Spectroscopy Instrument for Studies of Industrially Relevant Catalytic Reactions at Pressures of Several Bars. *Rev. Sci. Instrum.* **2019**, *90* (10), 103102.

(24) Wallace, P. R. The Band Theory of Graphite. *Phys. Rev.* **1947**, *71* (9), 622–634.

(25) Boehm, H. P. Graphene—How a Laboratory Curiosity Suddenly Became Extremely Interesting. *Angew. Chemie Int. Ed.* **2010**, *49* (49), 9332–9335.

(26) Boehm, H. P.; Eckel, M.; Scholz, W. Untersuchungen Am Graphitoxid V. Über Den Bildungsmechanismus Des Graphitoxids. *Zeitschrift für Anorg. und Allg. Chemie* **1967**, *353* (5–6), 236–242.

(27) Novoselov, K. S.; Geim, A. K.; Morozov, S. V; Jiang, D.; Zhang, Y.; Dubonos, S. V; Grigorieva, I. V; Firsov, A. A.; K. S. Novoselov, A. K. Geim, S. V. Morozov, D. Jiang, Y. Zhang, S. V. Dubonos, I. V. G. and A. A. F. Electric Field Effect in Atomically Thin Carbon Films. *Science* **2004**, *306* (5696), 666–669.

(28) Nobel Prize Outreach AB. The Nobel Prize in Physics 2010. NobelPrize.org https://www.nobelprize.org/prizes/physics/2010/summary/ (accessed Oct 13, 2022).

(29) Lee, C.; Wei, X.; Kysar, J. W.; Hone, J. Measurement of the Elastic Properties and Intrinsic Strength of Monolayer Graphene. *Science* **2008**, *321* (5887), 385–388.

(30) Geim, A. K.; Novoselov, K. S. The Rise of Graphene. *Nat. Mater.* **2007**, *6*.

(31) Balandin, A. A.; Ghosh, S.; Bao, W.; Calizo, I.; Teweldebrhan, D.; Miao, F.; Lau, C. N. Superior Thermal Conductivity of Single-Layer Graphene. *Nano Lett.* **2008**, *8* (3), 902–907.

(32) Kuzmenko, A. B.; Van Heumen, E.; Carbone, F.; Van Der Marel, D. Universal Optical Conductance of Graphite. *Phys. Rev. Lett.* **2008**, *100* (11), 117401.

(33) Ferrand, A.; Siaj, M.; Claverie, J. P. Graphene, the Swiss Army Knife of Nanomaterials Science. *ACS Appl. Nano Mater.* **2020**, *3* (8), 7305–7313.

(34) Kolmakov, A.; Dikin, D. A.; Cote, L. J.; Huang, J.; Abyaneh, M. K.; Amati, M.; Gregoratti, L.; Günther, S.; Kiskinova, M. Graphene Oxide Windows for in Situ Environmental Cell Photoelectron Spectroscopy. *Nat. Nanotechnol. 2011 610* **2011**, *6* (10), 651–657.

(35) Velasco-Velez, J. J.; Pfeifer, V.; Hävecker, M.; Weatherup, R. S.; Arrigo, R.; Chuang, C. H.; Stotz, E.; Weinberg, G.; Salmeron, M.; Schlögl, R.; Knop-Gericke, A. Photoelectron Spectroscopy at the Graphene–Liquid Interface Reveals the Electronic Structure of an Electrodeposited Cobalt/Graphene Electrocatalyst. *Angew. Chemie Int. Ed.* **2015**, *54* (48), 14554–14558.

(36) Weatherup, R. S.; Eren, B.; Hao, Y.; Bluhm, H.; Salmeron, M. B. Graphene Membranes for Atmospheric Pressure Photoelectron Spectroscopy. *J. Phys. Chem. Lett.* **2016**, *7* (9), 1622–1627.

(37) Comrie, C. M.; Weinberg, W. H. The Chemisorption of Carbon Monoxide on the Iridium (111) Surface. *J. Chem. Phys.* **1976**, *64* (1), 250.

(38) Andersen, M.; Hornekær, L.; Hammer, B. Understanding Intercalation Structures Formed under Graphene on Ir(111). *Phys. Rev. B* **2014**, *90* (15), 155428.

(39) Johansson, N.; Andersen, M.; Monya, Y.; Andersen, J. N.; Kondoh, H.; Schnadt, J.; Knudsen, J. Ambient Pressure Phase Transitions over Ir(111): At the Onset of CO Oxidation. *J. Phys. Condens. Matter* **2017**, *29* (44), 444002.

(40) Attard, G.; Barnes, C. *Surfaces, Oxford Chemistry Primers*, 1st edition; Oxford University Press: New York, 1998.

(41) Nobel Prize Outreach AB. The Nobel Prize in Chemistry 1909. NobelPrize.org https://www.nobelprize.org/prizes/physics/1909/summary/ (accessed Oct 13, 2022).

(42) Nobel Prize Outreach AB. Wilhelm Ostwald – Nobel Lecture. NobelPrize.org. https://www.nobelprize.org/prizes/chemistry/1909/ostwald/lecture/ (accessed Oct 13, 2022).

(43) Hüfner, S. *Photoelectron Spectroscopy Principles and Applications*, Third edit.; Springer-Verlag Berlin Heidelberg, 1995.

(44) Liao, Y. Practical Electron Microscopy and Database https://www.globalsino.com/micro/TEM/TEM9923.html (accessed Oct 13, 2022).

(45) Redhead, P. A. *Extreme High Vacuum*; 1999.

(46) Schröder, U. A.; Petrović, M.; Gerber, T.; Martínez-Galera, A. J.; Grånäs, E.; Arman, M. A.; Herbig, C.; Schnadt, J.; Kralj, M.; Knudsen, J.; Michely, T. Core Level Shifts of Intercalated Graphene. *2D Mater.* **2017**, *4* (1), 15013.

(47) Shirley, D. A. High-Resolution X-Ray Photoemission Spectrum of the Valence Bands of Gold. *Phys. Rev. B* **1972**, *5* (12), 4709.

(48) Doniach, S.; Sunjic, M. Many-Electron Singularity in X-Ray Photoemission and X-Ray Line Spectra from Metals. *J. Phys. C Solid State Phys.* **1970**, *3* (2), 285.

(49) Schmid, M.; Steinrück, H. P.; Gottfried, J. M. A New Asymmetric Pseudo-Voigt Function for More Efficient Fitting of XPS Lines. *Surf. Interface Anal.* **2014**, *46* (8), 505–511.

(50) Atomic Calculation of Photoionization Cross-Sections and Asymmetry Parameters https://vuo.elettra.eu/services/elements/WebElements.html (accessed Oct 13, 2022).

(51) Powell, C. J.; Jablonski, A. Surface Sensitivity of X-Ray Photoelectron Spectroscopy. *Nucl. Instruments Methods Phys. Res. Sect. A Accel. Spectrometers, Detect. Assoc. Equip.* **2009**, *601* (1–2), 54–65.

(52) Powell, C. J.; Tanuma, S. Inelastic Mean Free Paths, Mean Escape Depths, Information Depths, and Effective Attenuation Lengths for Hard X-Ray Photoelectron Spectroscopy. In: Woicik, J. (Eds) Hard X-Ray Photoelectron Spectroscopy (HAXPES). In *Springer Series in Surface Sciences*; Springer, 2016; Vol. 59, pp 111–140.

(53) Tavares, P. F.; Leemann, S. C.; Sjöström, M.; Andersson, Å. The MAX IV Storage Ring Project. *Synchrotron Radiat.* **2014**, *21* (5), 862–877.

(54) Walker, R. P. The ELETTRA Synchrotron Radiation Facility. *Rev. Sci. Instrum.* **1992**, *63* (1), 1615.

(55) Hertel, N.; Hoffmann, S. V. ASTRID2: A New Danish Low-Emittance SR Source. *Syncrotron Radiat. News* **2011**, *24* (1), 19–23.

(56) Robinson, A. L. History of Synchrotron Radiation. *Syncrotron Radiat. News* **2015**, *28* (4), 4–9.

(57) Siegbahn, H.; Siegbahn, K. ESCA Applied to Liquids. *J. Electron Spectros. Relat. Phenomena* **1973**, *2* (3), 319–325.

(58) Siegbahn, H. Electron Spectroscopy for Chemical Analysis of Liquids and Solutions. *J. Phys. Chem.* **1985**, *89* (6), 897–909.

(59) Cai, J.; Dong, Q.; Han, Y.; Mao, B. H.; Zhang, H.; Karlsson, P. G.; Åhlund, J.; Tai, R. Z.; Yu, Y.; Liu, Z. An APXPS Endstation for Gas–Solid and Liquid–Solid Interface Studies at SSRF. *Nucl. Sci. Tech.* **2019**, *30* (5), 1–10.

(60) Knudsen, J.; Andersen, J. N.; Schnadt, J. A Versatile Instrument for Ambient Pressure X-Ray Photoelectron Spectroscopy: The Lund Cell Approach. *Surf. Sci.* **2016**, *646*, 160–169.

(61) Schnadt, J.; Knudsen, J.; Andersen, J. N.; Siegbahn, H.; Pietzsch, A.; Hennies, F.; Johansson, N.; Mårtensson, N.; Öhrwall, G.; Bahr, S.; Mähl, S.; Schaff, O. The New Ambient-Pressure X-Ray Photoelectron Spectroscopy Instrument at MAX-Lab. *J. Synchrotron Radiat.* **2012**, *19* (5), 701–704.

(62) Tersoff, J.; Hamann, D. R. Theory of the Scanning Tunneling Microscope. *Phys. Rev. B* **1985**, *31* (2), 805.

(63) N'Diaye, A. T.; Coraux, J.; Plasa, T. N.; Busse, C.; Michely, T. Structure of Epitaxial Graphene on Ir(111). *New J. Phys.* **2008**, *10* (4), 043033.

(64) Coraux, J.; N'Diaye, A. T.; Busse, C.; Michely, T. Structural Coherency of Graphene on Ir(111). *Nano Lett.* **2008**, *8* (2), 565–570.

(65) Coraux, J.; T N'Diaye, A.; Engler, M.; Busse, C.; Wall, D.; Buckanie, N.; Meyer zu Heringdorf, F.-J.; van Gastel, R.; Poelsema, B.; Michely, T. Growth of Graphene on Ir(111). *New J. Phys.* **2009**, *11* (2), 23006.

(66) Suzuki, T. Organic Synthesis Involving Iridium-Catalyzed Oxidation. *Chem. Rev.* **2011**, *111* (3), 1825–1845.

(67) Hagedorn, C. J.; Weiss, M. J.; Weinberg, W. H. Dissociative Chemisorption of Hydrogen on Ir(111): Evidence for Terminal Site Adsorption. *Phys. Rev. B - Condens. Matter Mater. Phys.* **1999**, *60* (20), 14016–14018.

(68) Singh, S. B. Iridium Chemistry and Its Catalytic Applications: A Brief. *Green Chem. Technol. Lett.* **2016**, *2* (4), 206–210.

(69) Sun, L.; Yuan, G.; Gao, L.; Yang, J.; Chhowalla, M.; Gharahcheshmeh, M. H.; Gleason, K. K.; Choi, Y. S.; Hong, B. H.; Liu, Z. Chemical Vapour Deposition. *Nat. Rev. Methods Prim.* **2021**, *5*.

(70) Rosmi, M. S.; Shinde, S. M.; Rahman, N. D. A.; Thangaraja, A.; Sharma, S.; Sharma, K. P.; Yaakob, Y.; Vishwakarma, R. K.; Bakar, S. A.; Kalita, G.; Ohtani, H.; Tanemura, M. Synthesis of Uniform Monolayer Graphene on Re-Solidified Copper from Waste Chicken Fat by Low Pressure Chemical Vapor Deposition. *Mater. Res. Bull.* **2016**, *83*, 573–580.

(71) Nieuwenhuys, B. .; Hagen, D. .; Rovida, G.; Somorjai, G. . LEED, AES and Thermal Desorption Studies of Chemisorbed Hydrogen and Hydrocarbons (C_2H_2, C_2H_4, C6H6, C_6H_{12}) on the (111) and Stepped [6(111) × (100)] Iridium Crystal Surfaces; Comparison with Platinum. *Surf. Sci.* **1976**, *59* (1), 155–176.

(72) N'Diaye, A. T.; Bleikamp, S.; Feibelman, P. J.; Michely, T. Two-Dimensional Ir Cluster Lattice on a Graphene Moiré on Ir(111). *Phys. Rev. Lett.* **2006**, *97* (21), 1–4.

(73) Busse, C.; Lazić, P.; Djemour, R.; Coraux, J.; Gerber, T.; Atodiresei, N.; Caciuc, V.; Brako, R.; N'Diaye, A. T.; Blügel, S.; Zegenhagen, J.; Michely, T. Graphene on Ir(111): Physisorption with Chemical Modulation. *Phys. Rev. Lett.* **2011**, *107* (3), 036101.

(74) Hattab, H.; N'Diaye, A. T.; Wall, D.; Jnawali, G.; Coraux, J.; Busse, C.; Van Gastel, R.; Poelsema, B.; Michely, T.; Meyer Zu Heringdorf, F. J.; Horn-Von Hoegen, M. Growth Temperature Dependent Graphene Alignment on Ir(111). *Appl. Phys. Lett.* **2011**, *98* (14), 141903.

(75) Hattab, H.; N'Diaye, A. T.; Wall, D.; Klein, C.; Jnawali, G.; Coraux, J.; Busse, C.; Van Gastel, R.; Poelsema, B.; Michely, T.; Meyer Zu Heringdorf, F. J.; Horn-Von Hoegen, M. Interplay of Wrinkles, Strain, and Lattice Parameter in Graphene on Iridium. *Nano Lett.* **2012**, *12* (2), 678–682.

(76) Hämäläinen, S. K.; Boneschanscher, M. P.; Jacobse, P. H.; Swart, I.; Pussi, K.; Moritz, W.; Lahtinen, J.; Liljeroth, P.; Sainio, J. Structure and Local Variations of the Graphene Moiré on Ir(111). *Phys. Rev. B - Condens. Matter Mater. Phys.* **2013**, *88* (20), 201406.

(77) Cosma, D. A.; Wallbank, J. R.; Cheianov, V.; Fal'Ko, V. I. Moiré Pattern as a Magnifying Glass for Strain and Dislocations in van Der Waals Heterostructures. *Faraday Discuss.* **2014**, *173*, 137–143.

(78) Schröder, U. A.; Grånäs, E.; Gerber, T.; Arman, M. A.; Martínez-Galera, A. J.; Schulte, K.; Andersen, J. N.; Knudsen, J.; Michely, T. Etching of Graphene on Ir(111) with Molecular Oxygen. *Carbon N. Y.* **2016**, *96*, 320–331.

(79) Preobrajenski, A. B.; Ng, M. L.; Vinogradov, A. S.; Mårtensson, N. Controlling Graphene Corrugation on Lattice-Mismatched Substrates. *Phys. Rev. B - Condens. Matter Mater. Phys.* **2008**, *78* (7), 2–5.

(80) Knudsen, J.; Feibelman, P. J.; Gerber, T.; Grånäs, E.; Schulte, K.; Stratmann, P.; Andersen, J. N.; Michely, T. Clusters Binding to the Graphene Moiré on Ir(111): X-Ray Photoemission Compared to Density Functional Calculations. *Phys. Rev. B* **2012**, *85* (3), 035407.

(81) Balog, R.; Andersen, M.; Jørgensen, B.; Sljivancanin, Z.; Hammer, B.; Baraldi, A.; Larciprete, R.; Hofmann, P.; Hornekær, L.; Lizzit, S. Controlling Hydrogenation of Graphene on Ir(111). *ACS Nano* **2013**, *7* (5), 3823–3832.

(82) Lacovig, P.; Pozzo, M.; Alfè, D.; Vilmercati, P.; Baraldi, A.; Lizzit, S. Growth of Dome-Shaped Carbon Nanoislands on Ir(111): The Intermediate between Carbidic Clusters and Quasi-Free-Standing Graphene. *Phys. Rev. Lett.* **2009**, *103* (16), 14–17.

(83) Gråsäs, E.; Knudsen, J.; Schröder, U. A.; Gerber, T.; Busse, C.; Arman, M. A.; Schulte, K.; Andersen, J. N.; Michely, T. Oxygen Intercalation under Graphene on Ir(111): Energetics, Kinetics, and the Role of Graphene Edges. *ACS Nano* **2012**, *6* (11), 9951–9963.

(84) Geim, A. K.; Grigorieva, I. V. Van Der Waals Heterostructures. *Nature* **2013**, *499* (7459), 419–425.

(85) Lotsch, B. V. Vertical 2D Heterostructures. *Annu. Rev. Mater. Res.* **2015**, *45*, 85–109.

(86) Kim, C. H.; Kymissis, I. Graphene–Organic Hybrid Electronics. *J. Mater. Chem. C* **2017**, *5* (19), 4598–4613.

(87) Hong, G.; Wu, Q. H.; Ren, J.; Wang, C.; Zhang, W.; Lee, S. T. Recent Progress in Organic Molecule/Graphene Interfaces. *Nano Today* **2013**, *8* (4), 388–402.

(88) Jariwala, D.; Marks, T. J.; Hersam, M. C. Mixed-Dimensional van Der Waals Heterostructures. *Nat. Mater. 2016 162* **2016**, *16* (2), 170–181.

(89) N'Diaye, A. T.; Gerber, T.; Busse, C.; Mysliveček, J.; Coraux, J.; Michely, T. A Versatile Fabrication Method for Cluster Superlattices. *New J. Phys.* **2009**, *11*, 1–19.

(90) Macleod, J. M.; Rosei, F. Molecular Self-Assembly on Graphene. *Small* **2014**, *10* (6), 1038–1049.

(91) Tian, T.; Shih, C. J. Molecular Epitaxy on Two-Dimensional Materials: The Interplay between Interactions. *Ind. Eng. Chem. Res.* **2017**, *56* (38), 10552–10581.

(92) Koma, A. Van Der Waals Epitaxy—a New Epitaxial Growth Method for a Highly Lattice-Mismatched System. *Thin Solid Films* **1992**, *216* (1), 72–76.

(93) Lin, Y. C.; Lu, N.; Perea-Lopez, N.; Li, J.; Lin, Z.; Peng, X.; Lee, C. H.; Sun, C.; Calderin, L.; Browning, P. N.; Bresnehan, M. S.; Kim, M. J.; Mayer, T. S.; Terrones, M.; Robinson, J. A. Direct Synthesis of van Der Waals Solids. *ACS Nano* **2014**, *8* (4), 3715–3723.

(94) Heilmann, M.; Bashouti, M.; Riechert, H.; Lopes, J. M. J. Defect Mediated van Der Waals Epitaxy of Hexagonal Boron Nitride on Graphene. *2D Mater.* **2018**, *5* (2).

(95) Liu, Z.; Song, L.; Zhao, S.; Huang, J.; Ma, L.; Zhang, J.; Lou, J.; Ajayan, P. M. Direct Growth of Graphene/Hexagonal Boron Nitride Stacked Layers. *Nano Lett.* **2011**, *11* (5), 2032–2037.

(96) Lopes, J. M. J.; Czubak, D.; Zallo, E.; Figueroa, A. I.; Guillemard, C.; Valvidares, M.; Rubio-Zuazo, J.; López-Sanchéz, J.; Valenzuela, S. O.; Hanke, M.; Ramsteiner, M. Large-Area van Der Waals Epitaxy and Magnetic Characterization of Fe_3GeTe_2 films on Graphene. *2D Mater.* **2021**, *8* (4), 041001.

(97) Shi, Y.; Zhou, W.; Lu, A. Y.; Fang, W.; Lee, Y. H.; Hsu, A. L.; Kim, S. M.; Kim, K. K.; Yang, H. Y.; Li, L. J.; Idrobo, J. C.; Kong, J. Van Der Waals Epitaxy of MoS_2 Layers Using Graphene as Growth Templates. *Nano Lett.* **2012**, *12* (6), 2784–2791.

(98) Hall, J.; Pielić, B.; Murray, C.; Jolie, W.; Wekking, T.; Busse, C.; Kralj, M.; Michely, T. Molecular Beam Epitaxy of Quasi-Freestanding Transition Metal Disulphide Monolayers on van Der Waals Substrates: A Growth Study. *2D Mater.* **2018**, *5* (2), 025005.

(99) Murray, C.; Jolie, W.; Fischer, J. A.; Hall, J.; Van Efferen, C.; Ehlen, N.; Grüneis, A.; Busse, C.; Michely, T. Comprehensive Tunneling Spectroscopy of Quasifreestanding MoS_2 on Graphene on Ir(111). *Phys. Rev. B* **2019**, *99* (11), 115434.

(100) Ehlen, N.; Hall, J.; Senkovskiy, B. V.; Hell, M.; Li, J.; Herman, A.; Smirnov, D.; Fedorov, A.; Yu Voroshnin, V.; Di Santo, G.; Petaccia, L.; Michely, T.; Grüneis, A. Narrow Photoluminescence and Raman Peaks of Epitaxial MoS_2 on Graphene/Ir(111). *2D Mater.* **2018**, *6* (1), 011006.

(101) Jadriško, V.; Radatović, B.; Pielić, B.; Gadermaier, C.; Kralj, M.; Vujičić, N. Structural and Optical Characterization of Nanometer Sized MoS_2/Graphene Heterostructures for Potential Use in Optoelectronic Devices. *FlatChem* **2022**, *34*, 100397.

(102) Loi, F.; Sbuelz, L.; Lacovig, P.; Lizzit, D.; Bignardi, L.; Lizzit, S.; Baraldi, A. Growth Mechanism and Thermal Stability of a MoS_2-Graphene Interface: A High-Resolution Core-Level Photoelectron Spectroscopy Study. *J. Phys. Chem. C* **2020**, *124* (38), 20889–20897.

(103) Utke, I.; Hoffmann, P.; Melngailis, J. Gas-Assisted Focused Electron Beam and Ion Beam Processing and Fabrication. *J. Vac. Sci. Technol. B Microelectron. Nanom. Struct. Process. Meas. Phenom.* **2008**, *26* (4), 1197–1276.

(104) van Dorp, W. F.; Hagen, C. W. A Critical Literature Review of Focused Electron Beam Induced Deposition. *J. Appl. Phys.* **2008**, *104* (8), 81301.

(105) Hwang, B.; Kwon, J.; Lee, M.; Lim, S. J.; Jeon, S.; Kim, S.; Ham, U.; Song, Y. J.; Kuk, Y. Electron-Beam Assisted Growth of Hexagonal Boron-Nitride Layer. *Curr. Appl. Phys.* **2013**, *13* (7), 1365–1369.

(106) Sprenger, J. K.; Sun, H.; Cavanagh, A. S.; Roshko, A.; Blanchard, P. T.; George, S. M. Electron-Enhanced Atomic Layer Deposition of Boron Nitride Thin Films at Room Temperature and 100 °C. *J. Phys. Chem. C* **2018**, *122* (17), 9455–9464.

(107) Enderlein, C. Graphene and Its Interaction with Different Substrates Studied by Angular-Resolved Photoemission Spectroscopy, Universität Berlin, 2010.

(108) Voloshina, E. N.; Dedkov, Y. S. General Approach to Understanding the Electronic Structure of Graphene on Metals. *Mater. Res. Express* **2014**, *1* (3), 035603.

(109) Presel, F.; Jabeen, N.; Pozzo, M.; Curcio, D.; Omiciuolo, L.; Lacovig, P.; Lizzit, S.; Alfè, D.; Baraldi, A. Unravelling the Roles of Surface Chemical Composition and Geometry for the Graphene–Metal Interaction through C1s Core-Level Spectroscopy. *Carbon N. Y.* **2015**, *93*, 187–198.

(110) Guo, N.; Yam, K. M.; Zhang, C. Substrate Engineering of Graphene Reactivity: Towards High-Performance Graphene-Based Catalysts. *npj 2D Mater. Appl.* **2018**, *2*.

(111) Schumacher, S.; Wehling, T. O.; Lazić, P.; Runte, S.; Förster, D. F.; Busse, C.; Petrović, M.; Kralj, M.; Blügel, S.; Atodiresei, N.; Caciuc, V.; Michely, T. The Backside of Graphene: Manipulating Adsorption by Intercalation. *Nano Lett.* **2013**, *13* (11), 5013–5019.

(112) Huttmann, F.; Martínez-Galera, A. J.; Caciuc, V.; Atodiresei, N.; Schumacher, S.; Standop, S.; Hamada, I.; Wehling, T. O.; Blügel, S.; Michely, T. Tuning the van Der Waals Interaction of Graphene with Molecules via Doping. *Phys. Rev. Lett.* **2015**, *115* (23), 236101.

(113) Sutter, P.; Sadowski, J. T.; Sutter, E. A. Chemistry under Cover: Tuning Metal-Graphene Interaction by Reactive Intercalation. *J. Am. Chem. Soc.* **2010**, *132* (23), 8175–8179.

(114) Meiwes-Broer, K.-H. *Metal Clusters at Surfaces*; Springer Series in Cluster Physics; Springer Berlin, Heidelberg, 2000.

(115) Will, M.; Atodiresei, N.; Caciuc, V.; Valerius, P.; Herbig, C.; Michely, T. A Monolayer of Hexagonal Boron Nitride on Ir(111) as a Template for Cluster Superlattices. *ACS Nano* **2018**, *12* (7), 6871–6880.

(116) Martínez-Galera, A. J.; Schröder, U. A.; Herbig, C.; Arman, M. A.; Knudsen, J.; Michely, T.; Martinez-Galera, A. J.; Schroeder, U. A.; Herbig, C.; Arman, M. A.; Knudsen, J.; Michely, T. Preventing Sintering of Nanoclusters on Graphene by Radical Adsorption. *Nanoscale* **2017**, *9* (36), 13618–13629.

(117) Gerber, T.; Granäs, E.; Schröder, U. A.; Stratmann, P.; Schulte, K.; Andersen, J. N.; Knudsen, J.; Michely, T. Stability and Reactivity of Graphene-Templated Nanoclusters. *J. Phys. Chem. C* **2016**, *120* (46), 26290–26299.

(118) Schedin, F.; Geim, A. K.; Morozov, S. V.; Hill, E. W.; Blake, P.; Katsnelson, M. I.; Novoselov, K. S. Detection of Individual Gas Molecules Adsorbed on Graphene. *Nat. Mater. 2007 69* **2007**, *6* (9), 652–655.

(119) Johns, J. E.; Hersam, M. C. Atomic Covalent Functionalization of Graphene. *Acc. Chem. Res.* **2013**, *46* (1), 77–86.

(120) Schulte, K.; Vinogradov, N. A.; Ng, M. L.; Mårtensson, N.; Preobrajenski, A. B. Bandgap Formation in Graphene on Ir(111) through Oxidation. *Appl. Surf. Sci.* **2013**, *267*, 74–76.

(121) Jørgensen, J. H.; Čabo, A. G.; Balog, R.; Kyhl, L.; Groves, M. N.; Cassidy, A. M.; Bruix, A.; Bianchi, M.; Dendzik, M.; Arman, M. A.; Lammich, L.; Pascual, J. I.; Knudsen, J.; Hammer, B.; Hofmann, P.; Hornekaer, L. Symmetry-Driven Band Gap Engineering in Hydrogen Functionalized Graphene. *ACS Nano* **2016**, *10* (12), 10798–10807.

(122) Balog, R.; Jørgensen, B.; Nilsson, L.; Andersen, M.; Rienks, E.; Bianchi, M.; Fanetti, M.; Lægsgaard, E.; Baraldi, A.; Lizzit, S.; Sljivancanin, Z.; Besenbacher, F.; Hammer, B.; Pedersen, T. G.; Hofmann, P.; Hornekær, L. Bandgap Opening in Graphene Induced by Patterned Hydrogen Adsorption. *Nat. Mater.* **2010**, *9* (4), 315–319.

(123) Yamamoto, S.; Takeuchi, K.; Hamamoto, Y.; Liu, R. Y.; Shiozawa, Y.; Koitaya, T.; Someya, T.; Tashima, K.; Fukidome, H.; Mukai, K.; Yoshimoto, S.; Suemitsu, M.; Morikawa, Y.; Yoshinobu, J.; Matsuda, I. Enhancement of CO_2 Adsorption on Oxygen-Functionalized Epitaxial Graphene Surface under near-Ambient Conditions. *Phys. Chem. Chem. Phys.* **2018**, *20* (29), 19532–19538.

(124) Kyhl, L.; Balog, R.; Cassidy, A.; Jørgensen, J.; Grubisic-Čabo, A.; Trotochaud, L.; Bluhm, H.; Hornekær, L. Enhancing Graphene Protective Coatings by Hydrogen-Induced Chemical Bond Formation. *ACS Appl. Nano Mater* **2018**, *1*, 4509–4515.

(125) Ng, M. L.; Balog, R.; Hornekær, L.; Preobrajenski, A. B.; Vinogradov, N. A.; Mårtensson, N.; Schulte, K. Controlling Hydrogenation of Graphene on Transition Metals. *J. Phys. Chem. C* **2010**, *114* (43), 18559–18565.

(126) Sun, T.-Y.; Hao, Y.; Lin, C.-T.; Wang, L.; Huang, L.-F. Unraveling the Strong Coupling between Graphene/Nickel Interface and Atmospheric Adsorbates for Versatile Realistic Applications. *Carbon Trends* **2021**, *2*, 100013.

(127) Tang, Q.; Zhou, Z.; Chen, Z. Graphene-Related Nanomaterials: Tuning Properties by Functionalization. *Nanoscale* **2013**, *5* (11), 4541–4583.

(128) Kong, L.; Enders, A.; Rahman, T. S.; Dowben, P. A. Molecular Adsorption on Graphene. *J. Phys. Condens. Matter* **2014**, *26* (44), 443001.

(129) Shifa, T. A.; Vomiero, A. Confined Catalysis: Progress and Prospects in Energy Conversion. *Adv. Energy Mater.* **2019**, *9* (40), 1–15.

(130) Fu, Q.; Bao, X. Surface Chemistry and Catalysis Confined under Two-Dimensional Materials. *Chem. Soc. Rev.* **2017**, *46* (7), 1842–1874.

(131) Li, H.; Xiao, J.; Fu, Q.; Bao, X. Confined Catalysis under Two-Dimensional Materials. *Proc. Natl. Acad. Sci.* **2017**, *114* (23), 5930–5934.

(132) Boscoboinik, J. A. Chemistry in Confined Space through the Eyes of Surface Science - 2D Porous Materials. *J. Phys. Condens. Matter* **2019**, *31* (6).

(133) Mu, R.; Fu, Q.; Jin, L.; Yu, L.; Fang, G.; Tan, D.; Bao, X. Visualizing Chemical Reactions Confined under Graphene. *Angew. Chemie - Int. Ed.* **2012**, *51* (20), 4856–4859.

(134) Zhou, Y.; Chen, W.; Cui, P.; Zeng, J.; Lin, Z.; Kaxiras, E.; Zhang, Z. Enhancing the Hydrogen Activation Reactivity of Nonprecious Metal Substrates via Confined Catalysis Underneath Graphene. *Nano Lett.* **2016**, *16* (10), 6058–6063.

(135) Ferrighi, L.; Datteo, M.; Fazio, G.; Di Valentin, C. Catalysis under Cover: Enhanced Reactivity at the Interface between (Doped) Graphene and Anatase TiO_2. *J. Am. Chem. Soc.* **2016**, *138* (23), 7365–7376.

(136) Wei, F.; Wan, Q.; Lin, S.; Guo, H. Origin of Confined Catalysis in Nanoscale Reactors between Two-Dimensional Covers and Metal Substrates: Mechanical or Electronic? *J. Phys. Chem. C* **2020**, *124* (21), 11564–11573.

(137) Novoselov, K. S.; Mishchenko, A.; Carvalho, A.; Castro Neto, A. H. 2D Materials and van Der Waals Heterostructures. *Science* **2016**, *353* (6298), 9439.

(138) Zhang, L.; Chen, H.; Wei, Z. Recent Advances in Nanoparticles Confined in Two-Dimensional Materials as High-Performance Electrocatalysts for Energy-Conversion Technologies. *ChemCatChem* **2021**, *13* (11), 2541–2558.

(139) Han, X.; Gao, Q.; Yan, Z.; Ji, M.; Long, C.; Zhu, H. Electrocatalysis in Confined Spaces: Interplay between Well-Defined Materials and the Microenvironment. *Nanoscale* **2021**, *13* (3), 1515–1528.

(140) Goel, S.; Wu, Z.; Zones, S. I.; Iglesia, E. Synthesis and Catalytic Properties of Metal Clusters Encapsulated within Small-Pore (SOD, GIS, ANA) Zeolites. *J. Am. Chem. Soc.* **2012**, *134* (42), 17688–17695.

(141) Ma, L.; Zeng, X. C.; Wang, J. Oxygen Intercalation of Graphene on Transition Metal Substrate: An Edge-Limited Mechanism. *J. Phys. Chem. Lett.* **2015**, *6* (20), 4099–4105.

(142) Larciprete, R.; Ulstrup, S.; Lacovig, P.; Dalmiglio, M.; Bianchi, M.; Mazzola, F.; Hornekær, L.; Orlando, F.; Baraldi, A.; Hofmann, P.; Lizzit, S. Oxygen Switching of the Epitaxial Graphene-Metal Interaction. *ACS Nano* **2012**, *6* (11), 9551–9558.

(143) Grånäs, E. Above and Below Graphene: Nanoparticle Chemistry and Interface Reactions | Lund University Publications, Lund University, 2014.

(144) Bianchi, M.; Cassese, D.; Cavallin, A.; Comin, R.; Orlando, F.; Postregna, L.; Golfetto, E.; Lizzit, S.; Baraldi, A. Surface Core Level Shifts of Clean and Oxygen Covered Ir(111). *New J. Phys.* **2009**, *11* (6), 063002.

(145) Stampfl, C.; Soon, A.; Piccinin, S.; Shi, H.; Zhang, H. Bridging the Temperature and Pressure Gaps: Close-Packed Transition Metal Surfaces in an Oxygen Environment. *J. Phys. Condens. Matter* **2008**, *20* (18), 184021.

(146) Zhdan, P. A.; Boreskov, G. K.; Boronin, A. I.; Egelhoff, W. F.; Weinberg, W. H. An XPS Investigation of the Chemisorption of Oxygen on the Iridium (111) Surface. *Surf. Sci.* **1976**, *61* (1), 25–36.

(147) Chan, C. M.; Weinberg, W. H. Low-energy Electron Diffraction Structural Analysis of the (2×2) Oxygen Overlayer on the Iridium (111) Surface. *J. Chem. Phys.* **1979**, *71*, 2788.

(148) Kueppers, J.; Plagge, A. Interaction of CO and O_2 with Ir(111) Surfaces. *J. Vac. Sci. Technol.* **1998**, *13* (1), 259.

(149) Hagen, D. I.; Nieuwenhuys, B. E.; Rovida, G.; Somorjai, G. A. Low-Energy Electron Diffraction, Auger Electron Spectroscopy, and Thermal Desorption Studies of Chemisorbed CO and O_2 on the (111) and Stepped [6(111) × (100)] Iridium Surfaces. *Surf. Sci.* **1976**, *57* (2), 632–650.

(150) Ueda, K.; Suzuki, K.; Toyoshima, R.; Monya, Y.; Yoshida, M.; Isegawa, K.; Amemiya, K.; Mase, K.; Mun, B. S.; Arman, M. A.; Grånäs, E.; Knudsen, J.; Schnadt, J.; Kondoh, H. Adsorption and Reaction of CO and NO on Ir(111) under Near Ambient Pressure Conditions. *Top. Catal.* **2016**, *59* (5–7), 487–496.

(151) Grånäs, E.; Andersen, M.; Arman, M. A.; Gerber, T.; Hammer, B.; Schnadt, J.; Andersen, J. N.; Michely, T.; Knudsen, J. CO Intercalation of Graphene on Ir(111) in the Millibar Regime. *J. Phys. Chem. C* **2013**, *117* (32), 16438–16447.

(152) Eads, C. N.; Boscoboinik, J. A.; Head, A. R.; Hunt, A.; Waluyo, I.; Stacchiola, D. J.; Tenney, S. A. Enhanced Catalysis under 2D Silica: A CO Oxidation Study. *Angew. Chemie - Int. Ed.* **2021**, *60* (19), 10888–10894.

(153) Cored, J.; Wang, M.; Akter, N.; Darbari, Z.; Xu, Y.; Karagoz, B.; Waluyo, I.; Hunt, A.; Stacchiola, D.; Head, A. R.; Concepcion, P.; Lu, D.; Boscoboinik, J. A. Water Formation Reaction under Interfacial Confinement: $Al_{0.25}Si_{0.75}O_2$ on O-Ru(0001). *Nanomaterials* **2022**, *12* (2), 183.

(154) Sun, P. Z.; Yang, Q.; Kuang, W. J.; Stebunov, Y. V.; Xiong, W. Q.; Yu, J.; Nair, R. R.; Katsnelson, M. I.; Yuan, S. J.; Grigorieva, I. V.; Lozada-Hidalgo, M.; Wang, F. C.; Geim, A. K. Limits on Gas Impermeability of Graphene. *Nature* **2020**, *579* (7798), 229–232.

(155) Gråsä, E.; Gerber, T.; Schröder, U. A.; Schulte, K.; Andersen, J. N.; Michely, T.; Knudsen, J. Hydrogen Intercalation under Graphene on Ir(111). *Surf. Sci.* **2016**, *651* (651), 57–61.

(156) Sezen, H.; Al-Hada, M.; Amati, M.; Gregoratti, L. In Situ Chemical and Morphological Characterization of Copper under near Ambient Reduction and Oxidation Conditions. *Surf. Interface Anal.* **2018**, *50* (10), 921–926.

(157) Yu, F.; Camilli, L.; Wang, T.; Mackenzie, D. M. A.; Curioni, M.; Akid, R.; Bøggild, P. Complete Long-Term Corrosion Protection with Chemical Vapor Deposited Graphene. *Carbon N. Y.* **2018**, *132*, 78–84.

(158) Xu, X.; Yi, D.; Wang, Z.; Yu, J.; Zhang, Z.; Qiao, R.; Sun, Z.; Hu, Z.; Gao, P.; Peng, H.; Liu, Z.; Yu, D.; Wang, E.; Jiang, Y.; Ding, F.; Liu, K.; Z Xu, A. X.; Yu, J. C.; Zhang, Z. H.; Qiao, R. X.; Sun, Z. H.; Yu, D. P.; Liu, K. H.; Xu, X. Z.; Yi, D.; Ding, F.; Wang, Z. C.; Wang, E. G.; Jiang, Y.; Hu, Z. H.; Gao, P.; Peng, H. L.; Liu, Z. F. Greatly Enhanced Anticorrosion of Cu by Commensurate Graphene Coating. *Adv. Mater.* **2018**, *30* (6), 1702944.

(159) Scardamaglia, M.; Struzzi, C.; Zakharov, A.; Reckinger, N.; Zeller, P.; Amati, M.; Gregoratti, L. Highlighting the Dynamics of Graphene Protection toward the Oxidation of Copper under Operando Conditions. *ACS Appl. Mater. Interfaces* **2019**, *11* (32), 29448–29457.

(160) Camilli, L.; Yu, F.; Cassidy, A.; Hornekær, L.; Bøggild, P. Challenges for Continuous Graphene as a Corrosion Barrier. *2D Mater.* **2019**, *6* (2).

(161) Liu, Z.; Gong, Y.; Zhou, W.; Ma, L.; Yu, J.; Idrobo, J. C.; Jung, J.; Macdonald, A. H.; Vajtai, R.; Lou, J.; Ajayan, P. M. Ultrathin High-Temperature Oxidation-Resistant Coatings of Hexagonal Boron Nitride. *Nat. Commun. 2013 41* **2013**, *4* (1), 1–8.

(162) Shen, L.; Zhao, Y.; Wang, Y.; Song, R.; Yao, Q.; Chen, S.; Chai, Y. A Long-Term Corrosion Barrier with an Insulating Boron Nitride Monolayer. *J. Mater. Chem. A* **2016**, *4* (14), 5044–5050.

(163) Zhang, K.; Feng, Y.; Wang, F.; Yang, Z.; Wang, J. Two Dimensional Hexagonal Boron Nitride (2D-hBN): Synthesis, Properties, and Applications. *J. Mater. Chem. C* **2017**, *5* (46), 11992–12022.

(164) Zhang, C.; Zhao, S.; Jin, C.; Koh, A. L.; Zhou, Y.; Xu, W.; Li, Q.; Xiong, Q.; Peng, H.; Liu, Z. Direct Growth of Large-Area Graphene and Boron Nitride Heterostructures by a Co-Segregation Method. *Nat. Commun.* **2015**, *6* (1), 6519.

(165) Yao, Y.; Fu, Q.; Zhang, Y. Y.; Weng, X.; Li, H.; Chend, M.; Jin, L.; Dong, A.; Mu, R.; Jiang, P.; Liu, L.; Bluhm, H.; Liu, Z.; Zhang, S. B.; Bao, X. Graphene Cover-Promoted Metal-Catalyzed Reactions. *Proc. Natl. Acad. Sci. U. S. A.* **2014**, *111* (48), 17023–17028.

(166) Grånäs, E.; Schröder, U. A.; Arman, M. A.; Andersen, M.; Gerber, T.; Schulte, K.; Andersen, J. N.; Michely, T.; Hammer, B.; Knudsen, J. Water Chemistry beneath Graphene: Condensation of a Dense OH–H_2O Phase under Graphene. *J. Phys. Chem. C* **2022**, *126* (9), 4347–4354.

(167) Politano, A.; Cattelan, M.; Boukhvalov, D. W.; Campi, D.; Cupolillo, A.; Agnoli, S.; Apostol, N. G.; Lacovig, P.; Lizzit, S.; Farías, D.; Chiarello, G.; Granozzi, G.; Larciprete, R. Unveiling the Mechanisms Leading to H_2 Production Promoted by Water Decomposition on Epitaxial Graphene at Room Temperature. *ACS Nano* **2016**, *10* (4), 4543–4549.

(168) Stubbe, J. Effects of Carbon Functionalization on Hydrogen Oxidation Underneath Graphene Flakes | LUP Student Papers, Lund University, 2020.

(169) Wang, Z. J.; Liang, Z.; Kong, X.; Zhang, X.; Qiao, R.; Wang, J.; Zhang, S.; Zhang, Z.; Xue, C.; Cui, G.; Zhang, Z.; Zou, D.; Liu, Z.; Li, Q.; Wei, W.; Zhou, X.; Tang, Z.; Yu, D.; Wang, E.; Liu, K.; Ding, F.; Xu, X. Visualizing the Anomalous Catalysis in Two-Dimensional Confined Space. *Nano Lett.* **2022**, *22* (12), 4661–4668.

(170) Salmeron, M.; Eren, B. High-Pressure Scanning Tunneling Microscopy. *Chem. Rev.* **2021**, *121* (2), 962–1006.

(171) Gura, L.; Yang, Z.; Brinker, M.; Kalaß, F.; Kirstaedter, W.; Marschalik, P.; Junkes, H.; Heyde, M.; Freund, H. J. Spiral High-Speed Scanning Tunneling Microscopy: Tracking Atomic Diffusion on the Millisecond Timescale. *Appl. Phys. Lett.* **2021**, *119* (25), 251601.

(172) Ning, Y.; Fu, Q.; Li, Y.; Zhao, S.; Wang, C.; Breitschaft, M.; Hagen, S.; Schaff, O.; Bao, X. A near Ambient Pressure Photoemission Electron Microscope (NAP-PEEM). *Ultramicroscopy* **2019**, *200*, 105–110.

(173) Barth, S.; Huth, M.; Jungwirth, F. Precursors for Direct-Write Nanofabrication with Electrons. *J. Mater. Chem. C* **2020**, *8* (45), 15884–15919.

(174) Liu, G.; Teweldebrhan, D.; Balandin, A. A. Tuning of Graphene Properties via Controlled Exposure to Electron Beams. *IEEE Trans. Nanotechnol.* **2011**, *10* (4), 865–870.

(175) Kretschmer, S.; Lehnert, T.; Kaiser, U.; Krasheninnikov, A. V. Formation of Defects in Two-Dimensional MoS_2 in the Transmission Electron Microscope at Electron Energies below the Knock-on Threshold: The Role of Electronic Excitations. *Nano Lett.* **2020**, *20* (4), 2865–2870.

(176) Kim, S. S.; Kulkarni, D. D.; Davis, R.; Kim, S. S.; Naik, R. R.; Voevodin, A. A.; Russell, M.; Jang, S. S.; Tsukruk, V. V.; Fedorov, A. G. Controlling the Physicochemical State of Carbon on Graphene Using Focused Electron-Beam-Induced Deposition. *ACS Nano* **2014**, *8* (7), 6805–6813.

(177) Bueno, R. A.; Martínez, J. I.; Luccas, R. F.; Del Árbol, N. R.; Munuera, C.; Palacio, I.; Palomares, F. J.; Lauwaet, K.; Thakur, S.; Baranowski, J. M.; Strupinski, W.; López, M. F.; Mompean, F.; García-Hernández, M.; Martín-Gago, J. A. Highly Selective Covalent Organic Functionalization of Epitaxial Graphene. *Nat. Commun. 2017 81* **2017**, *8* (1), 1–10.

(178) Johnson, R. W.; Hultqvist, A.; Bent, S. F. A Brief Review of Atomic Layer Deposition: From Fundamentals to Applications. *Mater. Today* **2014**, *17* (5), 236–246.

(179) Vervuurt, R. H. J.; Kessels, W. M. M. E.; Bol, A. A. Atomic Layer Deposition for Graphene Device Integration. *Adv. Mater. Interfaces* **2017**, *4* (18), 1700232.

(180) Giannazzo, F.; Schilirò, E.; Nigro, R. Lo; Roccaforte, F.; Yakimova, R. Atomic Layer Deposition of High-k Insulators on Epitaxial Graphene: A Review. *Appl. Sci. 2020, Vol. 10, Page 2440* **2020**, *10* (7), 2440.

(181) Grebel, H.; Stan, L.; Sumant, A. V.; Liu, Y.; Gosztola, D.; Ocola, L.; Fisher, B. Transfer of Graphene with Protective Oxide Layers. *ChemEngineering 2018, Vol. 2, Page 58* **2018**, *2* (4), 58.

(182) Shivayogimath, A.; Eriksson, L.; Whelan, P. R.; Mackenzie, D. M. A.; Luo, B.; Bøggild, P.; Booth, T. J. Atomic Layer Deposition Alumina-Mediated Graphene Transfer for Reduced Process Contamination. *Phys. status solidi – Rapid Res. Lett.* **2019**, *13* (11), 1900424.

(183) Yam, K.; Guo, N.; Jiang, Z.; Li, S.; Zhang, C. Graphene-Based Heterogeneous Catalysis: Role of Graphene. *Catalysts* **2020**, *10* (1), 53.

Printed by Media-Tryck, Lund 2022 NORDIC SWAN ECOLABEL 3041 0903

ISBN 978-91-8039-447-5
Division of Synchrotron Radiation Research
Department of Physics
Faculty of Science
Lund University